CHAPTER 5 STRUCTURAL BEHAVIOR OF JOINTS

Page

5.1 INTRODUCTION

It would be difficult to conceive of a structure that did not involve some type of joint. Joints often occur in transitions between major composite parts and a metal feature or fitting. In aircraft, such a situation is represented by articulated fittings on control surfaces as well as on wing and tail components which require the ability to pivot the element during various stages of operation. Tubular elements such as power shafting often use metal end fittings for connections to power sources or for articulation where changes in direction are needed. In addition, assembly of the structure from its constituent parts will involve either bonded or mechanically fastened joints or both.

Joints represent one of the greatest challenges in the design of structures in general and in composite structures in particular. The reason for this is that joints entail interruptions of the geometry of the structure and often, material discontinuities, which almost always produce local highly stressed areas, except for certain idealized types of adhesive joint such as scarf joints between similar materials. Stress concentrations in mechanically fastened joints are particularly severe because the load transfer between elements of the joint have to take place over a fraction of the available area. For mechanically fastened joints in metal structures, local yielding, which has the effect of eliminating stress peaks as the load increases, can usually be depended on; such joints can be designed to some extent by the "P over A" approach, i.e., by assuming that the load is evenly distributed over load bearing sections so that the total load (the "P") divided by the available area (the "A") represents the stress that controls the strength of the joint. In organic matrix composites, such a stress reduction effect is realized only to a minor extent, and stress peaks predicted to occur by elastic stress analysis have to be accounted for, especially for one-time monotonic loading. In the case of composite adherends, the intensity of the stress peaks varies with the orthotropy of the adherend in addition to various other material and dimensional parameters which affect the behavior of the joint for isotropic adherends.

In principle, adhesive joints are structurally more efficient than mechanically fastened joints because they provide better opportunities for eliminating stress concentrations; for example, advantage can be taken of ductile response of the adhesive to reduce stress peaks. Mechanically fastened joints tend to use the available material inefficiently. Sizeable regions exist where the material near the fastener is nearly unloaded, which must be compensated for by regions of high stress to achieve a particular required average load. As mentioned above, certain types of adhesive joints, namely scarf joints between components of similar stiffness, can achieve a nearly uniform stress state throughout the region of the joint.

In many cases, however, mechanically fastened joints can not be avoided because of requirements for disassembly of the joint for replacement of damaged structure or to achieve access to underlying structure. In addition, adhesive joints tend to lack structural redundancy, and are highly sensitive to manufacturing deficiencies, including poor bonding technique, poor fit of mating parts and sensitivity of the adhesive to temperature and environmental effects such as moisture. Assurance of bond quality has been a continuing problem in adhesive joints; while ultrasonic and X-ray inspection may reveal gaps in the bond, there is no present technique which can guarantee that a bond which appears to be intact does, in fact, have adequate load transfer capability. Surface preparation and bonding techniques have been well developed, but the possibility that lack of attention to detail in the bonding operation may lead to such deficiencies needs constant alertness on the part of fabricators. Thus mechanical fastening tends to be preferred over bonded construction in highly critical and safety rated applications such as primary aircraft structural components, especially in large commercial transports, since assurance of the required level of structural integrity is easier to guarantee in mechanically fastened assemblies. Bonded construction tends to be more prevalent in smaller aircraft. For non-aircraft applications as well as in non-flight critical aircraft components, bonding is likewise frequently used.

This chapter describes design procedures and analytical methods for determining stresses and deformations in structural joints for composite structures. Section 5.2 which follows deals with adhesive joints. (Mechanically fastened joints will be the subject of a future revision of the Handbook.)

In the case of adhesive joints, design considerations which are discussed include: effects of adherend thickness as a means of ensuring adherend failure rather than bond failure; the use of adherend tapering to minimize peel stresses; effects of adhesive ductility; special considerations regarding composite adherends; effects of bond layer defects, including surface preparations defects, porosity and thickness variations; and, considerations relating to long term durability of adhesive joints. In addition to design considerations, aspects of joint behavior which control stresses and deformations in the bond layer are described, including both shear stresses and transverse normal stresses which are customarily referred to as "peel" stresses when they are tensile. Finally, some principles for finite element analysis of bonded joints are described.

Related information on joints in composite structures which is described elsewhere in this handbook includes Volume 1, Chapter 7, Section 7.2 (Mechanically Fastened Joints) and 7.3 (Bonded Joints) together with Volume 3, Chapter 2, Section 2.7.8 on Adhesive Bonding.

5.2 ADHESIVE JOINTS

5.2.1 Introduction

Adhesive joints are capable of high structural efficiency and constitute a resource for structural weight saving because of the potential for elimination of stress concentrations which cannot be achieved with mechanically fastened joints. Unfortunately, because of a lack of reliable inspection methods and a requirement for close dimensional tolerances in fabrication, aircraft designers have generally avoided bonded construction in primary structure. Some notable exceptions include: bonded step lap joints used in attachments for the F-14 and F-15 horizontal stabilizers as well as the F-18 wing root fitting, and a majority of the airframe components of the Lear Fan and the Beech Starship.

While a number of issues related to adhesive joint design were considered in the earlier literature cited in Reference 5.2.1(a)- 5.2.1(h), much of the methodology currently used in the design and analysis of adhesive joints in composite structures is based on the approaches evolved by L.J. Hart-Smith in a series of NASA/Langley-sponsored contracts of the early 70's (Reference 5.2.1(i) - 5.2.1(n)) as well as from the Air Force's Primary Adhesively Bonded Structures Technology (PABST) program (Reference 5.2.1(o) - 5.2.1(r)) of the mid-70's. The most recent such work developed three computer codes for bonded and bolted joints, designated A4EG, A4EI and A4EK (References 5.2.1(s) - 5.2.1(u)), under Air Force contract. The results of these efforts have also appeared in a number of open literature publications (Reference 5.2.1(v) - (z)). In addition, such approaches found application in some of the efforts taking place under the NASA Advanced Composite Energy Efficient Aircraft (ACEE) program of the early to mid 80's (Reference 5.2.1(x) and 5.2.1(y)).

Some of the key principles on which these efforts were based include: (1) the use of simple 1-dimensional stress analyses of generic composite joints wherever possible; (2) the need to select the joint design so as to ensure failure in the adherend rather than the adhesive, so that the adhesive is never the weak link; (3) recognition that the ductility of aerospace adhesives is beneficial in reducing stress peaks in the adhesive; (4) careful use of such factors as adherend tapering to reduce or eliminate peel stresses from the joint; and (5) recognition of slow cyclic loading, corresponding to such phenomena as cabin pressurization in aircraft, as a major factor controlling durability of adhesive joints, and the need to avoid the worst effects of this type of loading by providing sufficient overlap length to ensure that some of the adhesive is so lightly loaded that creep cannot occur there, under the most severe extremes of humidity and temperature for which the component is to be used.

Much of the discussion to follow will retain the analysis philosophy of Hart-Smith, since it is considered to represent a major contribution to practical bonded joint design in both composite and metallic structures. On the other hand, some modifications are introduced here. For example, the revisions of the Goland-Reissner single lap joint analysis presented in Reference 5.2.1(k) have again been revised according to the approach presented in References 5.2.1(z) and 5.2.1(aa).

Certain issues which are specific to composite adherends but were not dealt with in the Hart-Smith efforts will be addressed. The most important of these is the effect of transverse shear deformations in organic composite adherends.

Although the main emphasis of the discussion is on simplified stress analysis concepts allowed by shear lag models for shear stress prediction and beam-on-elastic foundation concepts for peel stress prediction, a brief discussion will be provided on requirements for finite element modeling of adhesive joints. Similarly, although joint failure will be considered primarily from the standpoint of stress and strain energy considerations, some discussion of fracture mechanics considerations for adhesive joints will also be included.

5.2.2 Joint design considerations

5.2.2.1 Effects of adherend thickness: adherend failures vs. bond failures

Figure 5.2.2.1(a) shows a series of typical bonded joint configurations. Adhesive joints in general are characterized by high stress concentrations in the adhesive layer. These originate, in the case of shear stresses, because of unequal axial straining of the adherends, and in the case of peel stresses, because of eccentricity in the load path. Considerable ductility is associated with shear response of typical adhesives, which is beneficial in minimizing the effect of shear stress joint strength. Response to peel stresses tends to be much more brittle than that to shear stresses, and reduction of peel stresses is desirable for achieving good joint performance.

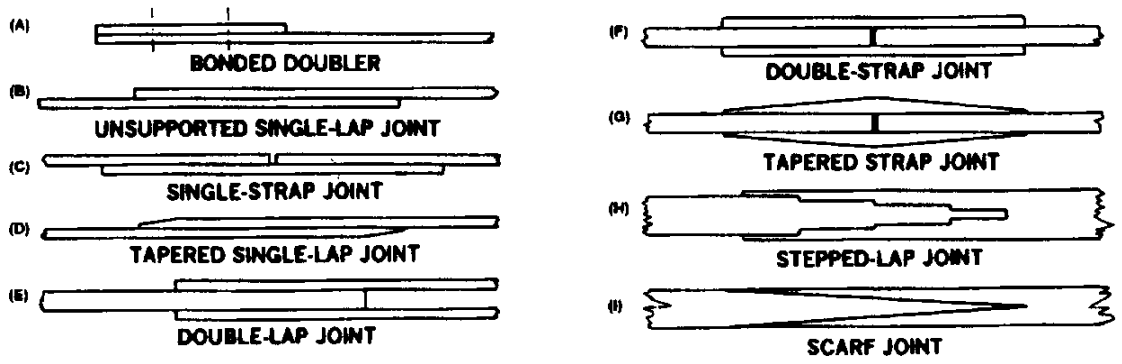

FIGURE 5.2.2.1(a) *Adhesive joint types (Reference 5.2.1(n) and 5.2.2.1(a)).*

From the standpoint of joint reliability, it is vital to avoid letting the adhesive layer be the weak link in the joint; this means that, whenever possible, the joint should be designed to ensure that the adherends fail before the bond layer. This is because failure in the adherends is fiber controlled, while failure in the adhesive is resin dominated, and thus subject to effects of voids and other defects, thickness variations, environmental effects, processing variations, deficiencies in surface preparation and other factors that are not always adequately controlled. This is a significant challenge, since adhesives are inherently much weaker than the composite or metallic elements being joined. However, the objective can be accomplished by recognizing the limitations of the joint geometry being considered and placing appropriate restrictions on the thickness dimensions of the joint for each geometry. Figure 5.2.2.1(b),which has frequently been used by Hart-Smith (References 5.2.1(n), 5.2.2.1(a)) to illustrate this point, shows a progression of joint types which represent increasing strength capability from the lowest to the highest in the figure. In each type of joint, the adherend thickness may be increased as an approach to achieving higher

load capacity. When the adherends are relatively thin, results of stress analyses show that for all of the joint types in Figure 5.2.2.1(b), the stresses in the bond will be small enough to guarantee that the adherends will reach their load capacity before failure can occur in the bond. As the adherend thicknesses increase, the bond stresses become relatively larger until a point is reached at which bond failure occurs at a lower load than that for which the adherends fail. This leads to the general principle that for a given joint type, the adherend thicknesses should be restricted to an appropriate range relative to the bond layer thickness. Because of processing considerations and defect sensitivity of the bond material, bond layer thicknesses are generally limited to a range of 0.005-0.015 in. (0.125-0.39 mm). As a result, each of the joint types in Figure 5.2.2.1(a) and 5.2.2.1(b) corresponds to a specific range of adherend thicknesses and therefore of load capacity, and as the need for greater load capacity arises, it is preferable to change the joint configuration to one of higher efficiency rather than to increasing the adherend thickness indefinitely.

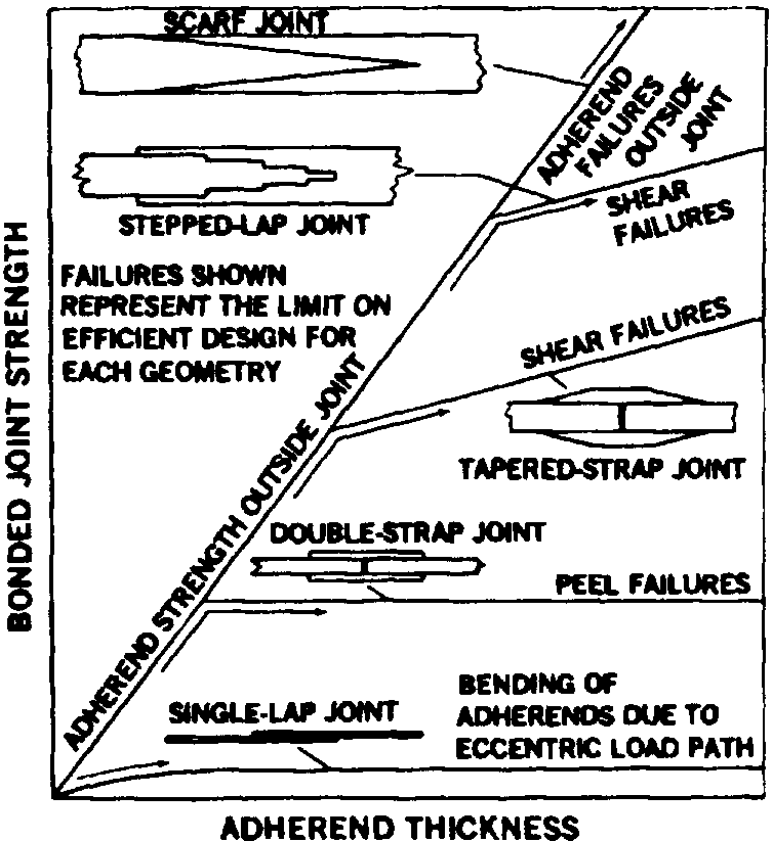

FIGURE 5.2.2.1(b) *Joint geometry effects (Reference 5.2.1(n)).*

5.2.2.2 Joint geometry effects

Single and double lap joints with uniformly thick adherends (Figure 5.2.2.1(a) - Joints (B), (E) and (F)) are the least efficient joint type and are suitable primarily for thin structures with low running loads (load per unit width, i.e., stress times element thickness). Of these, single lap joints are the least capable because the eccentricity of this type of geometry generates significant bending of the adherends that magnifies the peel stresses. Peel stresses are also present in the case of symmetric double lap and double strap joints, and become a limiting factor on joint performance when the adherends are relatively thick.

Tapering of the adherends (Figure 5.2.2.1(a) - Joints (D) and (G)) can be used to eliminate peel stresses in areas of the joint where the peel stresses are tensile, which is the case of primary concern. No tapering is needed at ends of the overlap where the adherends butt together because the transverse normal stress at that location is compressive and rather small. Likewise, for double strap joints under compressive loading, there is no concern with peel stresses at either location since the transverse extensional stresses that do develop in the adhesive are compressive in nature rather than tensile; indeed, where the gap occurs, the inner adherends bear directly on each other and no stress concentrations are present there for the compression loading case.

For joints between adherends of identical stiffness, scarf joints (Figure 5.2.2.1(a) - Joint (I)) are theoretically the most efficient, having the potential for complete elimination of stress concentrations. (In practice, some minimum thickness corresponding to one or two ply thicknesses must be incorporated at the thin end of the scarfed adherend leading to the occurrence of stress concentrations in these areas.) In theory, any desirable load capability can be achieved in the scarf joint by making the joint long enough and thick enough. However, practical scarf joints may be less durable because of a tendency toward creep failure associated with a uniform distribution of shear stress along the length of the joint unless care is taken to avoid letting the adhesive be stressed into the nonlinear range. As a result, scarf joints tend to be used only for repairs of very thin structures. Scarf joints with unbalanced stiffnesses between the adherends do not achieve the uniform shear stress condition of those with balanced adherends, and are somewhat less structurally efficient because of rapid buildup of load near the thin end of the thicker adherend.

Step lap joints (Figure 5.2.2.1(a) - Joint (H)) represent a practical solution to the challenge of bonding thick members. These types of joint provide manufacturing convenience by taking advantage of the layered structure of composite laminates. In addition, high loads can be transferred if sufficiently many short steps of sufficiently small "rise" (i.e., thickness increment) in each step are used, while maintaining sufficient overall length of the joint.

5.2.2.3 Effects of adherend stiffness unbalance

All types of joint geometry are adversely affected by unequal adherend stiffnesses, where stiffness is defined as axial or in-plane shear modulus times adherend thickness. Where possible, the stiffnesses should be kept approximately equal. For example, for step lap and scarf joints between quasi-isotropic carbon/epoxy (Young's modulus = 8 Msi (55 GPa)) and titanium (Young's modulus = 16 Msi (110 GPa)) ideally, the ratio of the maximum thickness (the thickness just beyond the end of the joint) of the composite adherend to that of the titanium should be 16/8=2.0.

5.2.2.4 Effects of ductile adhesive response

Adhesive ductility is an important factor in minimizing the adverse effects of shear and peel stress peaks in the bond layer. Figure 5.2.2.4(a) reconstructed from Reference 5.2.2.4(a) shows the shear stress-strain response characteristics of typical adhesives used in the aerospace industry as obtained from thick adherend tests (Volume 1, Section 7.3). Figure 5.2.2.4(a), part (A) represents a relatively ductile film adhesive, FM73, under various environmental conditions, while Figure 5.2.2.4(a), part (B) represents a more brittle adhesive (FM400) under the same conditions. Similar curves can be found in other sources such as Reference 5.2.2.4(b). Even for the less ductile material such as that represented in Figure 5.2.2.4(a), part (B), ductility has a pronounced influence on mechanical response of bonded joints, and restricting the design to elastic response deprives the application of a significant amount of additional structural capability. In addition to temperature and moisture, effects of porosity in the bond layer can have an influence on ductile response. Porosity effects are illustrated in Figure 5.2.2.4(b) (Reference 5.2.1(s)) which compares the response of FM73 for porous (x symbols) and non-porous (diamond symbols) bond layers for various environmental conditions. This will be further discussed in Section 5.2.2.6.

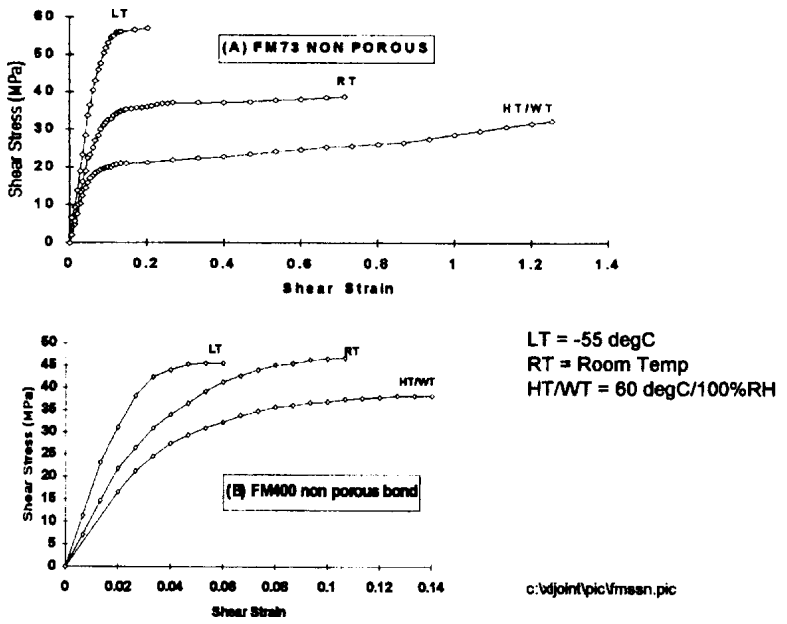

FIGURE 5.2.2.4(a) *Typical characteristics of aerospace adhesives (Reference 5.2.2.4(a)).*

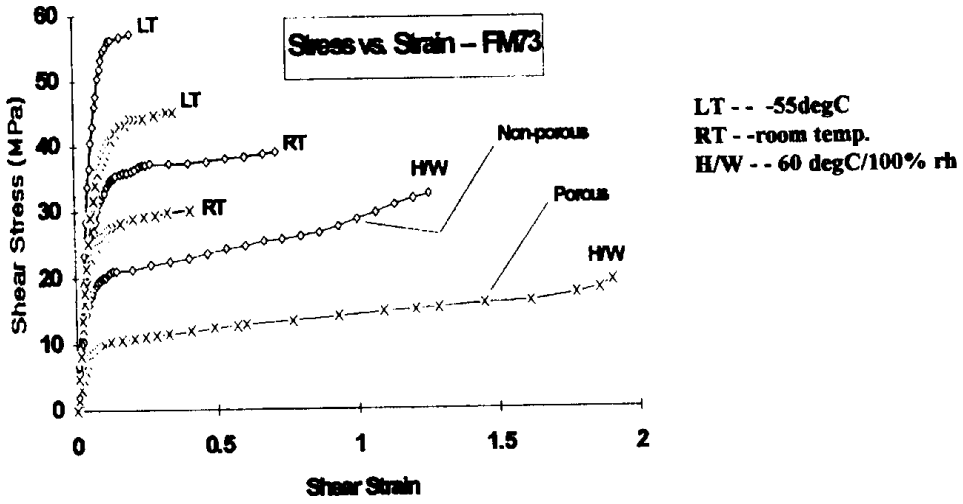

FIGURE 5.2.2.4(b) *Effect of porosity on adhesive stress-strain characteristics (Reference 5.2.1(s)).*

If peel stresses can be eliminated from consideration by such approaches as adherend tapering, strain energy to failure of the adhesive in shear has been shown by Hart-Smith (Reference 5.2.1(i)) to be the key parameter controlling joint strength; thus the square root of the adhesive strain energy density to failure determines the maximum static load that can be applied to the joint. The work of Hart-Smith has also shown that for predicting mechanical response of the joint, the detailed stress-strain curve of the adhesive can be replaced by an equivalent curve consisting of a linear rise followed by a constant stress plateau (i.e. elastic-perfectly plastic response) if the latter is adjusted to provide a strain energy density to failure equal to that of the actual stress-strain curve gives. Test methods for adhesives (see Volume 1, Section 7.3) should be aimed at providing data on this parameter . Once the equivalent elastic-perfectly

plastic stress strain curve has been identified for the selected adhesive in the range of the most severe environmental conditions (temperature and humidity) of interest, the joint design can proceed through the use of relatively simple one-dimensional stress analysis, thus avoiding the need for elaborate finite element calculations. Even the most complicated of joints, the step lap joints designed for root-end wing and tail connections for the F-18 and other aircraft, have been successfully designed (Reference 5.2.1(t)) and experimentally demonstrated using such approaches. Design procedures for such analyses which were developed under Government contract have been incorporated into the public domain in the form of the "A4EG", "A4EI" and "A4EK" computer codes mentioned previously in Section 5.2.1 and are currently available from the Air Force's Aerospace Structures Information and Analysis Center (ASIAC) . Note that the A4EK code permits analysis of bonded joints in which local disbonds are repaired by mechanical fasteners.

5.2.2.5 Behavior of composite adherends

Polymer matrix composite adherends are considerably more affected by interlaminar shear stresses than metals, so that there is a significant need to account for such effects in stress analyses of adhesively bonded composites. Transverse shear deformations of the adherends have an effect analogous to thickening of the bond layer and result in a lowering of both shear and peel stress peaks. (See Section 5.2.3.4.4).

In addition, because the resins used for adherend matrices tend to be less ductile than typical adhesives, and are weakened by stress concentrations due to the presence of the fibers, the limiting element in the joint may be the interlaminar shear and transverse tensile strengths of the adherends rather than the bond strength (Figure 5.2.2.5(a)). In the case of single lap joints (Figure 5.2.2.5(a), part (A)) bending failures of the adherends may occur because of high moments at the ends of the overlap. For metal adherends, bending failures take the form of plastic bending and hinge formation, while for composite adherends the bending failures are brittle in nature. In the case of double lap joints, peel stress build up in thicker adherends can cause the types of interlaminar failures in the adherends illustrated in Figure 5.2.2.5(a), part (B).

The effect of the stacking sequence of the laminates making up the adherends in composite joints is significant. For example, 90-degree layers placed adjacent to the bond layer theoretically act largely as additional thicknesses of bond material, leading to lower peak stresses, while 0-degree layers next to the bond layer give stiffer adherend response with higher stress peaks. In practice it has been observed that 90-degree layers next to the bond layer tend to seriously weaken the joint because of transverse cracking which develops in those layers, and advantage cannot be taken of the reduced peak stresses.

Large differences in thermal expansion characteristics between metal and composite adherends can cause severe problems. (See Section 5.2.3.4.2) Adhesives with high curing temperatures may be unsuitable for some low temperature applications because of large thermal stresses which develop as the joint cools down from the curing temperature.

In contrast with metal adherends, composite adherends are subject to moisture diffusion effects . As a result, moisture is more likely to be found over wide regions of the adhesive layer, as opposed to confinement near the exposed edges of the joint in the case of metal adherends, and response of the adhesive to moisture may be an even more significant issue for composite joints than for joints between metallic adherends.

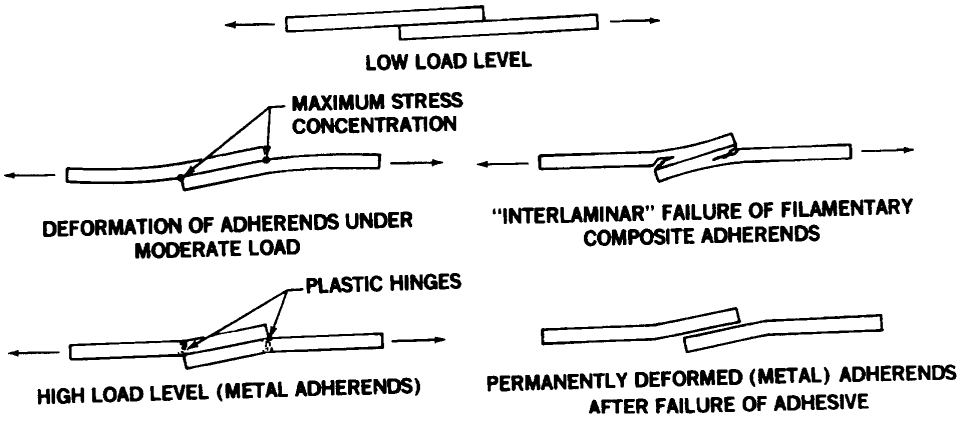

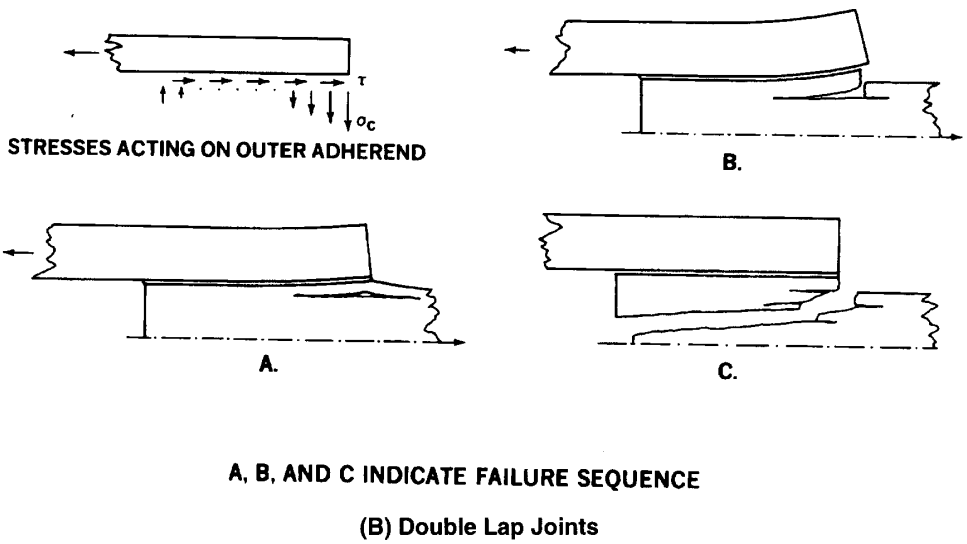

FIGURE 5.2.2.5(a) *Failure modes in composite adherends (References 5.2.1(w) and (x)).*

5.2.2.6 Effects of bond defects

Defects in adhesive joints which are of concern include surface preparation deficiencies, voids and porosity, and thickness variations in the bond layer.

Of the various defects which are of interest, surface preparation deficiencies are probably the greatest concern. These are particularly troublesome because there are no current nondestructive evaluation techniques which can detect low interfacial strength between the bond and the adherends. Most joint design principles are academic if good adhesion between the adherends and bond layer is poor. The principles for achieving this (Reference 5.2.2.6(a) - 5.2.2.6(c)) are well established for adherend and adhesive combinations of interest. Hart-Smith, Brown and Wong (Reference 5.2.2.6.(a)) give an account of the most crucial features of the surface preparation process. Results shown in Reference 5.2.2.6.(a) suggest that surface preparation which is limited to removal of the peel ply from the adherends may be suspect,

since some peel plies leave a residue on the bonding surfaces that makes adhesion poor. (However, some manufacturers have obtained satisfactory results from surface preparation consisting only of peel ply removal.) Low pressure grit blasting (Reference 5.2.2.6(b)) is preferable over hand sanding as a means of eliminating such residues and mechanically conditioning the bonding surfaces.

For joints which are designed to ensure that the adherends rather than the bond layer are the critical elements, tolerance to the presence of porosity and other types of defect is considerable (Reference 5.2.1(t)). Porosity (Reference 5.2.1(z)) is usually associated with over-thickened areas of the bond, which tend to occur away from the edges of the joint where most of the load transfer takes place, and thus is a relatively benign effect, especially if peel stresses are minimized by adherend tapering. Reference 5.2.1(z) indicates that in such cases, porosity can be represented by a modification of the assumed stress-strain properties of the adhesive as determined from thick-adherend tests, allowing a straightforward analysis of the effect of such porosity on joint strength as in the A4EI computer code. If peel stresses are significant, as in the case of over-thick adherends, porosity may grow catastrophically and lead to non-damage-tolerant joint performance.

In the case of bond thickness variations (Reference 5.2.1(aa)), these usually take place in the form of thinning due to excess resin bleed at the joint edges, leading to overstressing of the adhesive in the vicinity of the edges. Inside tapering of the adherends at the joint edges can be used to compensate for this condition; other compensating techniques are also discussed in Reference 5.2.1(aa). Bond thicknesses per se should be limited to ranges of 0.005-0.01 in. (0.12-0.24 mm) to prevent significant porosity from developing, although greater thicknesses may be acceptable if full periphery damming or high minimum viscosity paste adhesives are used. Common practice involves the use of film adhesives containing scrim cloth, some forms of which help to maintain bond thicknesses. It is also common practice to use mat carriers of chopped fibers to prevent a direct path for access by moisture to the interior of the bond.

5.2.2.7 Durability of adhesive joints

Two major considerations in the joint design philosophy of Hart-smith are: (1) either limiting the adherend thickness or making use of more sophisticated joint configurations such as scarf and step lap joints, to insure that adherend failure takes precedence over bond failure; (2) designing to minimize peel stresses, either by keeping the adherends excessively thin or, for intermediate adherend thicknesses, by tapering the adherends (see discussion of effects of adherend tapering, Section 5.2.2.2 and 5.2.3.5.). In addition, it is essential that good surface treatment practices (Section 5.2.2.6) be maintained to insure that the bond between the adhesive and adherends does not fail. When these conditions are met, reliable performance of the joint can be expected for the most part, except for environmental extremes, i.e., hot-wet conditions. The Hart-Smith approach focuses primarily on creep failure associated with slow cyclic loading (i.e., 1 cycle in several minutes to an hour) under hot wet conditions; this corresponds, for example, to cyclic pressurization of aircraft fuselages. In the PABST program, References 5.2.1(n)-(q) (see also Reference 5.2.1(v)), 18 thick adherend specimens, when tested at high cycling rates (30 Hz) were able to sustain more than 10 million loading cycles without damage, while tests conducted at the same loads at one cycle per hour produced failures within a few hundred cycles. Similar conclusions regarding the effects of cycling rate were presented in Reference 5.2.2.7(a). On the other hand, specimens representative of structural joints, which have a nonuniform shear stress distribution that peaks at the ends of the joint and is essentially zero in the middle (see Section 5.2.3.4.3 on ductile response of joints and Figure 5.2.3.4.3(b), part (B) in particular) are able to sustain hot-wet conditions even at low cycling rates if ℓ_e, the length of the region of elastic response in the bond layer, is sufficient. Based on experience of the PABST program, the Hart-Smith criterion for avoidance of creep failure requires that $\tau_b|_{min}$, the minimum shear stress along the bond length, be no greater than one tenth the yield stress of the adhesive. But the stress analysis for the elastic-plastic case (Section 5.2.3.4.3) using a bilinear adhesive response model leads to an expression for the minimum shear stress in double lap joints with identical adherends given by

$$\tau_b|_{min} = \frac{\tau_p}{\sinh \beta_{bd} \ell_e / 2 t_o} \qquad 5.2.2.7(a)$$

where t_p is the adhesive yield stress and β_{bd} is given by

$$\beta_{bd} = [2\, G_{b0}\, t_o / E_o t_b]^{1/2}$$

where G_{bo} is the initial shear modulus, t_b the bond thickness and E_0 and t_0 the adherend axial modulus and thickness. Because $\sinh(3) \approx 10$, this amounts to a requirement that $\beta_{bd}\ell_e / 2t_0$ be at least 3, i.e., that the elastic zone length be greater than $6t_0 / \beta_{bd}$. Since ℓ_e, is equivalent to the total overlap length, ℓ, minus twice the plastic zone length ℓ_p, then making use of the expression given in Section 5.2.3.4.3 for ℓ_p:

$$\ell_p = \left(\bar{\sigma}_x / 2\,\tau_p - 1/\beta_{bd}\right) t_o$$

where $\bar{\sigma}_x$ is the nominal adherend loading stress, the criterion for elastic zone length reduces to a criterion for total overlap length corresponding to a lower bound on ℓ which can be stated as

$$\ell \geq \left(\frac{\bar{\sigma}_x}{\tau_p} + \frac{4}{\beta_{bd}}\right) t_o \qquad \text{5.2.2.7(b)}$$

Equation 5.2.2.7(b) for the joint overlap length is the heart of the Hart-Smith approach to durability of bonded joints for cases where adherend failure is enforced over bond failure for static loading, and in which peel stresses are eliminated from the joint design. This type of requirement has been used in several contexts. In Reference 5.2.1(s) for example, it becomes part of the requirement for acceptable void volume, since in this case the voids, acting essentially as gaps in the bond layer, reduce the effective length of the overlap. The criterion has to be modified numerically for joints other than symmetric double lap joints with equal stiffness adherends and uniform thickness. For more sophisticated joint configurations such as step lap joints, the A4EI computer code provides for a step length requirement equivalent to that of Equation 5.2.2.7(b) for simple double lap joints.

In addition to creep failures under hot-wet conditions, the joint may fail due to cracking in the bond layer. Johnson and Mall (Reference 5.2.2.7(b)) presented the data in Figure 5.2.2.7(a) which shows the effect of adherend taper angle on development of cracks at ends of test specimens consisting of composite plates with bonded composite doublers, at 10^6 cycles of fatigue loading; here the open symbols represent the highest load levels that could be identified at which cracks failed to appear, while the solid symbols are for the lowest loads at which cracks just begin to appear. The predicted lines consist of calculated values of applied cyclic stress required to create a total strain energy release rate threshold value, G_{th}, at the debond tip for a given taper angle. The values of G_{th} for the two adhesives were experimentally determined on untapered specimens. The angle of taper at the end of the doubler was used to control the amount of peel stress present in the specimen for static loading. It is noted that even for taper angles as low as 5^o (left-most experimental points in Figure 5.2.2.7(a)) for which peel stresses are essentially nonexistent for static loading, crack initiation was observed when the alternating load was raised to a sufficient level. A number of factors need to be clarified before the implications of these results are clear. In particular, it is of interest to establish the occurrence of bond cracking at shorter cycling times, say less than $3x10^5$ cycles corresponding to expected lifetimes of typical aircraft. Effects of cycling rate and environmental exposure are also of interest. Nevertheless, the data presented in Reference 5.2.2.7(b) suggests the need for consideration of crack growth phenomena in bonded composite joints. Indeed, a major part of the technical effort that has been conducted on the subject of durability of adhesive joints (see Reference 5.2.2.7(c)-(i) for example) has been based on the application of fracture mechanics based concepts. The issue of whether or not a fracture mechanics approach is valid needs further examination. Apparently, no crack-like failures occurred in the PABST program, which was a metal bonding program, even when brittle adhesives were examined at low temperatures. The amount of effort which has been expended by a number of respected workers on development of energy release rate calculations for bonded joints certainly suggests that there is some justification for that approach, and the results obtained by Johnson and Mall appear to substantiate their need for composite joints in particular.

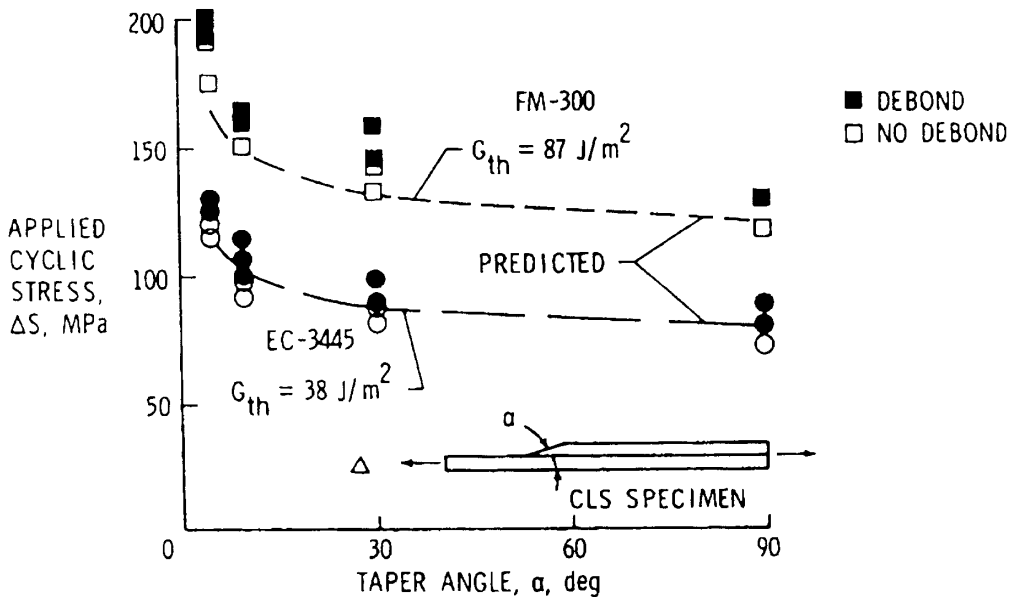

FIGURE 5.2.2.7(a) *Crack development in bonds of tapered composite doublers at 10^6 loading cycles.*

5.2.3 Stress and structural behavior of adhesive joints

5.2.3.1 General

Stress analyses of adhesive joints have ranged from very simplistic "P over A" formulations in which only average shear stresses in the bond layer are considered, to extremely elegant elasticity approaches that consider fine details, e.g., the calculation of stress singularities for application of fracture mechanics concepts. A compromise between these two extremes is desirable, since the adequacy of structural joints does not usually depend on a knowledge of details at the micromechanics level, but rather only at the scale of the bond thickness. Since practical considerations force bonded joints to incorporate adherends which are thin relative to their dimensions in the load direction, stress variations through the thickness of the adherend and the adhesive layer tend to be moderate. Such variations do tend to be more significant for polymer matrix composite adherends because of their relative softness with respect to transverse shear and thickness normal stresses. However, a considerable body of design procedure has been developed based on ignoring thickness-wise adherend stress variations. Such approaches involve using one-dimensional models in which only variations in the axial direction are accounted for. Accordingly, the bulk of the material to be covered in this chapter is based on simplified one-dimensional approaches characterized by the work of Hart-Smith, and emphasizes the principles which have been obtained from that type of effort, since it represents most of what has been successfully applied to actual joint design, especially in aircraft components. The Hart-Smith approach makes extensive use of closed form and classical series solutions since these are ideally suited for making parametric studies of joint designs. The most prominent of these have involved modification of Volkersen (Reference 5.2.1(a)) and Goland-Reissner (Reference 5.2.1(b)) solutions to deal with ductile response of adhesives in joints with uniform adherend thicknesses along their lengths, together with classical series expressions to deal with variable adherend thicknesses encountered with tapered adherends, and scarf joints. Simple lap joint solutions described below calculate shear stresses in the adhesive for various adherend stiffnesses and applied loadings. For the more practical step lap joints, the described expressions can be adapted to treat the joint as a series of separate joints each having uniform adherend thickness.

5.2.3.2 Adhesive shear stresses

Figure 5.2.3.2(a) shows a joint with ideally rigid adherends, in which neighboring points on the upper and lower adherends align vertically before sliding horizontally with respect to each other when the joint is loaded. This causes a displacement difference $\delta = u_U - u_L$ related to the bond layer shear strain by $\gamma_b = \delta / t_b$. The corresponding shear stress, τ_b, is given by $\tau_b = G_b \gamma_b$. The rigid adherend assumption implies that δ, γ_b and τ_b are uniform along the joint. Furthermore, the equilibrium relationship indicated in Figure 5.2.3.2(a) (C), which requires that the shear stress be related to the resultant distribution in the upper adherend by

$$d T_U / dx = \tau_b \qquad 5.2.3.2(a)$$

leads to a linear distribution of T_U and T_L (upper and lower adherend resultants) as well as the adherend axial stresses σ_{xU} and σ_{xL}, as indicated in Figure 5.2.3.2(b). These distributions are described by the following expressions:

$$T_U = \overline{T}\frac{x}{\ell} \quad ; \quad T_L = \overline{T}\left(1 - \frac{x}{\ell}\right) \quad \text{i.e.,} \quad \sigma_{xU} = \overline{\sigma}_{xU} = \overline{\sigma}_x \frac{x}{\ell} \quad ; \quad \sigma_{xL} = \overline{\sigma}_x\left(1 - \frac{x}{\ell}\right) \qquad 5.2.3.2(b)$$

where $\overline{\sigma}_x = \overline{T} / t$. In actual joints, adherend deformations will cause shear strain variations in the bond layer which are illustrated in Figure 5.2.3.2(c). For the case of a deformable upper adherend in combination with a rigid lower adherend shown in Figure 5.2.3.2(c) (A) (in practice, one for which $E_L t_L >> E_U t_U$), stretching elongations in the upper adherend lead to a shear strain increase at the right end of the bond layer. In the case shown in Figure 5.2.3.2(c) (B) in which the adherends are equally deformable, the bond shear strain increases at *both* ends of the joint. This is due to the increase in axial strain in whichever adherend is stressed (noting that only one adherend is under load) at a particular end of the joint. For both cases, the variation of shear strain in the bond results in an corresponding variation in shear stress which, when inserted into the equilibrium equation (Equation 5.2.3.2(a)) leads to a nonlinear variation of the bond and adherend stresses. The Volkersen shear lag analysis (Reference 5.2.1(a)) provides for calculations of these stresses for cases of deformable adherends.

Introducing the notation (see Figure 5.2.3.2(d))

E_U, E_L, t_U, and t_L = Young's moduli and thicknesses of upper and lower adherends
G_b and t_b = shear modulus and thickness of bond layer

with

$$B_U = E_U t_U, \quad B_L = E_L t_L$$

while, denoting $\overline{T}$ as the applied axial resultant with

$$\overline{\sigma}_{xU} = \overline{T} / t_U \quad \text{and} \quad \overline{\sigma}_{xKL} = \overline{T} / t_L$$

denoting the stresses in the two adherends at their loaded ends, together with

$$\beta = \left[G_b \frac{\bar{t}^2}{t_b}\left(\frac{1}{B_U} + \frac{1}{B_L}\right)\right]^{1/2} \quad ; \quad \bar{t} = \frac{t_U + t_L}{2} \quad ; \quad \rho_B = B_L / B_{LU} \qquad 5.2.3.2(c)$$

then the distribution for the axial stress in the upper adherend, $\sigma_{xU}(x)$, obtained from the Volkersen analysis is given by

$$\sigma_{xU} = \overline{\sigma}_{xU}\left\{\frac{B_U}{B_U + B_L}\left[1 + \frac{\sinh \beta(x - \ell)/\bar{t}}{\sinh \beta \ell / \bar{t}}\right] + \frac{B_U}{B_U + B_L}\frac{\sinh \beta x / \bar{t}}{\sinh \beta \ell / \bar{t}}\right\} \qquad 5.2.3.2(d)$$

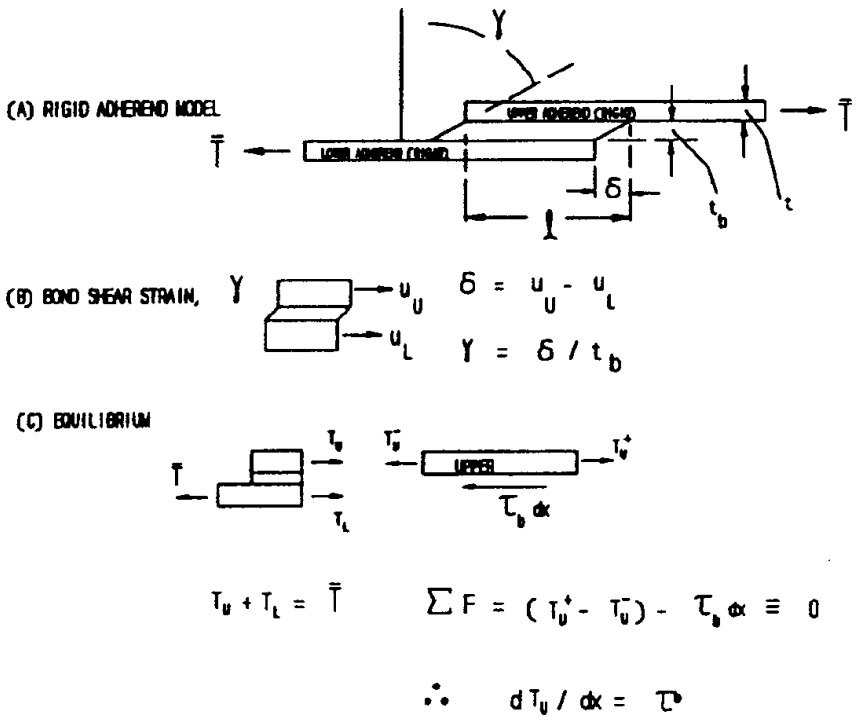

FIGURE 5.2.3.2(a) *Elementary joint analysis (Rigid adherend model).*

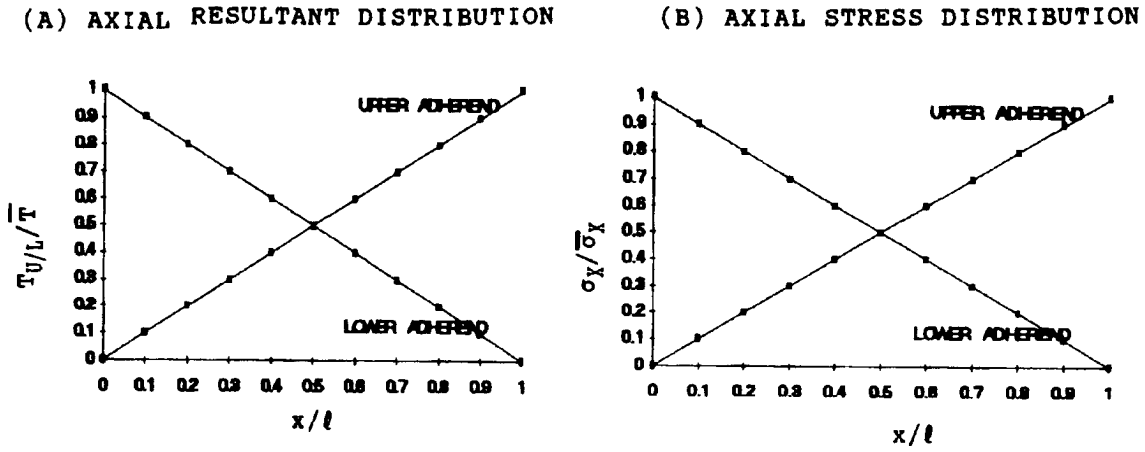

FIGURE 5.2.3.2(b) *Axial stresses in joint with rigid adherends.*

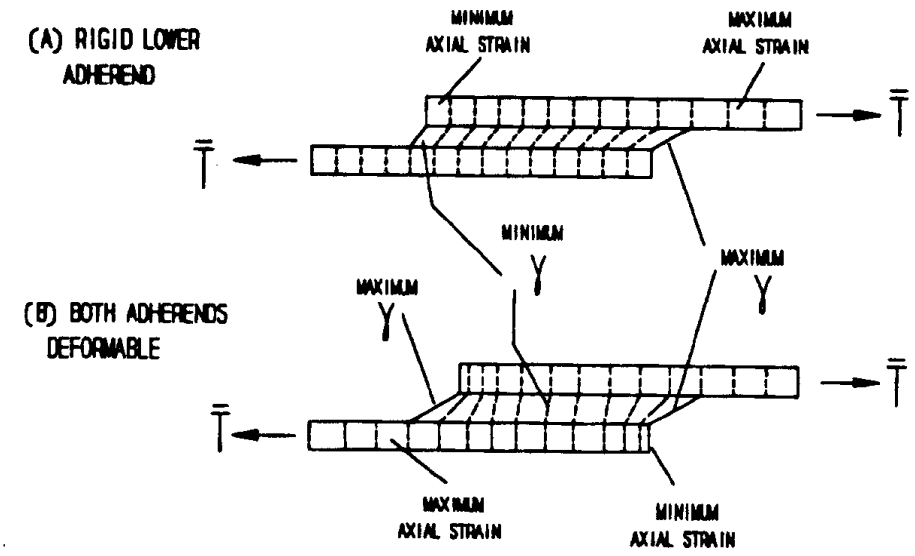

FIGURE 5.2.3.2(c) *Adherend deformations in idealized joints.*

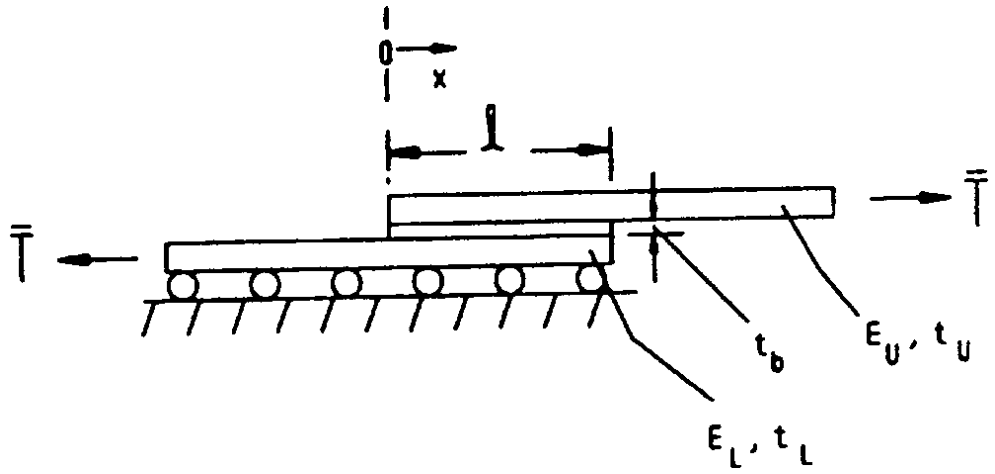

FIGURE 5.2.3.2(d) *Geometry for Volkersen solution.*

A comparison of the distribution of axial stresses together with the bond shear stresses for the case of equal thicknesses in the adherends but a relatively rigid lower adherend ($E_L = 10E_U$) vs. that of two equally deformable adherends ($E_L = E_U$) is given in Figure 5.2.3.2(e) below. The results in Figure 5.2.3.2(e) are for $t_U = t_L$ (so that the loading stresses at the adherend ends are equal) and for a bond shear modulus and thickness chosen so that $\beta = 0.387$ and $\ell / t = 20$ for both cases (giving $\beta\ell / t = 7.74$) and a nominal adher-

end stress $\sigma_{xU} = \sigma_{xL} = 10$ (in unspecified units). The maximum shear stresses are to a good approximation given by

$$x = 0 \quad \tau_b|_{max} \approx \bar{T}\frac{\beta}{\bar{t}}\frac{B_U}{B_U + B_L}$$
$$x = \ell \quad \tau_b|_{max} \approx \bar{T}\frac{\beta}{\bar{t}}\frac{B_L}{B_U + B_L} \qquad 5.2.3.2(e)$$

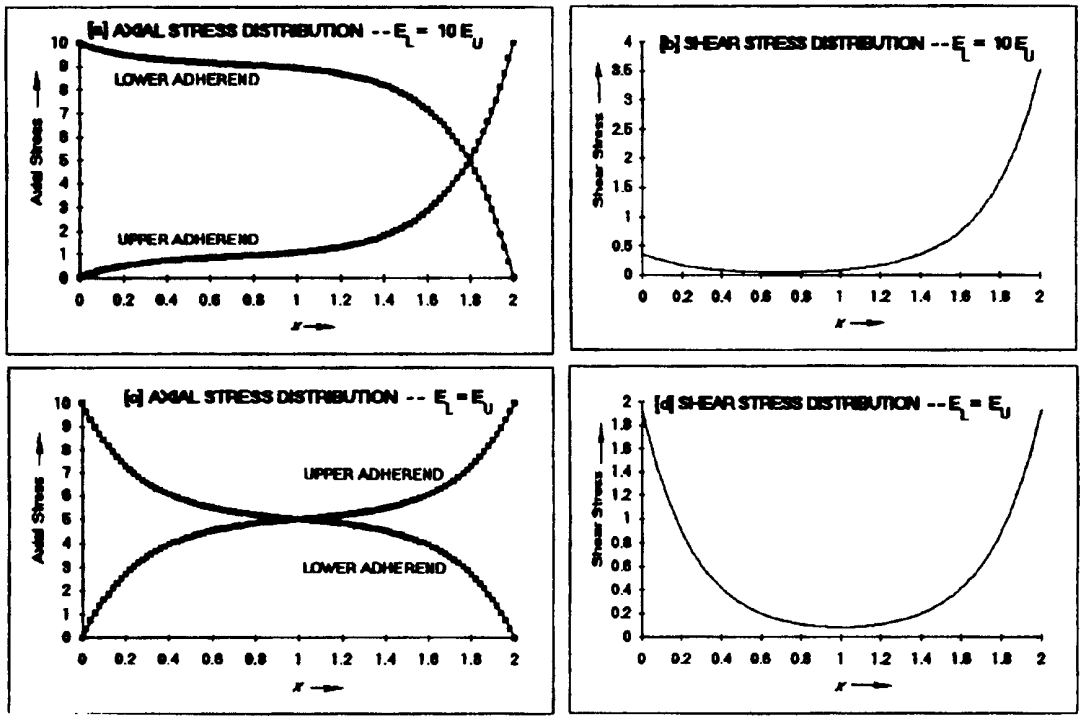

FIGURE 5.2.3.2(e) *Comparison of adherend stresses and bond shear stresses for $E_l = E_u$ vs. $E_l = 10E_u$, β and adherend thicknesses equal for both cases.*

Typical characteristics of the shear stress distributions are seen at the rights (parts (B) and (D)) in Figure 5.2.3.2(e) in the form of peaks at both ends for equally deformable adherends ($B_L = B_U$); for dissimilar adherends with the lower adherend more rigid ($B_L > B_U$), the higher peak stress obtained from Equation 5.2.3.2(e) occurs at the right end of the joint where $x = \ell$. Because of the shear strain characteristics which are illustrated in Figure 5.2.3.2(c) part (A), the higher peak generally occurs at the loaded end of the more flexible adherend.

As a practical consideration, we will be interested primarily in long joints for which $\beta\ell / t >> 1$. For these chases Equation 5.2.3.2(e) reduces to

$$\beta\ell / t >> 1$$
$$B_L >> B_U; \quad \tau_b|_{max} \approx \beta\bar{\sigma}_x; \quad B_L = B_U; \quad \tau_b|_{max} \approx \frac{1}{2}\beta\bar{\sigma}_x \qquad 5.2.3.2(f)$$

i.e., for long overlaps, the maximum shear stress for the rigid adherend case tends to be twice as great as that for the case of equally deformable adherends, again illustrating the adverse effect of adherend unbalance on shear stress peaks.

An additional point of interest is a typical feature of bonded joints illustrated in Figure 5.2.3.2(e) Part (d) which gives the shear stress distribution for equal adherend stiffness; namely, the fact that high adhesive shear stresses are concentrated near the ends of the joint. Much of the joint length is subjected to relatively low levels of shear stress, which implies in a sense that region of the joint is structurally inefficient since it doesn't provide much load transfer; however, the region of low stress helps to improve damage tolerance of the joint since defects such as voids, and weak bond strength may be tolerated in regions where the shear stresses are low, and in joints with long overlaps this may include most of the joint. As discussed in Section 5.2.2.7, Hart-Smith has suggested that when ductility and creep are taken into account, it is a good idea to have a minimum shear stress level no more than 10% of the yield strength of the adhesive, which requires the minimum value of overlap length given in Equation 5.2.2.7(a).

One other point of interest here is illustrated in Figure 5.2.3.2(f), which compares the behavior of the maximum shear stress in the bond with the average shear stress as a function of the dimensionless joint length, ℓ / t (for the particular case of equal adherend stiffnesses). The average shear stress in the bond line is always the same as the uniform shear stress in the hypothetical joint with rigid adherends discussed earlier, and from equilibrium is given by

$$\tau_{b|ave} = \frac{t}{\ell}\bar{\sigma}_x \quad (t_U = t_L \equiv t; \quad \bar{\sigma}_{xU} = \bar{\sigma}_{xL} \equiv \bar{\sigma}_x)$$

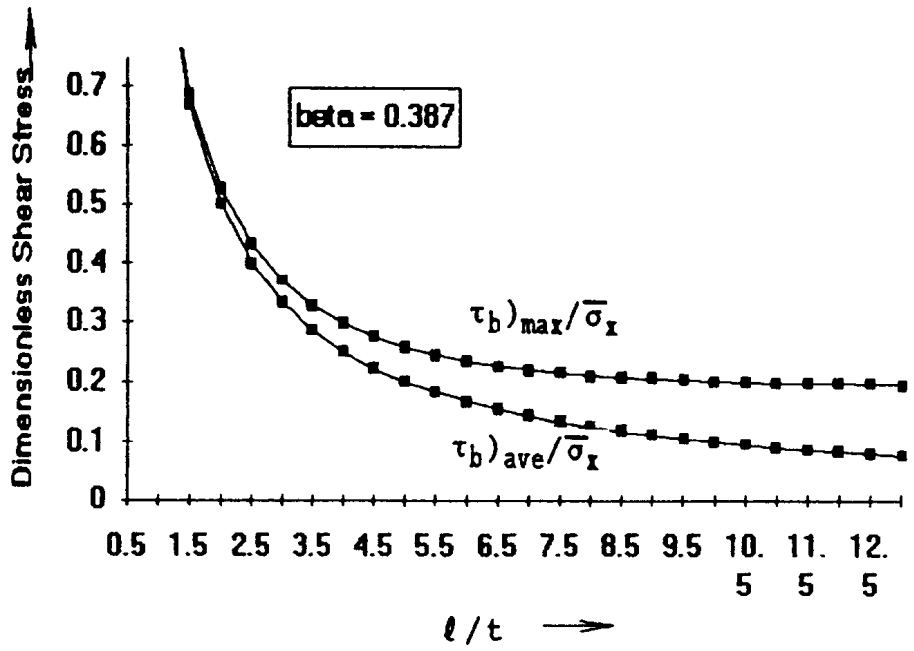

FIGURE 5.2.3.2(f) *Comparison of average and maximum shear stress vs.* ℓ / t.

The point illustrated here is the fact that although the *average* shear stress continuously decreases as the joint length increases, for the *maximum* shear stress which controls the load that can be applied without failure of the adhesive, there is a diminishing effect of the increased joint length when $\beta\ell / t$ gets much greater than about 2. Joint design has sometimes been considered only a matter of choosing the joint

length ℓ long enough to reduce the average shear stress given in Equation 5.2.3.2(f) to a value less than the allowable shear stress in the bond layer. Obviously if the adhesive responds elastically to failure and if the joint is long enough, the peak stresses at the joint ends will be much larger than the average stress, and joint failure will occur much below the load for which the average is equal to the allowable. On the other hand, ductility tends to dominate the behavior of structural adhesives, and design based on setting the peak stress equal to the allowable is too conservative. The effect of ductility which has already been discussed in Section 5.2.2.4 will be considered in the subsequent discussion.

5.2.3.3 Peel stresses

Peel stresses, i.e., through the thickness extensional stresses in the bond, are present because the load path in most adhesive joint geometries is eccentric. It is useful to compare the effect of peel stresses in single and double lap joints with uniform adherend thickness, since peel stresses are most severe for joints with uniform adherend thickness. The load path eccentricity in the single lap joint (Figure 5.2.3.3(a)) is relatively obvious due to the offset of the two adherends which leads to bending deflection as in Figure 5.2.3.3(a) (B). In the case of double lap joints, as exemplified by the configuration shown in Figure 5.2.3.3(b), the load path eccentricity is not as obvious, and there may be a tendency to assume that peel stresses are not present for this type of joint because, as a result of the lateral symmetry of such configurations, there is no overall bending deflection. However, a little reflection brings to mind the fact that while the load in the symmetric lap joint flows axially through the central adherend prior to reaching the overlap region, there it splits in two directions, flowing laterally through the action of bond shear stresses to the two outer adherends. Thus eccentricity of the load path is also present in this type of joint. As seen in Figure 5.2.3.3(b) (C), the shear force, designated as F_{SH}, which represents the accumulated effect of τ_b for one end of the joint, produces a component of the total moment about the neutral axis of the upper adherend equal to $F_{SH}t/2$. (Note that F_{SH} is equivalent to $\overline{T}/2$, since the shear stresses react this amount of load at each end.) The peel stresses, which are equivalent to the forces in the restraining springs shown in Figure 5.2.3.3(b) (B) and (C) have to be present to react the moment produced by the offset of F_{SH} about the neutral axis of the outer adherend. Peel stresses are highly objectionable. Later discussion will indicate that effects of ductility significantly reduce the tendency for failure associated with shear stresses in the adhesive. On the other hand, the adherends tend to prevent lateral contraction in the in-plane direction when the bond is strained in the thickness direction, which minimizes the availability of ductility effects that could provide the same reduction of adverse effects for the peel stresses. This is illustrated by what happens in the butt-tensile test shown in Figure 5.2.3.3(c) in which the two adherend surfaces adjacent to the bond are pulled away from each other uniformly. Here the shear stresses associated with yielding are restricted to a small region whose width is about equal to the thickness of the bond layer, near the outer edges of the system; in most of the bond, relatively little yielding can take place. For polymer matrix composite adherends, the adherends may fail at a lower peel stress level than that at which the bond fails, which makes the peel stresses even more undesirable.

It is important to understand that peel stresses are unavoidable in most bonded joint configurations. However, it will be seen that they can often be reduced to acceptable levels by selecting the adherend geometry appropriately.

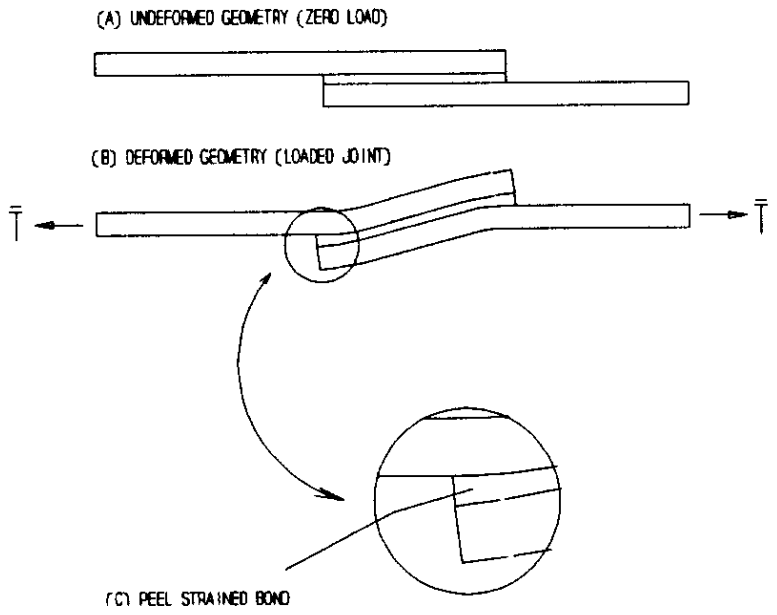

FIGURE 5.2.3.3(a) *Peel stress development in single lap joints.*

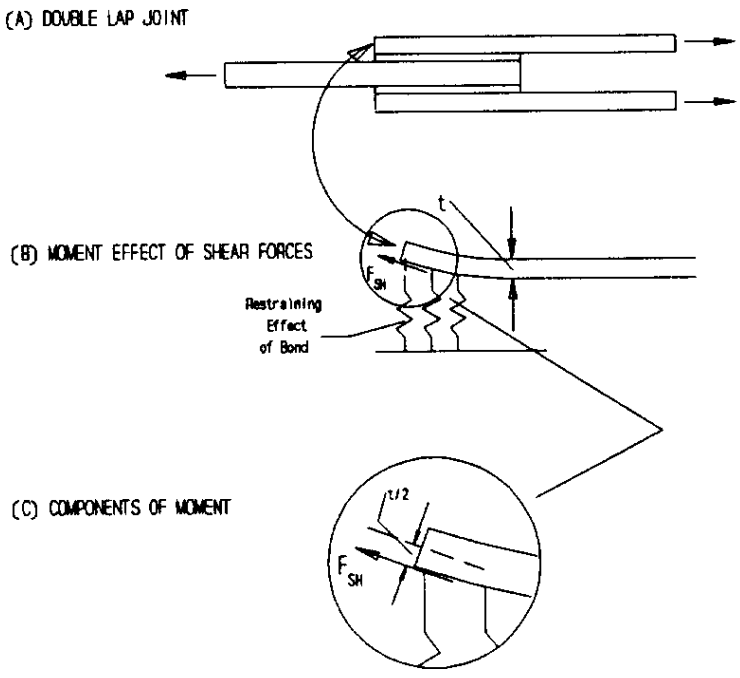

FIGURE 5.2.3.3(b) *Peel stress development in double lap joints.*

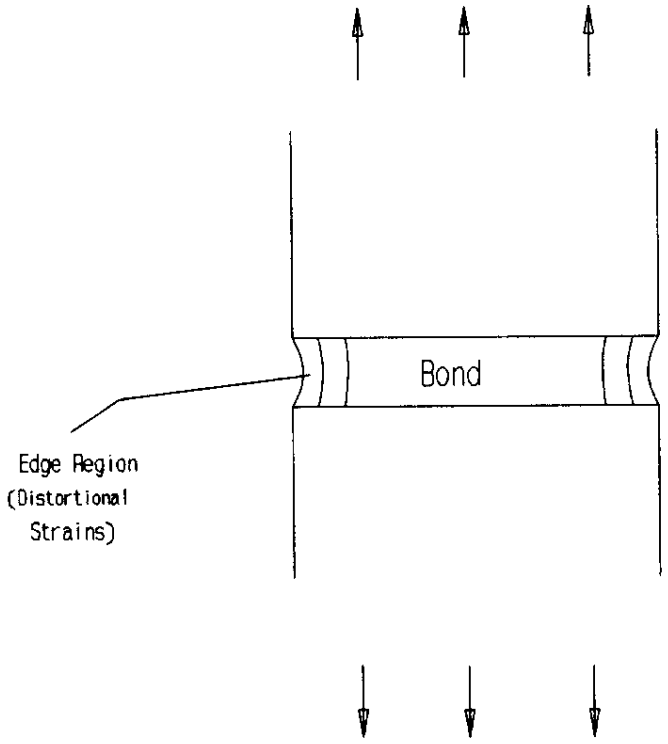

FIGURE 5.2.3.3(c) *Shear stresses near outer edges of butt tensile test.*

5.2.3.4 Single and double lap joints with uniform adherend thickness

In this section, joints with uniform adherend thickness are considered, since most important features of structural behavior of adhesive joints are illustrated by this case. Section 5.2.3.4.1 below deals with joint behavior under elastic response of the bond layer for structural loading alone. The effect of thermal stresses is treated in Section 5.2.3.4.2, while effects of adhesive ductility in the bond layer and transverse shear deformations in composite adherends are discussed in Sections 5.2.3.4.3 and 5.2.3.4.4, respectively.

5.2.3.4.1 Joint behavior with elastic response of the bond layer

Double lap joints will be considered first since they are somewhat simpler to discuss than single lap joints because of lateral deflection effects which occur in the latter. The following notation (see Figure 5.2.3.4.1(a)) is introduced for reference in the discussion:

E_i, t_i, E_o, t_o≡ axial moduli and thickness of inner and outer adherends
G_b, E_b, t_b≡ bond shear and peel modulus and thickness
σ_{xo}, σ_{xi} = axial adherend stresses ; T_o ≡σ_{xo} t_o, T≡ $\sigma_{xi}t_i$ - - axial resultants
$\tau_b\sigma_b$ - - bond shear and peel stress

5.2.3.4.1(a)

$$B_0 = t_0 E_0 \; ; B_i = t_i E_i \; ; \beta = \left[G_b \frac{\bar{t}^2}{t_b}\left(\frac{1}{B_0}+\frac{1}{B_i}\right)\right]^{1/2} \; ; \bar{t} = \frac{t_0 + t_i/2}{2} \; ; \rho_B = B_i / B_0$$

$$\hat{T}_{th} = \frac{B_0 B_i}{B_0 + B_i}(\alpha_0 - \alpha_i)\Delta T \; ; \bar{\sigma}_x = \bar{T}/\bar{t} \; ; \hat{\sigma}_{th} = \hat{T}_{th}/\bar{t}$$

(thermal expansion coefs α_0, α_i ; temperature change ΔT)

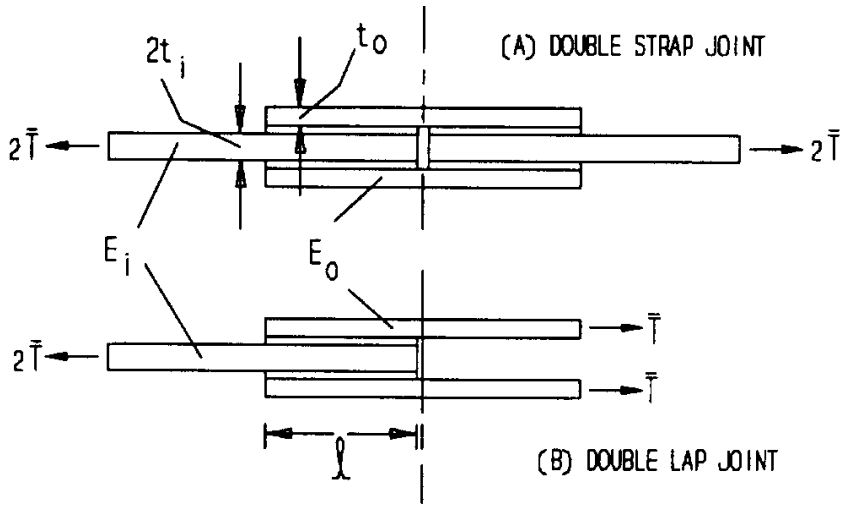

FIGURE 5.2.3.4.1(a) *Symmetric double strap/double lap joints.*

Shear and peel stresses in double lap joints with uniform adherend thickness, including thermal mismatch effects have been treated in a number of places, in particular by Hart-Smith in Reference 5.2.1(i). Using the notation of Equation 5.2.3.4.1(a), the structural response of the joint accounting for both shear and peel stresses in the bond layer can be modeled using a combination of the Volkersen shear lag analysis (Reference 5.2.1(a)) which gives

$$\frac{d^2 T_o}{dx^2} = \frac{G_b}{t_b}\left[\left(\frac{1}{B_o}+\frac{1}{B_i}\right)T_o - \frac{1}{B_i}\bar{T} + \Delta T(\alpha_o \alpha_i)\right] \qquad 5.2.3.4.1(b)$$

together with a beam-on-elastic foundation equation modified for the effect of tangential shear loading on the beam:

$$\frac{d^4\sigma_b}{dx^4} + 4\frac{\gamma_d^4}{t^4}\sigma_b = \frac{1}{2}t_o\frac{d\tau_b}{dx} \qquad 5.2.3.4.1(c)$$

$$\gamma_d = \left(3\frac{E_b}{E_o}\frac{t_o}{t_b}\right)^{1/4} \qquad 5.2.3.4.1(d)$$

Results from these equations will first be obtained in the absence of thermal stress effects. Modifying Equation 5.2.3.2a for the current notation gives

$$dT_o/dx = \tau_b \qquad 5.2.3.4.1(e)$$

so that solving Equation 5.2.3.4.1(b) under the end conditions $T_0|_x = 0;\ T_0|_{x=\ell} = \overline{T}$ and differentiating T_o with respect to x gives an expression for t_b.

$$\tau_b = \beta\overline{\sigma}_x\left[\frac{1}{1+\rho_B}\frac{\cosh\beta(x-\ell)/\bar{t}}{\sinh\beta\ell/\bar{t}} + \frac{\rho_B}{1+\rho_B}\frac{\cosh\beta x/\bar{t}}{\sinh\beta\ell/\bar{t}}\right] + \beta\hat{\sigma}_{th}\left[\frac{\cosh\beta x/\bar{t}}{\sinh\beta\ell/\bar{t}} - \frac{\cosh\beta(\ell-x)/\bar{t}}{\sinh\beta\ell/\bar{t}}\right] \qquad 5.2.3.4.1(f)$$

For the usual situation in which the overlap is long enough so that $\beta\ell/\bar{t}$ is greater than about 3, the peak shear stresses at the ends of the joint are given to a good approximation by

$$\mathbf{x = 0}\ ;\ \tau_{b0} = \beta\left(\frac{1}{1+\rho_B}\overline{\sigma}_x - -\hat{\sigma}_{th}\right);\ \mathbf{x} = \ell\ ;\ \tau_{b\ell} = \beta\left(\frac{\rho_B}{1+\rho_B}\overline{\sigma}_x + \hat{\sigma}_{th}\right) \qquad 5.2.3.4.1(g)$$

and for the special case of equal adherend stiffnesses (B_i=B_o) we have

$$\mathbf{B_i = B_o}\ (\rho_B = 1)\ ;\quad \tau_b|_{max} = \frac{1}{2}\beta\overline{\sigma}_x \pm \hat{\sigma}_{th} \qquad 5.2.3.4.1(h)$$

In the absence of thermal effects ($\overline{T}_{th} = 0$) and assuming that $B_i \geq B_o$, the maximum value of the shear stresses occurs at the ends of the joint as noted earlier (Figure 5.2.3.2(e)).

Once the shear stress distribution is determined, the peel stresses in the double lap joint are obtained from Equation 5.2.3.4.1(c). The solution to this equation depends (see Figure 5.2.3.4.1(a)) on whether a strap joint (outer adherend rotation restrained at $x = \ell$) or a lap joint (zero outer adherend moment at $x = \ell$) is considered. The exact form of the solution contains products of hyperbolic and trigonometric functions but for the practical situation of joints longer than one-or-two adherend thicknesses and $\beta << \gamma_d$, are given by

$$\textbf{Double lap joint}\quad \sigma_b \approx \sigma_b|_{max}\left(\cos\gamma_d\frac{x}{t}e^{-\gamma_d x/t} - \cos\gamma_d\frac{x-\ell}{t}e^{\gamma_d(x-\ell)/t}\right)$$

$$\textbf{Double strap joint}\quad \sigma_b \approx \sigma_b|_{max}\left(\cos\gamma_d\frac{x}{t}e^{-\gamma_d x/t} - \frac{1}{2}\cos\gamma_d\frac{x-\ell}{t}e^{\gamma_d(x-\ell)/t}\right) \qquad 5.2.3.4.1(i)$$

For the case of identical adherends, the maximum peel stresses, which occur at x=0, are given by

$$\sigma_b|_{max} = t_b)_{max}\gamma_d \qquad 5.2.3.4.1(j)$$

$$\tau_b|_{max} = \beta\overline{\sigma}_x/2 \quad \text{(identical adherends).}$$

Here $t_b|_{max}$ is taken to be the peak stress at *left* end of the joint. Note that the out-of-plane normal stresses are compressive at $x = \ell$ for $\overline{T} > 0$ (tensile load). For $\overline{T} < 0$ (compressive load), the situation would reverse for the double *lap* joint (Figure 5.2.3.4.1(a) part(B)), with the positive out-of-plane stresses occurring at the right end of the joint ($x = \ell$); in the case of the double *strap* joint (Figure 5.2.3.4.1(a) part(A)), the peak out-of-plane stresses would be compressive at the left end of the joint and would be zero at $x = \ell$ (i.e., where the gap between the inner adherends occurs), since the inner adherends would then butt against each other there and act as a continuous element.

Figure 5.2.3.4.1(b) compares the peel and shear stress distributions for $\hat{\sigma}_{th} = 0$, in a typical joint having balanced adherend stiffnesses (the sum of the outer adherend stiffnesses equal to the inner adherend stiffness) whose parameters are listed in Figure 5.2.3.4.1(b) part(B). The diagram at the top indicates the origin of x at the left end of the overlap. Note that the distribution of peel stresses is somewhat more concentrated near the ends than that of the shear stresses. Moreover, the peel stresses at the right end of the joint are negative. In addition, note that the compressive peak at the right end is half as great for the strap joint as for the lap joint, which is the result of the restraint of bending rotations in the strap joint for a gap which is essentially zero. If the loading were compressive rather than tensile, the inner adherends would bear directly on each other and no shear or peel stress peak would occur at the gap, whereas in the lap joint the right end of the overlap would experience the same peak stresses for compressive loading as the left end does for tensile loading.

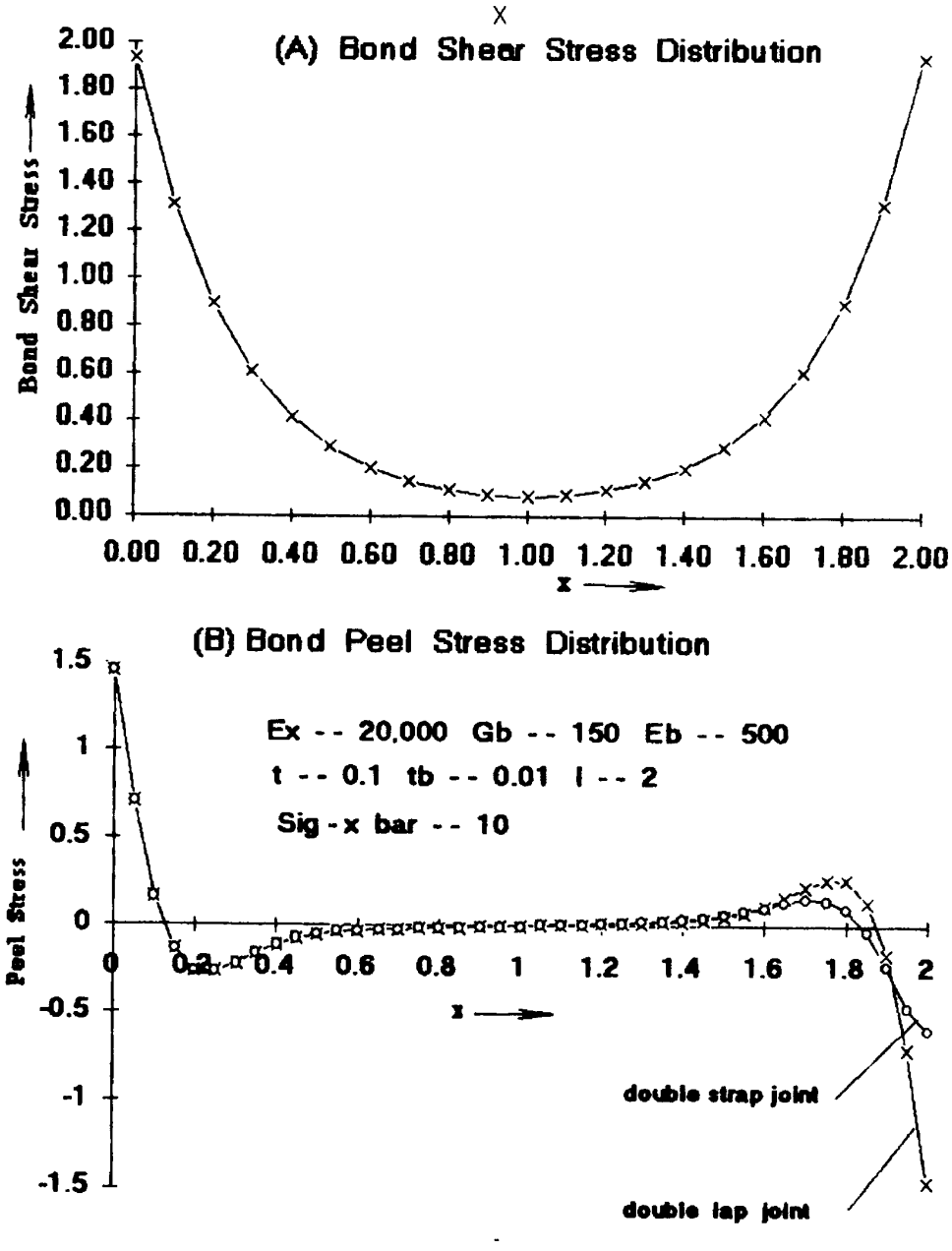

FIGURE 5.2.3.4.1(b) *Bond stresses in double lap/strap joints.*

The situation for the single lap joint (Figure 5.2.3.4.1(c)) is complicated by the effects of lateral deflection which are indicated in Figure 5.2.3.4.1(d). (The literature on the single lap joint is extensive. In addition to Reference 5.2.1(b), pertinent literature for the following discussion on the single lap joint is given in Reference 5.2.1(j), (ab) and (ac). See 5.2.1(ab) and (ac) for other sources.) The deflection effect is dependent on the joint load, given in terms of the quantity $U\ell / 2(8)^{1/2} t_U$ where

$$U = t_U \sqrt{\frac{\bar{T}}{D_U}} \equiv \sqrt{12 \frac{\bar{\sigma}_x}{E_U}} \quad ; \quad D_U = \frac{1}{12} E_U t_U^3 \qquad 5.2.3.4.1(k)$$

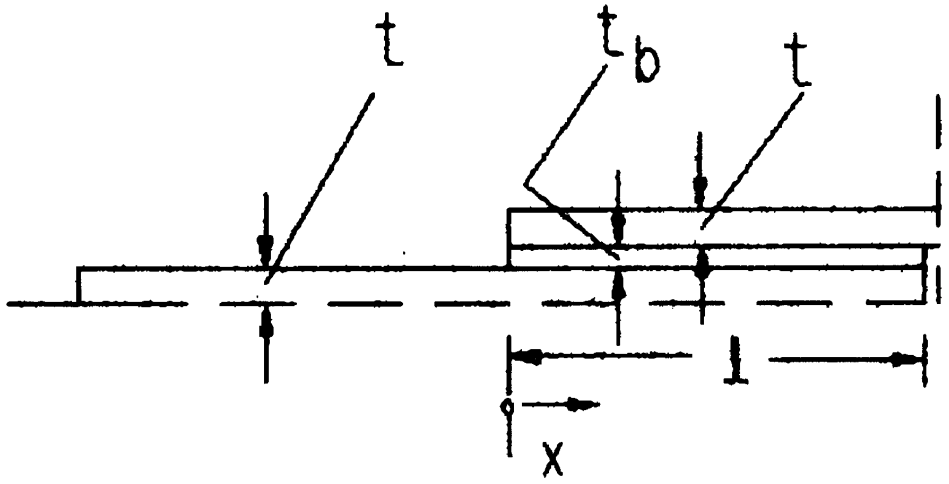

FIGURE 5.2.3.4.1(c) *Single lap joint geometry - A) Model.*

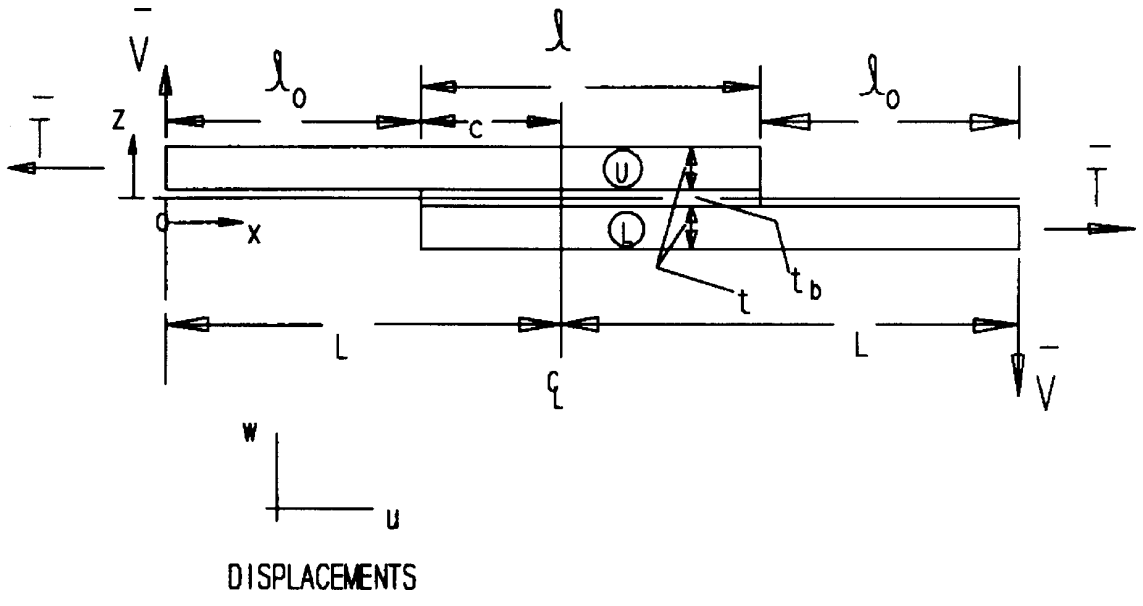

FIGURE 5.2.3.4.1(c) *Single lap joint geometry - B) Dimension.*

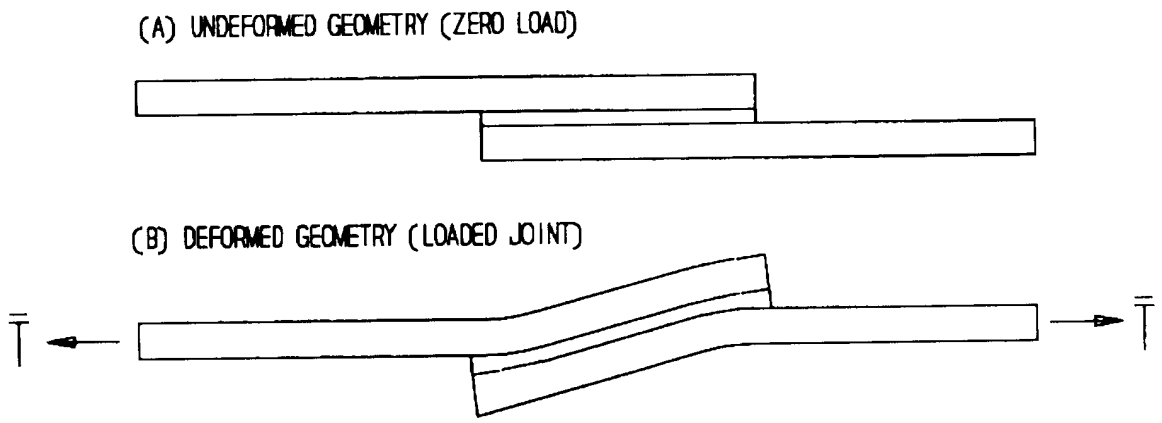

FIGURE 5.2.3.4.1(d) *Effects of bending deflections in single lap joints.*

The effects of lateral deflections on the bond stresses were first evaluated by Goland and Reissner (GR) in Reference 5.2.1(b). The GR analysis was restricted to the case of equal adherend thicknesses, so that t_U and t_L, which are equal, are denoted by t in the following. The lateral deflections can then be stated in terms of a dimensionless ratio, k, with respect to the adherend thickness, and are of the following form:

$$t_U = t_L \equiv t$$

$$x \le \ell_0 \;\; ; \;\; w = k\frac{t}{2}\frac{\sinh Ux/t}{\sinh U\ell_0/t} - \frac{1}{2}\frac{t+t_b}{L}x \qquad 5.2.3.4.1(l)$$

$$\ell_0 \le x \le \ell + \ell_0 \;\; ; \;\; w = W_2\frac{\sinh[U/\sqrt{8}(x-L)/t]}{\sinh[U\ell/\sqrt{8}t]} + \frac{t_U}{2} - \frac{1}{2}\frac{t+t_b}{L}x \;\; ; \;\; W_2 = \frac{t}{2}(1-k)$$

The GR expression given in Reference 5.2.1(b) for the parameter k has been reexamined by Hart-Smith (Reference 5.2.1(k)) and more recently by Oplinger (Reference 5.2.1(ab), (ac)); based on the discussion in Reference 5.2.1(ac), the GR expression appears to provide adequate accuracy unless the adherends are excessively thin, i.e., not much more than about twice the bond layer thickness, in which case the expressions given in Reference 5.2.1(ab) and (ac) provide corrections for the adherend thickness effects. A reasonable approximation to the expression for k given in Reference 5.2.1(ab) and (ac) is

$$k = \frac{\tanh U\lambda_o}{\tanh U\lambda_o + \sqrt{8}\,C_\rho \tanh(U\lambda/2C_\rho)} \qquad 5.2.3.4.1(m)$$

$$\text{where} \quad C_\rho = \left(1 + \frac{3}{2}\rho_t + \frac{3}{4}\rho_t^2\right)^{1/2} \;\; ; \;\; \rho_t = \frac{t_b}{t} \;\; ; \;\; \lambda = \ell/t \;\; ; \;\; \lambda_o = \ell_0/t \qquad 5.2.3.4.1(n)$$

The original GR expression for k is recovered if C_ρ is set equal to 1 corresponding to $t \gg t_b$ (i.e., relatively thick adherends) and $\tanh U\lambda_o$ is likewise set to 1 corresponding to very long outer adherend lengths. A plot of k vs. the adherend loading stress $\bar{\sigma}_x$ is given in Figure 5.2.3.4.1(e) for two different values of adherend thickness corresponding to bond thickness-to-adherend thickness ratios (ρ_t in Equation 5.2.3.4.1(m)) of 0.5 and 0.1. This plot suggests that k is fairly constant at a value of about 0.25 for a wide range of applied stress values once the initial drop has occurred. The effect of bond-to-adherend thickness ratio is not particularly great and can perhaps be ignored in many situations.

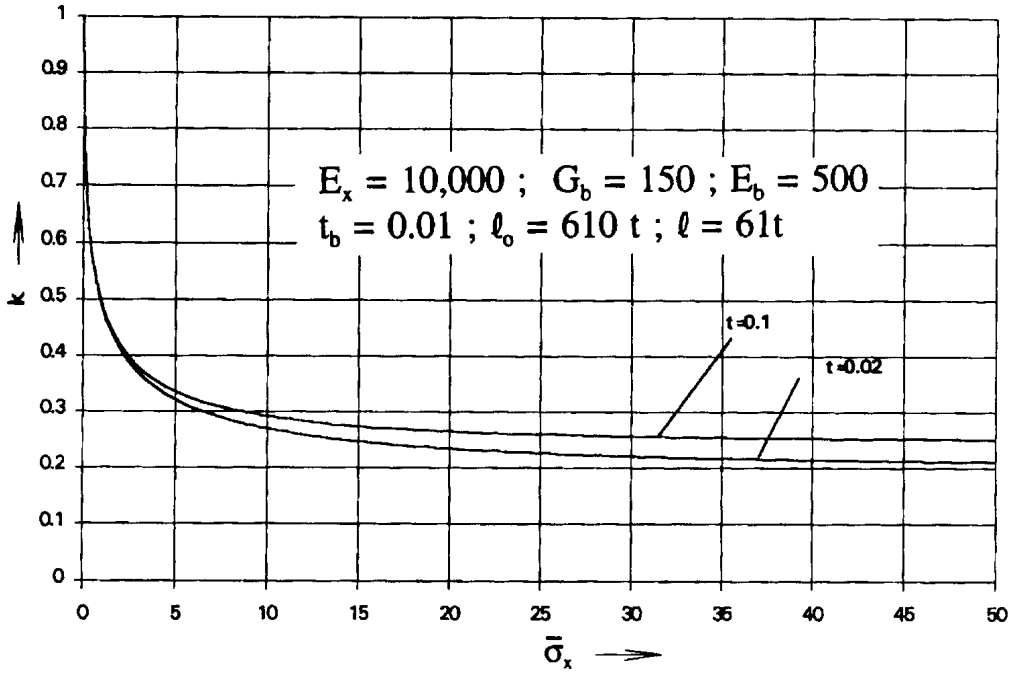

FIGURE 5.2.3.4.1(e) *k parameter vs. adherend loading stress.*

The lateral deflections of the joint have a significant influence on the stresses in the bond layer, which show this through the presence of the k parameter in expressions for them. The shear stress is given by

$$\tau_b = \bar{\sigma}_x \left\{ \frac{\beta_s}{4}(1+3k)\frac{\cosh\left[2\beta_s(x-L)/t\right]}{\sinh\left(\beta_s\gamma/t\right)} + \frac{3}{8\sqrt{8}}U(1=k)\frac{\cosh\left[U(x-L)/\sqrt{8}t\right]}{\sinh\left(u\gamma/2\sqrt{8}\right)} \right\} \qquad 5.2.3.4.1(o)$$

where $\beta_s \equiv \left(G_b t / E_x t_b\right)^{1/2}$, $E_x \equiv$ adherend axial modulus and U is given by Equation 5.2.3.4.1(k). Equation 5.2.3.4.1(o), which represents a slight modification of the GR expression, reduces to the latter for small values of $U\ell/t$. In addition, the peel stresses, for joints in which the overlap length is more than one or two adherend thicknesses (essentially the only case of practical interest) are given by

$$\sigma_b = \bar{\sigma}_x \frac{k\gamma_s}{2}$$

$$\left\{ \left[\gamma_s \left(\cos\gamma_s \frac{\ell_0+\ell-x}{t} + \sin\gamma_s \frac{\ell_0+\ell-x}{t} \right) + U\cos\gamma_s \frac{\ell_0+\ell-x}{t} \right] \exp\gamma_s \frac{x-\ell_0-\ell}{t} \right. \qquad 5.2.3.4.1(p)$$

$$\left. + \left[\gamma_s \left(\cos\gamma_s \frac{x-\ell_o}{t} - \sin\gamma_s \frac{x-\ell_o}{t} \right) + U\cos\gamma_s \frac{x-\ell_o}{t} \right] \exp\gamma_s \frac{\ell_o - x}{t} \right\}$$

where

$$\gamma_s = \left(6E_b t / E_x t_b\right)^{1/4} \qquad 5.2.3.4.1(q)$$

The maximum stresses in the bond layer are given by

$$\tau_{b|max} = \bar{\sigma}_x \left[\frac{\beta_s}{4}(1+3k)1/\tanh\beta_s\lambda + \frac{3}{8\sqrt{8}}U(1-k)/\tanh\left(\frac{U\lambda}{2\sqrt{8}}\right) \right] \qquad 5.2.3.4.1(r)$$

Maximum Bond Shear Stress Maximum bond peel stress:

$$\sigma_{b|max} = \bar{\sigma}_x \frac{k\gamma_s}{2}(\gamma_s + U) \qquad 5.2.3.4.1(s)$$

Figure 5.2.3.4.1(f) gives a comparison of the maximum bond stresses as functions of the loading stress $\bar{\sigma}_x$ for two different adherend thicknesses in a joint with a bond layer thickness of 0.01. It is interesting to note that the peel and shear stresses take on quite similar values. Since the maximum peel stress varies approximately as γ_s^2 according to Equation 5.2.3.4.1(s) (the contribution of U being relatively minor), the relationship for γ_s given in Equation 5.2.3.4.1(q) suggests that the peel stresses should be expected to vary as $(t/t_b)^{1/2}$, while the same variation is seen from Equation 5.2.3.4.1(r) for the maximum shear stresses since β_s also contains $(t/t_b)^{1/2}$ as a factor. Thus both stresses should vary with the thickness ratio by the same factor. The fact that they are numerically close together for all stresses is partly due to the effect of other parameters that enter into Equations 5.2.3.4.1(r) and 5.2.3.4.1(s) and partly due to the fact that k does not vary much with load for $\bar{\sigma}_x$ greater than 5. A slight nonlinearity can be observed in the curves of Figure 5.2.3.4.1(f) for the lower loading stresses.

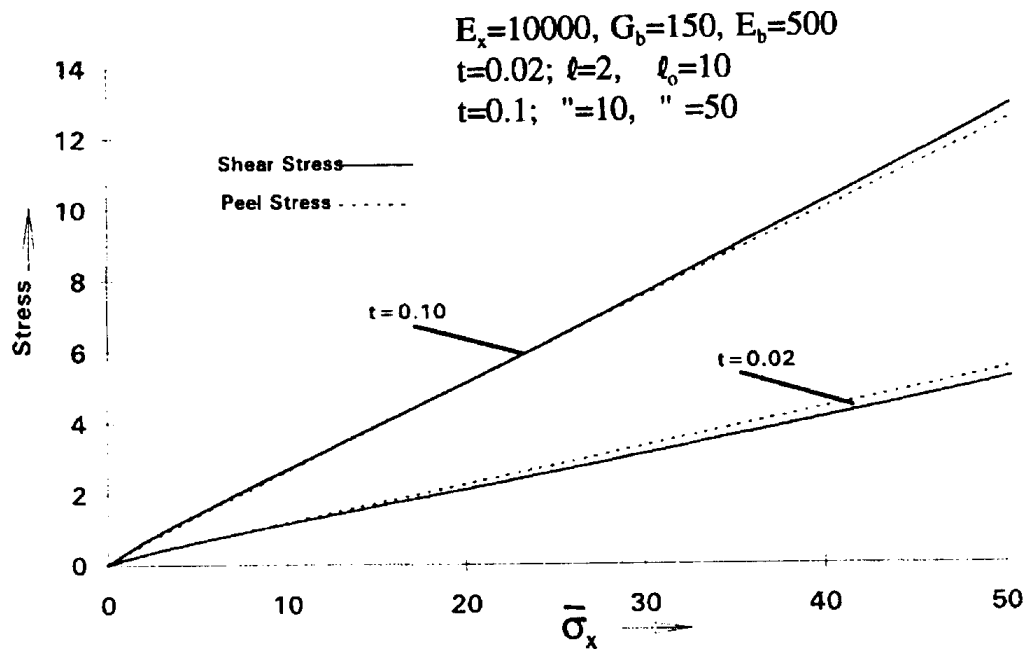

FIGURE 5.2.3.4.1(f) *Maximum bond stresses in single lap joint, bond thickness = 0.01.*

Figure 5.2.3.4.1(g) gives a comparison of maximum bond stresses in single and double lap joints for a fixed value of the loading stress $\bar{\sigma}_x$. For loading stresses above this value the bond stresses vary essentially in proportion to the load even in the single lap joint, as just discussed. The stresses are plotted in this figure as a function of adherend thickness with the adherend axial modulus as a parameter. The trend discussed in Section 5.2.2 toward higher bond stresses and therefore a greater tendency toward bond failure with increasing adherend thickness is clearly born out in these curves. Note also that reduction of the adherend modulus tends to aggravate the bond stresses. In addition, it is apparent that there is considerable separation between the peel and shear stresses in the case of the double lap joint, the peel stresses for this case being smaller. This reflects the fact that the peel stresses vary linearly as γ_d defined in Equation 5.2.3.4.1(d) and therefore vary as $(t/t_b)^{1/4}$ rather than as $(t/t_b)^{1/2}$ as in the single lap case. Thus peel stresses for double lap joints are not as much of a factor in joint failure as they are in single lap joints, although they are still large enough relative to the shear stresses that they can not be ignored.

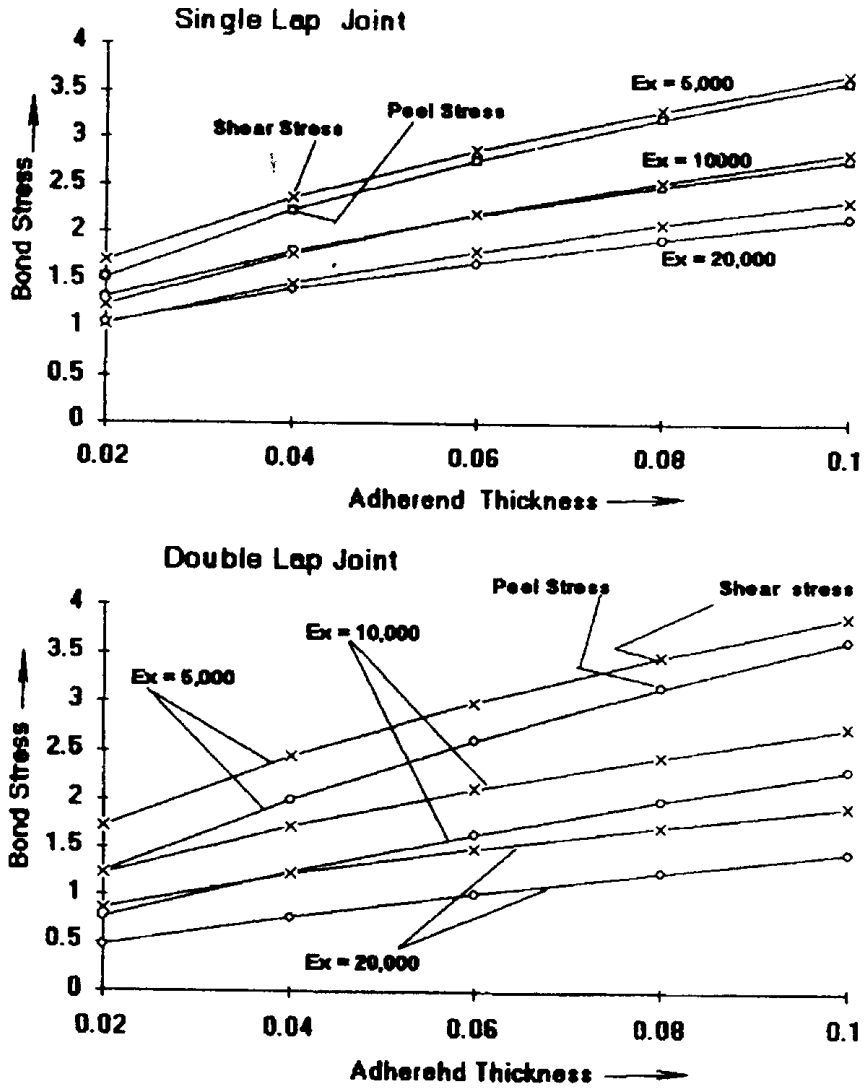

FIGURE 5.2.3.4.1(g) *Maximum bond stresses in single and double lap joints, fixed* $\bar{\sigma}_x = 10$.

Failure characteristics of single and double lap joints were discussed in Section 5.2.2.5. If the adherends are thin enough, failure in double lap joints should be in the form of adherend axial (tensile or compressive) failure. For single lap joints, adherend bending stresses are significant at the ends of the overlap because of the deflections indicated in Figure 5.2.3.4.1(d) part(D); using standard beam formulas, the maximum axial stress for combined bending and stretching (the latter stress corresponding to the single lap joint in tension loading) for the bending deflection given in Equation 5.2.3.4.1(l) can be expressed as

$$\sigma_x|_{max} = \bar{\sigma}_x\left(1 + 3\left(1 + t_b / t\right)k\right) \qquad 5.2.3.4.1(t)$$

The maximum adherend axial stress is largest for adherends which are particularly thin with respect to the bond thickness; these will be prone to brittle bending failures for composite adherends or to yielding associated with bending for metal adherends. Hart-Smith discusses difficulties with the use of standard single lap shear test specimens in Reference 5.2.1(v). The problem is that adherend bending failures rather than bond failures are likely to occur with such specimens and the test results obtained in these cases tend to be irrelevant and misleading. One additional characteristic difference between single and double lap joints should be discussed. The effect of lateral deflections on single lap joint performance are felt for a long distance along the joint compared with those of the shear and peel stresses. Figure 5.2.3.4.1(h) shows that for a joint with an adherend thickness of 0.1 inch (2.54 mm) and a loading stress of 10 ksi (70 MPa), the bond stresses do not reduce to their minimum values until the overlap length reaches about 40-50 adherend thicknesses, i.e., 4-5 inch (100-120 mm). Double lap joints also require some minimum length before stresses settle out as a function of overlap length, but in this case the stresses reach minimum values in much shorter lengths, on the order of 5 to 10 adherend thicknesses, in the present case amounting to 0.5 to 1 inch (13 to 25 mm).

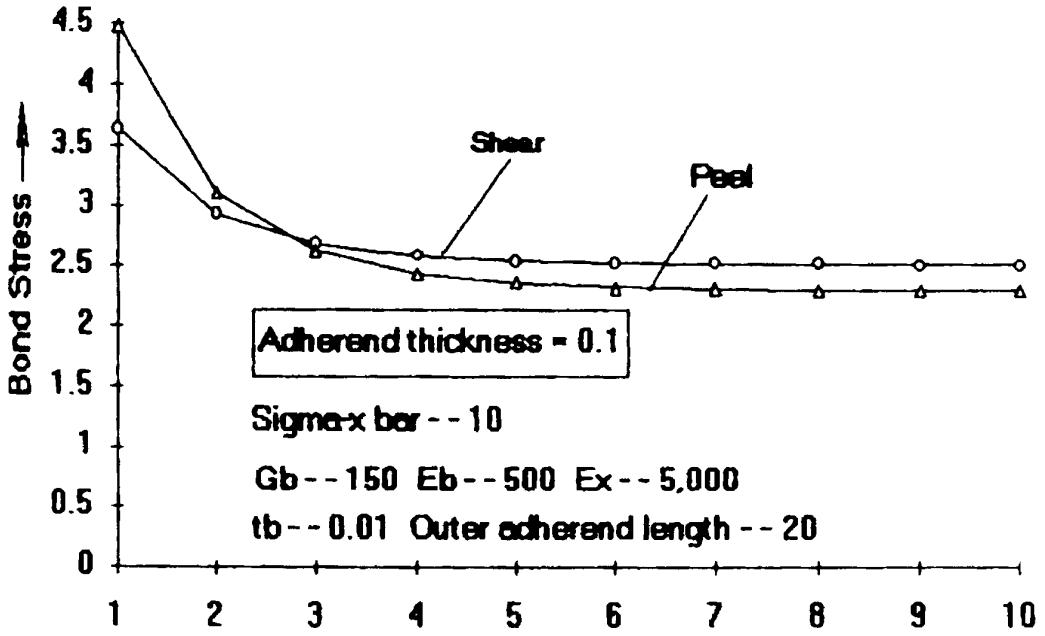

FIGURE 5.2.3.4.1(h) *Effects of overlap length in single lap joints.*

5.2.3.4.2 Thermal stress effects

Thermal stresses are a concern in joints with adherends having dissimilar thermal expansion coefficients. Thermal stresses in bond layers of double lap joints can be determined from the expressions given in Equations 5.2.3.5.1(a)-(e). (These calculations are all based and assumed elastic response of the adhesive. Hart-Smith (References 5.2.1(i)-(l)) provides corrections for ductile response in the presence of thermal effects.) Thermal effects for one specific combination of composite and metal adherends are considered in Figure 5.2.3.4.2(a) while peak peel and shear stresses for various combinations of metal and composite adherends (see Tables 5.2.3.4.2(a) and (b) for mechanical properties) are shown in Table 5.2.3.4.2(c).

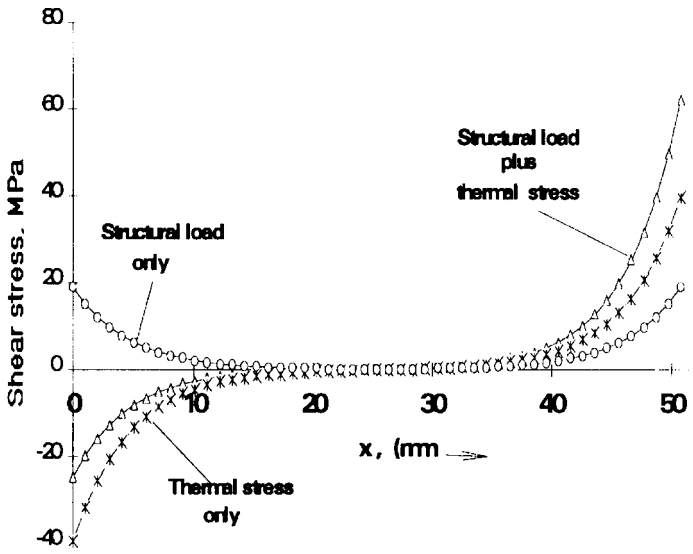

Outer adherend -- 0/90 carbon epoxy; Inner adherend -- aluminum
$E_i = E_o = 68.97$ GPa (10,000 ksi) ; $G_b = 1.04$ GPa (150 ksi)
$t_i = t_o = 2.54$ mm (0.1 in) ; $t_b = 0.254$ mm (0.01 in)
$\alpha_i = 23.4 \times 10^{-6}$ °C^{-1} (13×10^{-6} °F^{-1}) ; $\alpha_o = 1.8 \times 10^{-6}$ °C^{-1} (1×10^{-6} °F^{-1})
Cure temp. 121.1 °C (250° F) ; Application temp. 23.9°C (75°F)
Loading stress 68.97 MPa (10 ksi)

FIGURE 5.2.3.4.2(a) *Thermal shear stresses in double lap joint.*

TABLE 5.2.3.4.2(a) *Generic mechanical properties of composites (Reference 5.2.3.4.2(a))*.

	Unidirectional Lamina					0/90 Laminate	
Composite	E_L, Msi (GPa)	E_T, Msi (GPa)	ν_{LT}	α_L 10-6/F° (10^{-6}/C°)	α_T 10-6/F° (10^{-6}/C°)	E_x Msi (GPa)	α_x 10-6/F° (10^{-6}/C°)
Boron/ epoxy	29.1 (201)	2.91 (20.1)	0.17	6.50 (11.7)	16.9 (30.4)	16.5 (114)	4.8 (8.6)
S-glass/ epoxy	8.80 (60.7)	3.60 (24.8)	0.23	2.10 (3.78)	4.28 (16.7)	6.34 (43.7)	4.40 (7.92)
Carbon/ epoxy	20.0 (138)	1.00 (6.90)	0.25	0.40 (0.72)	16.4 (29.5)	10.5 (72.6)	1.30 (2.34)

Figure 5.2.3.4.2(a) illustrates the effect of thermal stresses in an aluminum - 0/90° carbon/epoxy joint. The stresses due to thermal mismatch between the aluminum and composite arise if the cure temperature of the bond is substantially different from the temperature at which the joint is used. The case considered here represents a 250°F (121°C) cure temperature for the adhesive and a room temperature application, a temperature difference of -175°F (-79°C), which (see Tables 5.2.3.4.2(a) and (b)) would result in a strain difference of 0.002 between the aluminum and composite if no bond were present. (The material combi-

nation considered here, aluminum and carbon/epoxy, represents the greatest extreme in terms of thermal mismatch between materials normally encountered in joints in composite structures.)

TABLE 5.2.3.4.2(b) *Generic metal properties (Reference 5.2.3.4.2(b)).*

	Ti-6-Al-4-4V	1025 Steel	2014 Aluminum
Young's Modulus, Msi (GPa)	16.0 (110.3)	30.0 (206.9)	10.0 (69.0)
Poisson Ratio	0.3	0.3	0.3
α, 10-6/F° (10^{-6}/C°)	4.90 (8.82)	5.70 (10.3)	13.0 (23.4)

TABLE 5.2.3.4.2(c) *Bond layer thermal stress in double lap joints (0/90 composite outer adherend, metal inner adherend)*

	Boron/epoxy	Glass/epoxy	Carbon/epoxy
TITANIUM			
shear stress – ksi	0.061	0.338	2.27
MPa	0.419	2.33	15.64
peel stress – ksi	-0.067	-0.541	-2.817
MPa	-0.465	-3.73	-19.43
STEEL			
shear stress – ksi	0.789	1.16	3.80
MPa	5.44	7.99	26.22
peel stress – ksi	-0.914	-2.17	-5.52
MPa	-6.30	-15.0	-38.1
peel stress – ksi	-3.54	-5.82	-6.47
MPa	-24.4	-40.1	-44.6
ALUMINUM			
shear stress – ksi	4.02	4.08	5.86
MPa	27.7	28.2	40.47
t_i -- 0.2 inch (5.08 mm); t_o adjusted for equal adherend stiffnesses; t_b= .01 inch (0.253 mm) Adhesive properties: shear modulus -- 150 ksi (1.03 GPa) peel modulus -- 500 ksi (3.49 GPa) Cure temperature 250°F (121°C); Application temperature 75°F (24°C)			

Figure 5.2.3.4.2(a) demonstrates how the thermal stresses combine with the stresses due to structural load to determine the actual stress distribution in the adhesive. The thermal stresses in themselves develop an appreciable fraction of the ultimate stress in the adhesive, and although they oppose the stresses due to structural loading at the left end of the joint, they add at the right end and give a total shear stress that is somewhat beyond the yield stress of typical adhesives, even with as small a structural loading stress as 10 ksi (69 MPa). Similar effects occur with the peel stresses, although the peel stresses due to thermal mismatch alone have the same sign at both ends of the joint; with a composite outer adherend,

the thermally induced peel stresses are negative, which is beneficial to joint performance. For joints with an aluminum inner adherend, the difference in thermal expansion between the adherends is relatively large, giving considerably higher thermal stresses for the most part. In addition, carbon/epoxy has a particularly low thermal expansion, so that carbon/epoxy adherends in combination with metals tend to produce higher thermal stresses with than other material combinations do. Note, for example, that boron/epoxy in combination with titanium gives particularly small thermal stresses because of similarity of the thermal expansion coefficients shown in Tables 5.2.3.4.2(a) and 5.2.3.4.2(b) for these materials. As discussed earlier, the "peel" stresses shown in Table 5.2.3.4.2(c) are all negative (i.e. compressive) because of the location of the composite on the outside of the joint, although the shear stresses are unaffected by this aspect of the joint. Composite repair patches on aluminum aircraft structure benefit from this type of behavior, in that peel stresses are not a problem for temperatures below the cure temperature. Placing the metal rather than the composite on the outside of a double lap joint would reverse the signs of the peel stresses, making them tensile and aggravating the effects of differential thermal expansion of the adherends.

5.2.3.4.3 Effect of ductility on joint stresses

Ductility of typical structural adhesives was discussed in Section 5.2.2.4 and illustrated in Figures 5.2.2.4(a) and 5.2.2.4(b) taken from Reference 5.2.2.4(a). Similar curves can be found in other sources such as Reference 5.2.2.4(b). Temperature and strain rate dependence of the stress-strain characteristics are important considerations; these are also addressed in Reference 5.2.2.7(a). Even for the less ductile materials such as FM400 (Figure 5.2.2.4(a) part(B)), ductility has a pronounced influence on mechanical response of bonded joints, and restricting the design to elastic response deprives the application of a significant amount of additional structural capability. In general, the maximum elastic strain of the adhesive provides to the limit load capability of the joint, while the maximum strain in the ductile part of the stress-strain curve provides the margin of ultimate load over limit load.

The work of Hart-Smith (Reference 5.2.1(i)-(q)) emphasized the importance of ductile adhesive response and introduced the relationship between the strain energy to failure of the adhesive and the load capacity of the joint. As a means of simplifying the stress analysis of the joint in the presence of ductile adhesive response, Hart-Smith showed that any bilinear stress-strain curve which has the same ultimate shear strain and maximum strain energy as that of the actual stress-strain curve will produce the same total load in the joint. Figure 5.2.3.4.3(a) (Reference 5.2.2.4(a)) gives an example of the method for fitting a bilinear curve to the actual stress-strain curve of the adhesive in shear. With the strain energy of the adhesive given by

$$SE = \tau_p \gamma_{max} - \tau_p^2 / 2G_{b0} \qquad 5.2.3.4.3(a)$$

where G_{b0}, γ_{max} and SE are the initial modulus of the stress-strain curve, the maximum strain and the strain energy of the adhesive at γ_{max}, respectively, then the equivalent bilinear curve consists of an initial straight line of slope G_{b0} together with a horizontal part at an abscissa which can be obtained by solving for τ_p from Equation (5.2.3.4.3a), using the expression

$$\tau_p = G_{b0}\gamma_{max} - \sqrt{(G_{b0}\gamma_{max})^2 - 2G_{b0}SE} \qquad 5.2.3.4.3(b)$$

Hart-Smith has also used an equivalent bilinear representation in which the horizontal part of the curve is set equal to τ_{max}, the maximum shear stress of the actual stress strain curve, and the initial modulus G_{bo} adjusted to give the strain energy match, using the expression

$$G_{bo} = \tau_{max}^2 / 2(\tau_{max}\gamma_{max} - SE) \qquad 5.2.3.4.3(c)$$

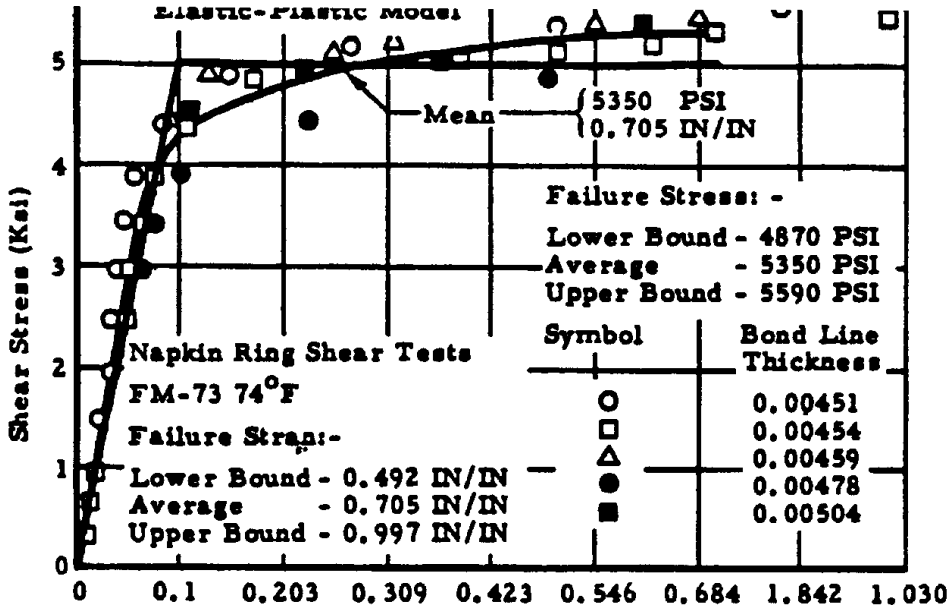

FIGURE 5.2.3.4.3(a) *Elastic-perfectly plastic adhesive response model* ***(FM73)*** *(Reference 5.2.2.4(a)).*

which is also obtained from Equation (5.2.3.4.3a) when τ_{max} is substituted for τ_p. In either case the use of a bilinear representation of the stress-strain curve for the response of the adhesive in shear makes it straightforward to obtain one dimensional stress distributions in various types of joint geometry with adhesive ductility accounted for; Reference 5.2.1(i)-(l) gave solutions for single and double lap joints with uniform and tapered adherends, as well as more sophisticated joint designs such as scarf and step lap geometries. These have been subsequently incorporated in the "A4Ex" series of computer programs (Reference 5.2.1(s)) mentioned previously in Section 5.2.2.4. Figure 5.2.3.4.3(b) shows the application of the bilinear stress-strain curve approximation to a symmetric double lap joint with equal adherend stiffnesses. Part (A) of Figure 5.2.3.4.3(b) gives the distribution of upper adherend axial stress resultant while part (B) gives the shear stress distribution in the bond layer. The linear portion at the ends of the resultant distribution in part (A) corresponds to the ends of the shear stress distribution in part (B) where the shear stress is a constant because of the plateau in the bilinear representation of the stress-strain curve. Following the analysis developed by Hart-Smith, the lengths of the plastic zones designated in Figure 5.2.3.4.3(b) part (B) as ℓ_p are given by

$$\ell_p = \left(\bar{\sigma}_x / 2\tau_p - 1/\beta_{bd}\right) t_o \quad ; \quad \beta_{bd} = \left[2 G_{b0} t_o / E_o t_b\right]^{1/2} \qquad 5.2.3.4.3(d)$$

Here β_{bd} (subscript "bd" denoting balanced double lap) is equivalent to β given in Equation (5.2.3.4.1a) when the latter is specialized for the case of equal-stiffness adherends, while $\bar{\sigma}_x$ is the nominal loading stress at either end of the overlap. The expression for ℓ_p given in Equation (5.2.3.4.3d) is valid only if greater than 0, of course, negative values of plastic zone length not having any meaning. As a result, if $\beta_{bd}\bar{\sigma}_x / 2 < \tau_p$, no plastic zone is present and the behavior of the joint can be considered to be purely elastic. The maximum value of $\bar{\sigma}_x$ for this case can be expressed by inverting the shear stress expression in Equation 5.2.3.4.1(f), for the case of equal adherend stiffnesses, and setting $\tau_b|_{max}$ to τ_p. For the case of $\beta_{bd}\bar{\sigma}_x / 2 \geq \tau_p$ which corresponds to ductile response of the adhesive, the Hart-Smith analysis given in Reference 5.2.1(i) provides the required expression for $\bar{\sigma}_x$. The two cases are summarized as follows:

$\beta_{bd}\overline{\sigma}_x / 2 < \tau_p$ (elastic response):

$$\overline{\sigma}_x|_{max} = 2\tau_p / \beta_{bd} = \sigma_e \qquad \text{5.2.3.4.3(e)}$$

$\beta_{bd}\overline{\sigma}_x / 2 \geq \tau_p$ (ductile response):

$$\overline{\sigma}_x|_{max} = \frac{2}{\beta_{bd}}\tau_p\sqrt{2\frac{G_{b0}\gamma_{max}}{\tau_p} - 1} \equiv \sigma_e\sqrt{2\frac{G_{b0}\gamma_{max}}{\tau_p} - 1} \qquad \text{5.2.3.4.3(f)}$$

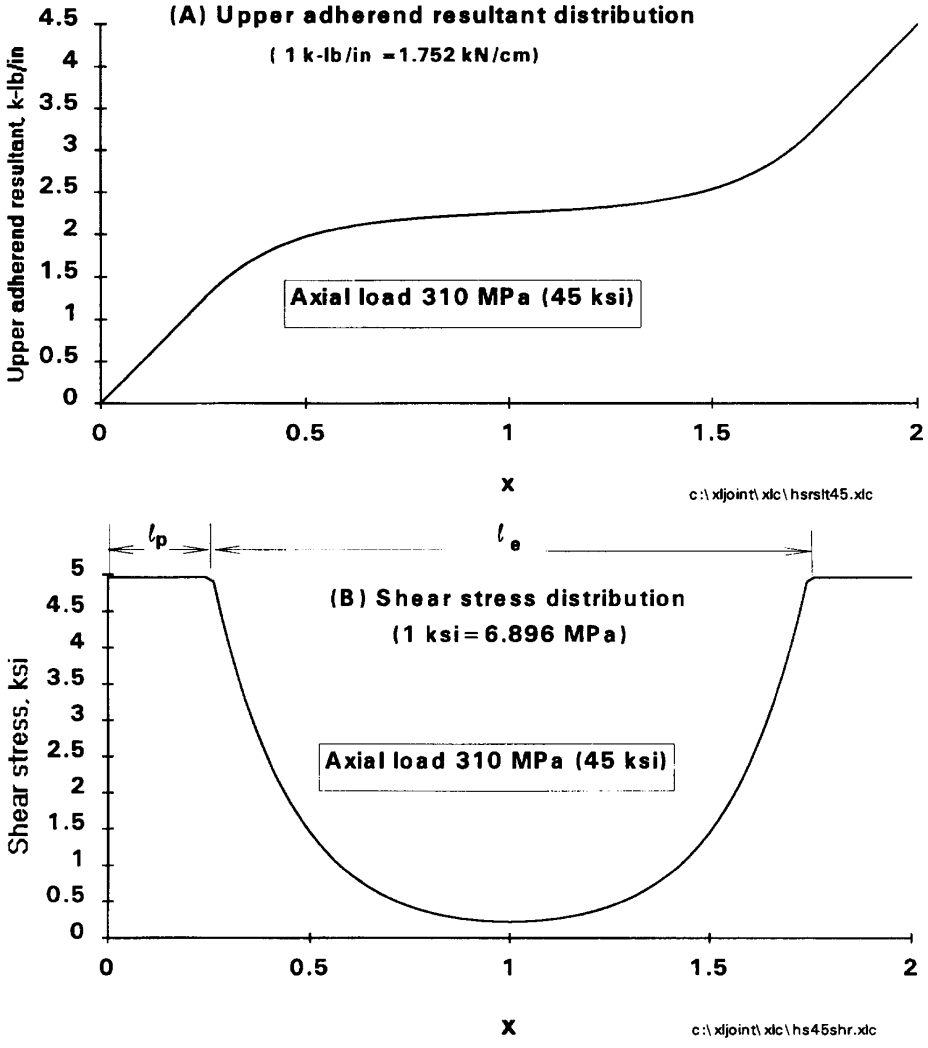

FIGURE 5.2.3.4.3(b) *Stress distributions in double lap joints – ductile adhesive response.*

Note that if $\gamma_{max} = \tau_p / G_{b0}$ which is the maximum strain in the elastic part of the bilinear representation, then Equations 5.2.3.4.3(e) and 5.2.3.4.3(f) give the same value. The factor $\left(2G_{b0}\gamma_{max} / \tau_p - 1\right)^{1/2}$ in Equation 5.2.3.4.3(f) acts as a load enhancement factor and represents the increase of joint load capacity due to ductile adhesive response over the maximum load allowed by elastic response of the adhesive.

Note that Equation 5.2.3.4.3(f) can be rearranged to express $\bar{\sigma}_x|_{max}$ in terms of the maximum strain energy of the adhesive:

$$SE = \tau_p^2 / G_{b0} + \tau_p(\gamma_{max} - \gamma_e) \quad \text{where} \quad \gamma_e = \tau_p / G_{b0} \qquad 5.2.3.4.3(g)$$

Equation 5.2.3.4.3(f) can then be written

$$\bar{\sigma}_x|_{max} = \frac{2}{\beta}\sqrt{2 G_{b0} SE} \qquad 5.2.3.4.3(h)$$

The Hart-Smith analysis based on the equivalent bilinear stress-strain law was shown in Reference 5.2.1(j) to give the same joint load capacity as the solution for the problem using the actual stress-strain curve of the adhesive. The convenience of the bilinear stress-strain description is in the simplicity of the solutions it allows; once the length of the plastic zone at each end is determined, the same types of solution apply for the elastic zone as were given in Equation 5.2.3.4.1(f) for the shear stress distributions, together with linear resultant and constant shear stress distributions in the plastic zones.

The most obvious effect of ductility in the adhesive behavior is the reduction of peak shear stresses. In addition, there is a beneficial effect on reduction of peel stresses. For the double lap joint considered in Figure 5.2.3.4.3(b), the maximum peel stresses denoted by $\bar{\sigma}_x|_{max}$, which occur at the ends of the joint, are given (Reference 5.2.1(l)) by

$$\sigma_b|_{max} = \gamma \tau_b|_{max} : \gamma = \left(3 \frac{E_b}{E_o} \frac{t_o}{t_b}\right)^{1/4} ; E_b = \text{peel modulus of adhesive} \qquad 5.2.3.4.3(i)$$

where $\bar{\tau}_b|_{max}$ is the maximum shear stress, either $\beta\bar{\sigma}_x / 2$ for the elastic case or τ_p for the case of ductile response. The maximum peel stresses are thus reduced by the same ratio as the maximum shear stresses in the case of ductile response of the adhesive.

As stated earlier, the ductile response of the adhesive provides additional structural capability of the joint over its limit load capacity. Under normal operation, it is advisable to keep the applied load in the joint low enough to insure purely elastic response for most practical situations where time-varying loading is encountered. Some damage to the adhesive probably occurs in the ductile regime which would degrade the long term response. The main benefit of ductile behavior is to provide increased capacity for peak loads and damage tolerance with regard to flaws -- voids, porosity and the like -- in the adhesive layer.

5.2.3.4.4 Transverse shear and stacking sequence effects in composite adherends

Classical analyses such as the Volkersen shear lag model for shear stresses in the bond layer (Sections 5.2.3.2 and 5.2.3.4.1) are based on the assumption that the only significant deformations in the adherends are axial, and that they are uniformly distributed through the adherend thicknesses. This is a good assumption for metal adherends which are relatively stiff with respect to transverse shear deformation, but for polymer matrix composite adherends which have low transverse shear moduli, transverse shear deformations are more significant and can have an important influence on bond layer shear stresses. Finite element analysis will take such effects into account in a routine manner, but for the closed form type of solutions on which most of the results of this chapter are based, allowance for transverse shear and thickness normal deformations is absent. A useful correction to the classical Volkersen solution which allows for transverse shear deformations in the adherends can be obtained by initially assuming that the axial stresses are constant through the adherend thickness and that as a result, (because of equilibrium with the axial stresses), the transverse shear stresses and strains are distributed linearly. (For a non-unidirectional laminate the shear stresses and strains will be **piecewise** linear, corresponding to the jumps in axial moduli of the laminate plies.) Integrating the shear strain distribution through the thickness then leads to a quadratic correction term to the distribution of axial displacements and stresses, which can be absorbed as a simple modification (Reference 5.2.3.4.4) of the Volkersen shear lag analysis . Modifying the shear modulus of the adhesive from its actual value, G_b, to an effective value, $G_b|_{eff}$, given by

$$G_b|_{eff} = G_b / K_{sh} \quad \text{where} \quad K_{sh} = 1 + \frac{1}{3}\left(\frac{G_b}{G_{xzo}} \frac{t_o}{t_b} + \frac{G_b}{G_{xzi}} \frac{t_i}{2\,t_b} \right) \qquad 5.2.3.4.4(a)$$

then the resulting $G_b|_{eff}$ can be substituted for G_b to obtain the parameter β in Equation 5.2.3.4.1(a) and the resulting β can be used to obtain the shear stress distribution using Equation 5.2.3.4.1(f). Note that G_{xzo} and G_{xzi} in Equation 5.2.3.4.4(a) are the transverse shear moduli of the adherends. A similar modification is also given in Reference 5.2.3.4.4 for the single lap joint analysis . The correction given here amounts to treating 1/3 the thickness of each adherend as an extension of the bond layer, and assigning the shear stiffness of the adherend for that part of the effective bond layer. The factor 1/3 corresponds to a linear distribution of shear stress through the adherend thicknesses, which as noted above, is consistent with the assumption that the axial deformations are approximately uniform through the adherend thickness.

As an example, consider a double lap joint with unidirectional carbon/epoxy inner and outer adherends, with adherend thicknesses of 0.1 in (2.53 mm) and 0.2 in (5.06 mm), respectively, and a 0.01 in (0.253 mm) bond thickness. Assume a shear modulus of the bond layer of 150 ksi (1.06 GPa) and transverse shear moduli of 700 ksi (4.82 GPa) for the adherends. A value of 2.48 is then obtained for K_{sh} in Equation 5.2.3.4.4(a), and the value of β and the maximum shear and peel stresses which depend on it are reduced by a factor of $(K_{sh})^{1/2}$ or 1.56 for this case. The shear and peel stresses are therefore approximately 36% lower than the values predicted in Equations 5.2.3.4.1(f) and 5.2.3.4.1(h) with the unmodified bond shear modulus. This type of correction appears to give relatively good predictions of the adhesive stresses in comparison with finite element analyses. An example will be presented in Section 5.2.3.6 (see Figure 5.2.3.6 (b)). The distribution of shear stress in the bond is shown there to be predicted with impressive accuracy by the Volkersen shear lag analysis with the modification of the effective bond shear modulus just discussed.

The modification presented above applies only to unidirectional reinforcement of the adherends. However, the same type of approach can be applied to adherends with general stacking sequences, although in this case, while the axial **strain** distribution is again initially assumed to be uniform through the thickness, the axial **stress** distribution will be piecewise uniform, varying from layer to layer with the axial moduli of the adherend plies. The resulting transverse shear stress- and therefore the shear-strain distribution will be piece-wise linear rather than continuously linear, and can be integrated through the thickness to get a correction to the conventional shear lag analysis which is similar to that described above, with a suitable modification of the formula for K_{sh} given in Equation 5.2.3.4.4(a). Similar modifications of the Hart-Smith analysis for ductile adhesive response are possible.

The approach presented here is a simplified version of a more elaborate method for correcting the classical closed form solutions developed in the early 1970's (References 5.2.1(d), (f) and (g)). The latter approach allowed for both bending and stretching deformations in the adherends. The present correction appears to be adequate for most practical purposes, however.

5.2.3.5 Tapered and multi-step adherends

In this section we will consider joints with adherend thicknesses that vary along the joint length. These include double strap joints with tapered outer adherends shown in Figure 5.2.3.5(a) part (A), scarf joints, Figure 5.2.3.4(a) part(B), and step lap joints, Figure 5.2.3.5(b) .

As discussed in Section 5.2.2.2, tapering the outer adherends of strap joints as in Figure 5.2.3.5(a) part (A) is beneficial mainly for reducing peel stresses, while scarf and step lap joints (Figures 5.2.3.5(a) part(B) and 5.2.3.5(b)) can reduce both shear- and peel-stress peaks. With both tapered-adherend lap joints and scarf joints it can be shown from equilibrium considerations that the bond stresses can be related to the ratio of thickness t to taper length ℓ by

$$\tau_b \approx \sigma_x\, t/\ell \quad ; \quad \sigma_b \approx \sigma_x\, t^2/\ell^2 \qquad 5.2.3.5(a)$$

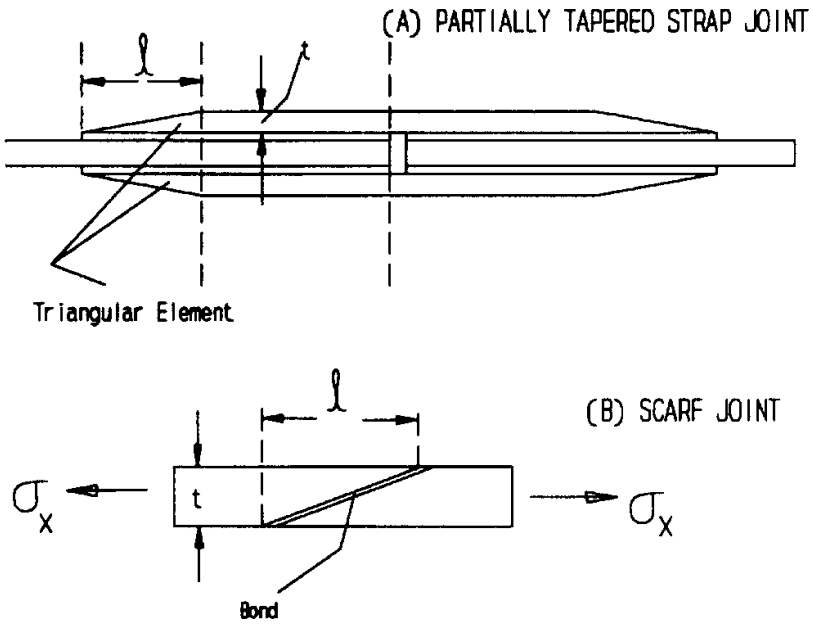

FIGURE 5.2.3.5(a) *Tapered double strap and scarf joints.*

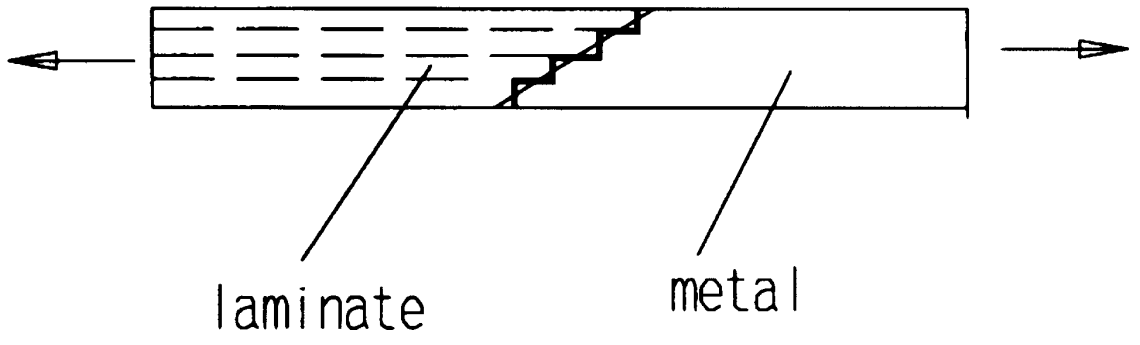

FIGURE 5.2.3.5(b) *Generic step lap joint.*

For a scarf joint, standard stress transformation relationships give this approximation, for small scarf angles, for the relation between axial stress in the adherend and resolved stresses in the inclined plane corresponding to the bond line. For the strap joint of Figure 5.2.3.5(a) part (A) it corresponds to the relation between the stresses in the triangular element at the left end of the joint for a traction free condition at the inclined upper surface of the element. Equation 5.2.3.5(a) is quite accurate for scarf joints having the same maximum stiffness (axial modulus times maximum thickness) in each adherend, although for unequal stiffnesses the stresses will vary along the joint and exhibit peaks at the ends of the joint (although not as severe as those for untapered joints) which causes a deviation from Equation 5.2.3.4(a). For tapered strap joints the equation holds approximately along the tapered part of the joint if the length of the taper is short enough to avoid stretching effects that cause the shear strain in the bond to vary, as discussed in Section 5.2.3.4.1 for the case of uniform adherend thickness. Note that Equation 5.2.3.5(a) implies that the bond stresses are constant along the length of the joint and can be reduced to any arbitrary level by making t / ℓ small enough, i.e., making the joint long enough with respect to the maximum adher-

end thickness. Note also that the effect of t / ℓ on the peel stresses is especially strong, being governed by the *square* of the thickness-to-length ratio. This is particularly important when outer adherend tapering used as a means of reducing peel stresses in strap and lap joints.

Aside from the finite element approach, various stress analysis methods are available for joints with tapered adherends. Hart-Smith, in Reference 5.2.1(k), presented power series solutions for stresses for such joints. In addition, Reference 5.2.3.5(a) discusses a finite difference approach leading to a PC-based computer code, `TJOINTNL`, that allows for ductile response of the bond layer along with tapered adherends. This code forms the basis for the results presented below on scarf joints and lap and strap joints with tapered outer adherends.

The following discussion will address the specific benefits of adherend tapering in adhesive joints. The objective is to achieve high joint efficiency by reducing effects of shear and peel stress concentrations at the ends of the joint. Ideally, we would like to achieve the joint strength provided by the "P over A" concept obtained with the case discussed in Section 5.2.3.2 for perfectly rigid adherends (Figure 5.2.3.2(a)), in which increasing the joint length indefinitely brings the shear stress in the bond down to any required level regardless of the magnitude of load being supported by the joint. For scarf and step lap joints this objective is achievable, although in tapered double lap and strap joints it is not. While tapering does reduce the peel stresses markedly in these types of joint as will be seen below, shear stress peaks can not be avoided completely, and the law of diminishing returns illustrated previously for uniform thickness adherends by Figure 5.2.3.2(f) continues to prevail with regard to the ultimate lack of effectiveness of increasing the joint length to obtain greater load capacity, although adhesive ductility will still enhance the strength beyond what elastic analysis predicts.

Various features of strap joints with tapered outer adherends are illustrated in Figure 5.2.3.5(c). Figure 5.2.3.5(d) gives shear stress predictions for joints with uniform adherend thickness to provide a basis for comparison with the tapered cases.) The "initial rise" feature of Figure 5.2.3.5(c) part (C) has been included in the joints considered here since bringing the tapered end of the joint to a knife edge may weaken the adherend and cause premature failure.

Figure 5.2.3.5(e) shows the bond stresses in various double strap joints with tapered outer adherends. Pertinent dimensions for the joint configurations on which these results are based are shown in Figure 5.2.3.5(c). The notation used in Figure 5.2.3.5(e), i.e., fully tapered outer adherends, partially tapered adherends (with the taper expressed as a percentage of joint length), and adherends with an initial rise (expressed in Figure 5.2.3.5(e) as a percentage of maximum adherend thickness) is also given in Figure 5.2.3.5(c). For the situation of no initial rise, two cases are considered in Figure 5.2.3.5(e), the case of 50% taper and that of full taper. There is an appreciable difference in the shear stress distribution at the left end of the joint for these two cases, the peak values agreeing reasonably well with the approximate predictions of Equation (5.2.3.5a). In the case of the peel stresses, these are too small to be distinguished in the plots, but the peak values at the left end of the joint, while appreciably less than the predictions of Equation 5.2.3.5(a), *are* found to be related to each other approximately as the square of the taper ratio which is 0.2 for the fully tapered case and 0.1 for the 50% taper. (The actual values for the peel stresses at the left end amount to 0.045 for the fully tapered case and 0.16 for the 50% taper) For both the full taper and 50% taper cases, a tensile secondary peel stress peak is present at the right end of the Figure 5.2.3.5(e) in the vicinity of the midpoint of the joint.

In the case of a 25% initial rise, much greater peel stresses , about 80% of the level occurring for the case of no tapering (the case of uniform adherend thickness considered in Section 5.2.3.4.1), arise at the left end of the joint than for the fully feathered cases. The initial rise also causes a greater increases in shear stress at the left end of the joint than the case of 50% taper with no initial rise does.

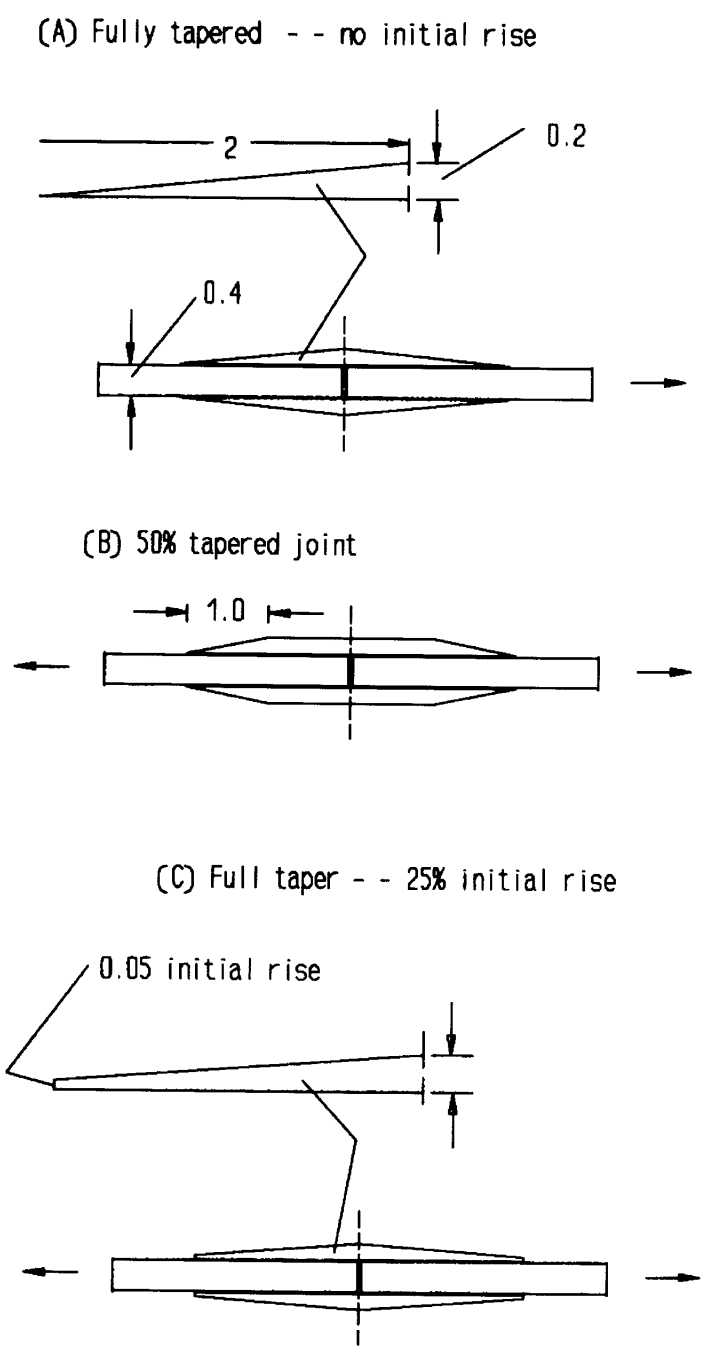

FIGURE 5.2.3.5(c) *Tapered strap joints under consideration.*

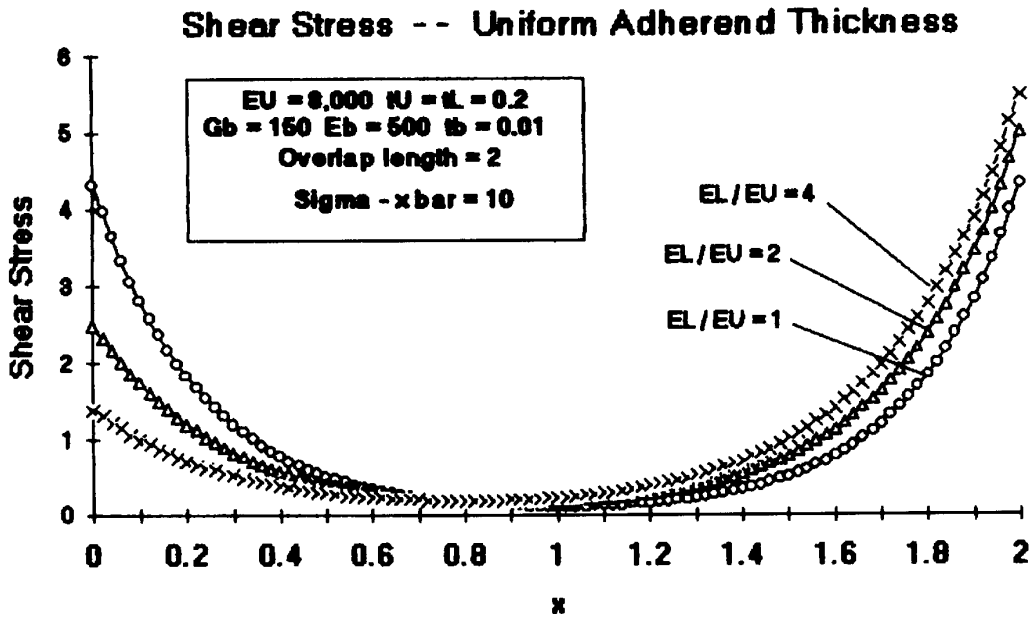

FIGURE 5.2.3.5(d) *Shear stresses in untapered strap joints.*

Thus, tapering is advantageous mainly as a way of eliminating the effects of peel stresses in double strap joints. Once this is accomplished, the effects of shear stress peaks can be controlled to a significant extent by taking advantage of adhesive ductility. Tapered strap joints can not achieve the ideal behavior which is possible with scarf joints, but they do provide a simpler solution to good joint performance if the adherends are sufficiently thin.

Shear stress distributions in scarf joints (Figure 5.2.3.5(f)) are given in Figure 5.2.3.5(g). Note that as in Figure 5.2.3.5(f), practical scarf joints can be arranged in a symmetric double lap configuration which avoids bending effects as well as providing a balanced stiffness design for dissimilar materials. In Figure 5.2.3.5(f) this is achieved by a continuous change of total (inner adherend + outer adherend) thickness over the length of the joint . The most important parameter for the scarf joint is the effect of adherend stiffness unbalance ($E_o \neq E_i$, "o" and "i" refer to the outer and inner adherends as in Figure 5.2.3.4.1(a)). The results given in Figure 5.2.3.5(g) which were obtained from the finite difference analysis discussed in Reference 5.2.3.5(a) represent the effect of varying degrees of stiffness unbalance and may be compared with the results for uniform thickness adherends given in Figure 5.2.3.5(d). The ratio of peak-to-average shear stresses in Figure 5.2.3.5(g) compare well with the values given by Hart-Smith in References 5.2.1(l) and 5.2.3.5(b), although the Hart-Smith analysis did not give the distribution of stresses along the length of the joint because of limitations of the power series solution approach which Hart-Smith used. Note that for fairly sizeable stiffness unbalances, up to 4:1, the maximum shear stress peak is not as great as that observed in Figure 5.2.3.5(d) for the uniform adherend case. However, it is clear that a stiffness unbalance *will* increase the maximum shear stress and weaken the joint in comparison with the performance in joints with balanced stiffnesses. It is emphasizes that for the equal stiffness case the shear stress in the bond is constant and equal to the average stress at all points.

It appears that most practical scarf joints can be configured for dissimilar materials as in Figure 5.2.3.5(f) to provide for balanced stiffnesses. In principle, the scarf joint then provides a near ideal solution to achieving as much load capacity as is required in any situation without overstressing the bond layer. However, the dimensions of the joint may grow too large to be practical for high joint load. In addition, an extremely good fit, for example, to tolerances on the order of the bond thickness over large lengths, has to be maintained to insure that the joint can provide uniform load transfer over its entire

length. Even with balanced stiffness configurations, thermal stresses which arise when the adherend materials are dissimilar will prevent the ideal form of behavior from being achieved.

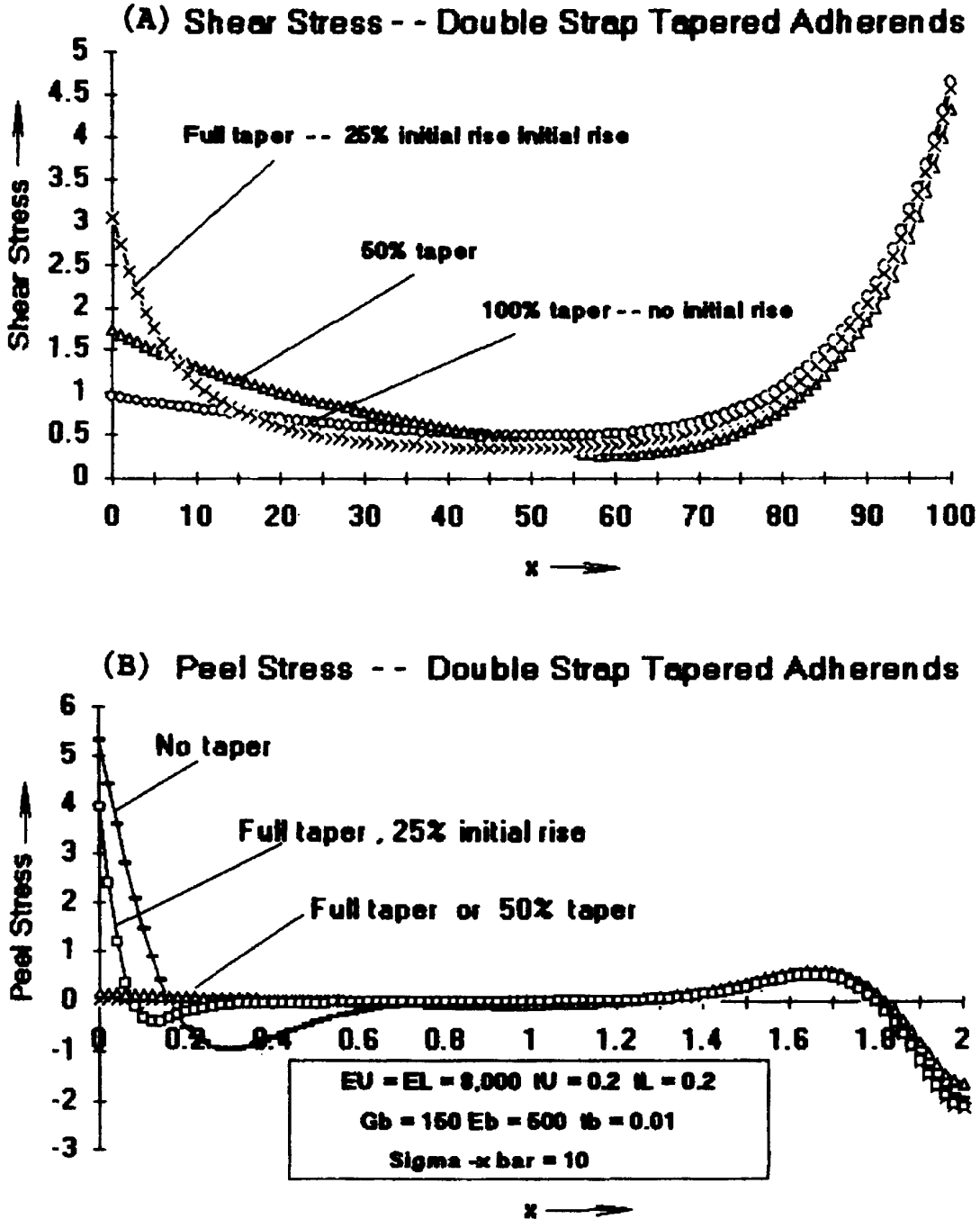

FIGURE 5.2.3.5(e) *Stresses in tapered double strap joints.*

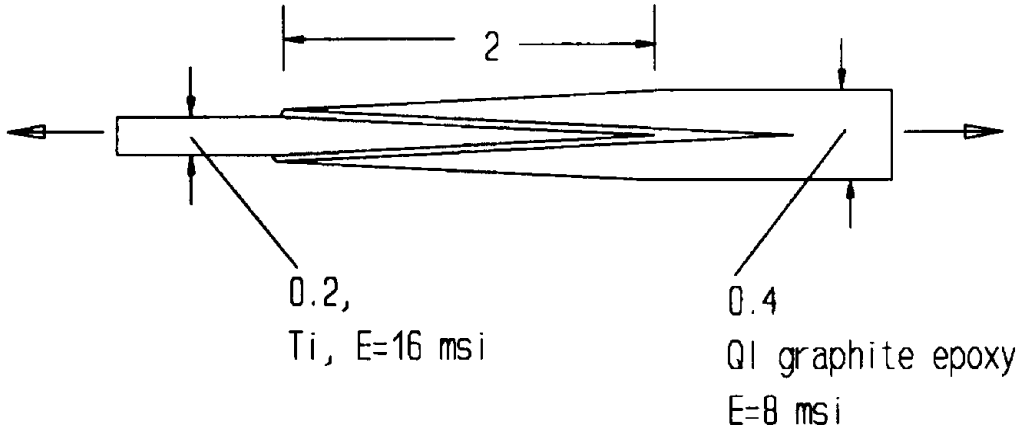

FIGURE 5.2.3.5(f) *Stiffness-balanced scarf joint configuration.*

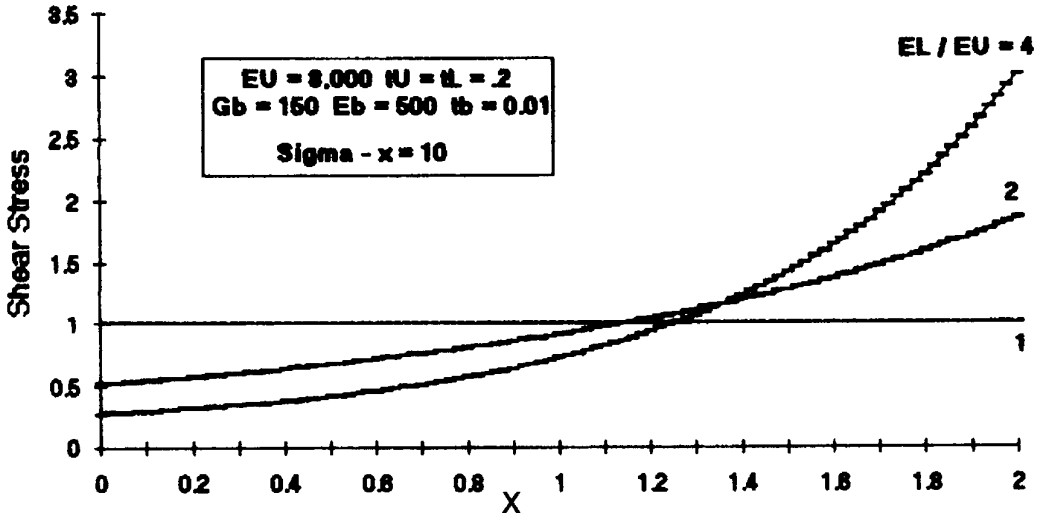

FIGURE 5.2.3.5(g) *Shear stresses in scarf joints.*

Step lap joints (Figure 5.2.3.5(b)) represent an approximation to the scarf joint which can take advantage of the layered structure of the composite adherend. The average slope of the region represented by the line through the steps in Figure 5.2.3.5(b) tends to control the average shear stresses developed in the bond. Within each horizontal section, equivalent to the tread of a staircase, the behavior is analogous to a joint with constant adherend thickness, and the differential equation given earlier as Equation 5.2.3.4.1(b) applies locally when t_U and t_L are adjusted to match the situation in each step. An expression similar to Equation 5.2.3.4.1(f):

$$\tau_{bj|max} = \beta_j \frac{\overline{T}}{\bar{t}} \left(\frac{1}{1+\rho_{Bj}} \frac{1}{\sinh \beta_j \ell_j / \bar{t}} + \frac{\rho_{B_j}}{1+\rho_{B_j}} \frac{1}{\tanh \beta_j \ell_j / \bar{t}} \right)$$

where 5.2.3.5(b)

$$\beta_j = \left[G_b \frac{\bar{t}^2}{t_b} \left(\frac{1}{B_{Uj}} + \frac{1}{B_{Lj}} \right) \right]^{1/2} \quad ; \quad \bar{t} = \frac{t_{Uj} + t_{Lj}}{2} \quad ; \quad \rho_{Bj} = B_{Lj} / B_{Uj}$$

gives the maximum shear stresses for the jth step, and the overall solution is a chain of such expressions with allowance for continuity of the shear strain and resultants, T_{Uj} and T_{Lj} at the points where neighboring steps join. In each step of the joint the shear stresses will have a distribution similar to that of Figure 5.2.3.4.1(b) part(A), the size of the peaks being governed primarily by the length of the step through the parameter $\eta_{sl} = \beta_j \ell_j / \bar{t}$. The aspect ratio for the step, $\ell_j / \bar{t}$, can in principle be kept small enough to almost completely avoid any peaking by using a large number of steps and keeping the length of each one small. In practice, the number of steps is governed by the number of plies in the laminate. In addition, if the joint is used to connect a composite adherend to a metal component, machining cost and tolerance requirements for the metal part enter into the selection of the number of steps.

Figure 5.2.3.5(h) shows a generic step lap joint configuration that illustrates some of the effects of design parameters on stresses in the joint. The results presented in Figures 5.2.3.5(i) and 5.2.3.5(j) were generated for this discussion using a linear elastic response model for the adhesive; in practice, considerable strength capability of the adhesive is unused if elastic response of the adhesive is assumed; Figure 5.2.3.5(k) taken from the discussion by Hart-Smith in Reference 5.2.3.5(b) is an example of joint design using elastic-plastic response for the adhesive. However, the elastic adhesive model used to generate Figure 5.2.3.5(i) and 5.2.3.5(j) is adequate for illustrating some of the parameters controlling the joint design. The results given in these figures are based on the classical Volkersen-type analysis which forms the basis of Equation 5.2.3.5(b).

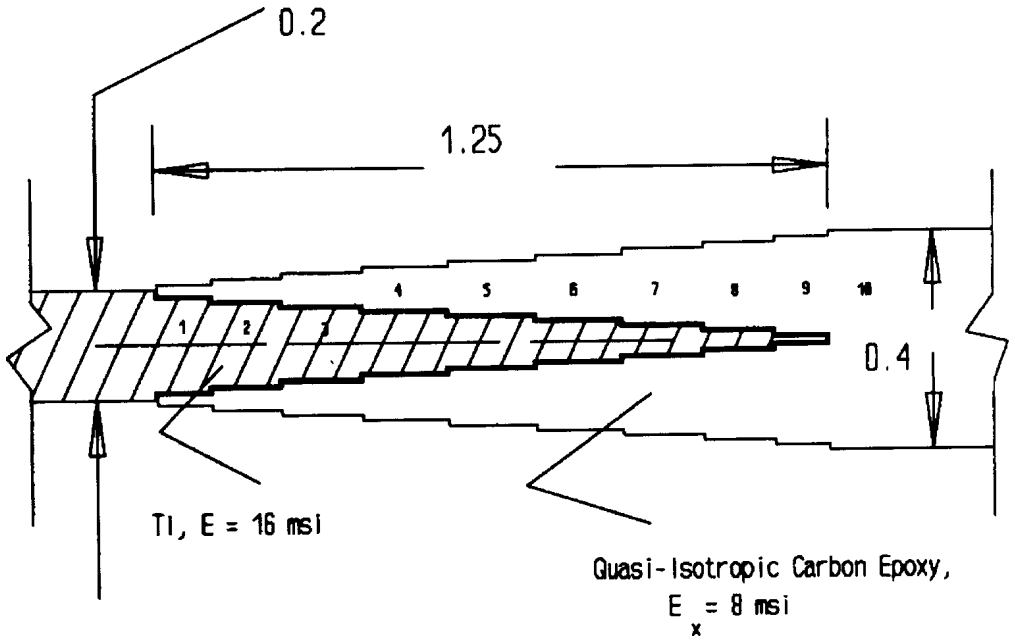

FIGURE 5.2.3.5(h) *Step lap joint configuration.*

The five-step design in Figure 5.2.3.5(i) and the ten-step design in Figure 5.2.3.5(j) were chosen with the following characteristics:

- Except for the first and last steps, the adherend thickness was incremented equally for each step
- For the first and last steps, the thickness increments were half those of the generic steps
- The lengths of each step were chosen with a fixed value of the parameter $\eta_{sl} = \beta_j \ell_j / \bar{t}_j$,where ℓ_j is the length of step j

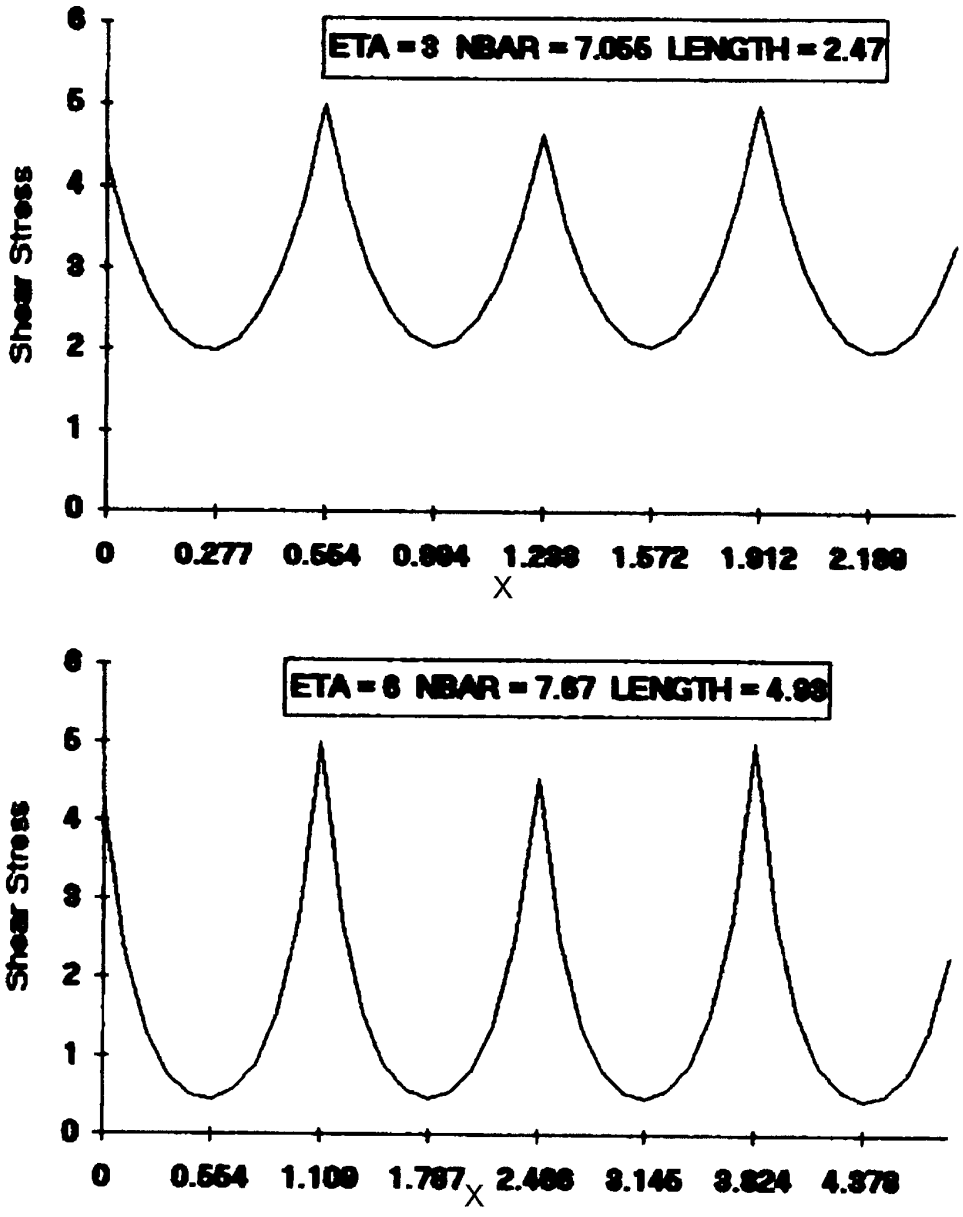

FIGURE 5.2.3.5(i) *Shear stresses in five-step joint.*

The half-thickness increments of the end steps gave a more uniform shear stress distribution than maintaining the same thickness increment for all steps. Note that for the symmetric joint configurations shown in Figures 5.2.3.5(h) and 5.2.3.5(k), the thickness increment for the outer adherend (composite) was greater than that for the inner adherend by the inverse of the modulus ratio, to achieve a stiffness balance for the dissimilar adherends. Note also that the parameter "ETA" listed in Figures 5.2.3.5(i) and 5.2.3.5(j) refers to η_{s1} defined above. This parameter essentially controls the length of the joint. Both Figures 5.2.3.5(i) and 5.2.3.5(j) show an increase in joint length with η_{s1} ("ETA" in the two figures). Note further that the load capacity of the joint in terms of the allowed resultant listed as "NBAR" in the Figures 5.2.3.5(i) and 5.2.3.5(j), corresponds to an assumed bond shear stress limitation of 5 ksi (34 MPa); this allowable load shows a general increase with joint length, but with diminishing increase when η_{s1} gets much beyond 3. Table 5.2.3.5 gives a summary of the results shown in the two figures. As discussed

above, the joint design shown in Figure 5.2.3.5(k) taken from References 5.2.1(l) and 5.2.3.5(b) represents a practical joint approach which accounts for several considerations that the simplified elastic analysis approach used for Figures 5.2.3.5(i) and 5.2.3.5(j) neglects. The neglect of ductility effects has already been mentioned. In addition, the use of as large a number of steps as 10 in Figure 5.2.3.5(j) may not be practical.

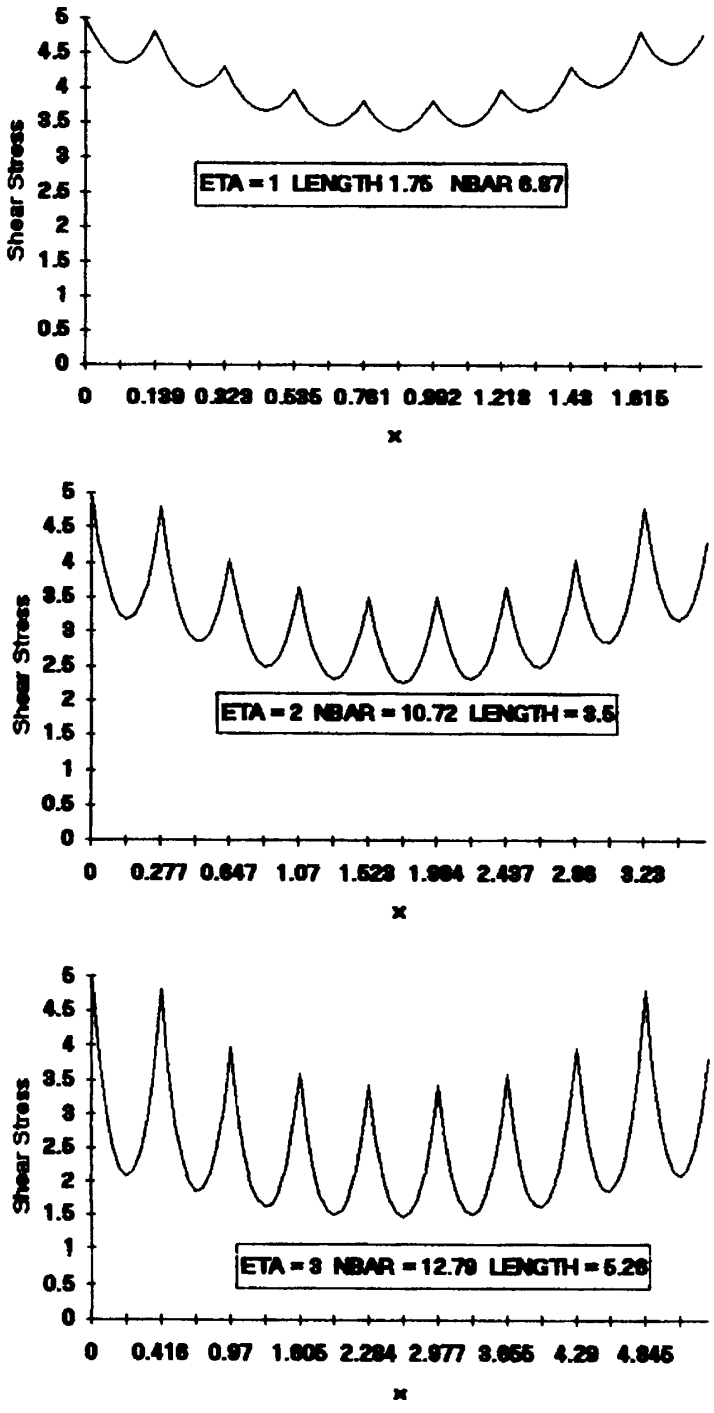

FIGURE 5.2.3.5(j) *Shear stresses in ten-step joint.*

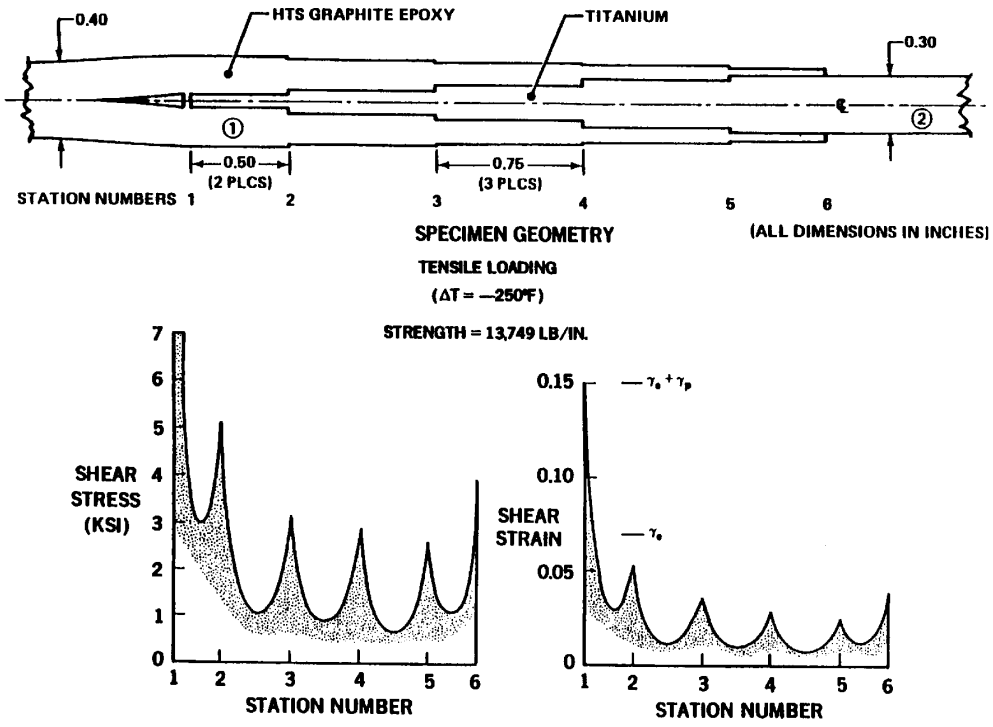

FIGURE 5.2.3.5(k) *Practical step lap joint design (Reference 5.2.3.5(b)).*

The joint design shown in Figure 5.2.3.5(k) represents the evolution of step-lap joint design over many years. Early analytical work was presented by Corvelli and Saleme (Reference 5.2.3.5(c)); this was later enhanced by Hart-Smith (Reference 5.2.1(l)), under NASA funding, to provide for elastic-plastic response, culminating in the A4EG and A4EI programs (Reference 5.2.1 (s)) discussed in Section 5.2.1, to allow for variations in thickness, porosity, flaw content, and moisture content in the bond layer. Hart-Smith (Reference 5.2.3.5(b)), notes that in mathematical treatments of step joints, all properties have to be constant within each step; however, in an actual joint such as that shown in Figure 5.2.3.5(k), artificial breaks may be inserted to permit changes in porosity or bond thickness.

TABLE 5.2.3.5 *Summary of step lap joint results (Figure 5.2.3.5(i), 5.2.3.5(j)).*

No. of Steps	10	10	10	5	5
η_{s1}	1	2	3	3	6
Joint length, in (cm)	1.75 (4.44)	3.5 (8.89)	5.25 (13.33)	2.47 (6.05)	4.93 (12.5)
Allowed resultant, kN/cm (10^3lb/in)	6.87 (12.03)	10.72 (12.03)	12.59 (22.05)	7.05(12.35)	7.67 (13.43)

5.2.3.6 Finite element modeling

Finite element methods have often been used for investigating various features of bonded joint behavior, but there are serious pitfalls which the analyst must be aware of to avoid problems in such analyses, mainly because of the tendency of the bond layer thinness to unbalance the finite element model. To achieve adequate accuracy, it is especially important to provide a high degree of mesh refinement around the ends of the overlap (see Figure 5.2.3.6(a)) and yet transition the mesh to a coarser representation away from the ends of the overlap to avoid unneeded computational costs. Without such approaches, the need for limiting the aspect ratios of elements will force either a crude representation of the bond layer or an excessively over-refined mesh for the adherends. The mesh shown in Figure 5.2.3.6(a) was generated with a custom designed automated mesh generator developed by C. E. Freese of the Army Research Laboratory Materials Directorate, Watertown, MA (Reference 5.2.3.6). The elements shown consist of 8-point isoparametric quadrilaterals and 6-point isoparametric triangles, providing a quadratic distribution of displacements within each element. A number of commercially available finite element codes are presently available for developing such refined meshes. The commonly used displacement-based finite element methods are not capable of satisfying exact boundary conditions such as the traction free condition shown at the left end of the upper adherend in Figure 5.2.3.6(a) (C). In addition, a mathematical stress infinity occurs at the corner formed by the left end of the bond layer and the lower adherend.

These characteristics cannot be represented exactly, but a measure of the adequacy of the mesh refinement is provided by the degree to which the solution achieves the traction free condition shown in Figure 5.2.3.6(a) (C). Pertinent results are shown in Figure 5.2.3.6(b) which gives a solution for a double lap joint with unidirectional carbon/epoxy adherends. The finite element results represented by the "x" and "Δ" symbols are relevant to the issue under consideration. These represent the distribution of shear stresses along the interface between the upper adherend and the bond layer as indicated in the insert at the top of Figure 5.2.3.6(b). Since this line intersects the left end at a point fairly near the corner where the singularity occurs, it is reasonable to expect some difficulty in satisfying traction free conditions at the left end. The computer results did not go to zero at the end (where x = 1.1953) but did show signs of heading in that direction since the end stress is slightly below the peaks for the two curves. Note that the Δ symbols represent a condition in which the bond is replaced by a continuation of the upper adherend, a considerably more difficult situation to deal with than that of the x's which allow for an actual bond layer. The third curve shown in Figure 5.2.3.6(b) indicated by open circles represents a modification of Volkersen's one-dimensional shear lag analysis which allows for transverse shear deformations in the adherends; the latter agrees surprisingly well with the prediction for the finite element analysis with the bond layer present (x's) for most of the joint length, although the peak stress predicted by the approximation is somewhat less than that of the FE analysis.

5.2.4 Failure criteria for adhesive joints

This section is reserved for future use.

5.2.5 Design case studies

This section is reserved for future use.

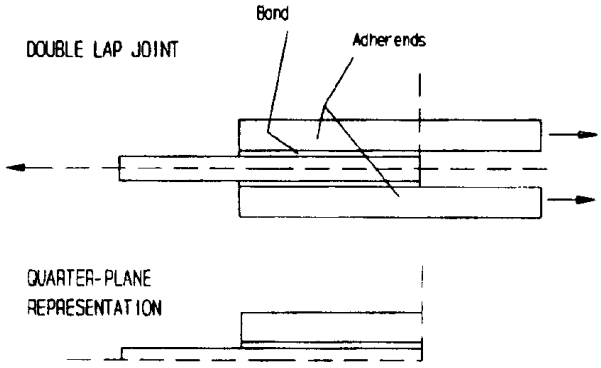

(A) Joint configuration

(B) Overall mesh

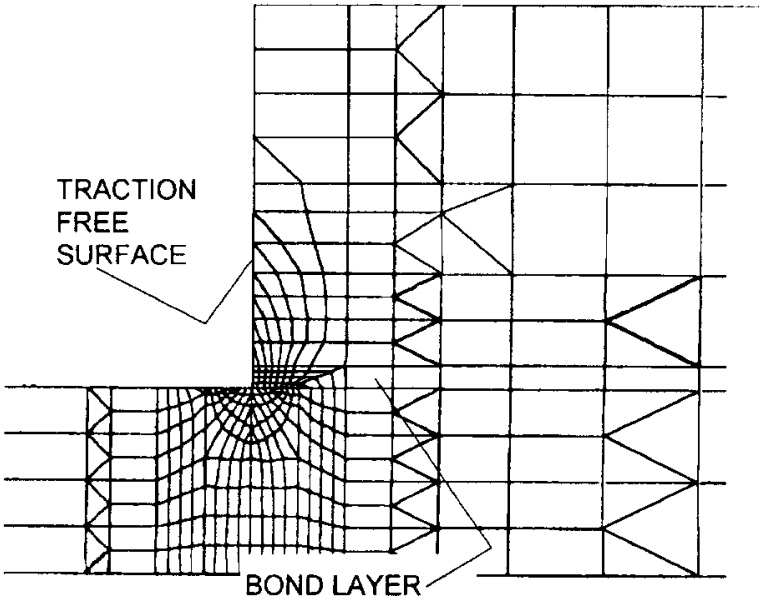

(C) Detailed Mesh

FIGURE 5.2.3.6(a) *Mesh details for finite element analysis of double lap joint.*

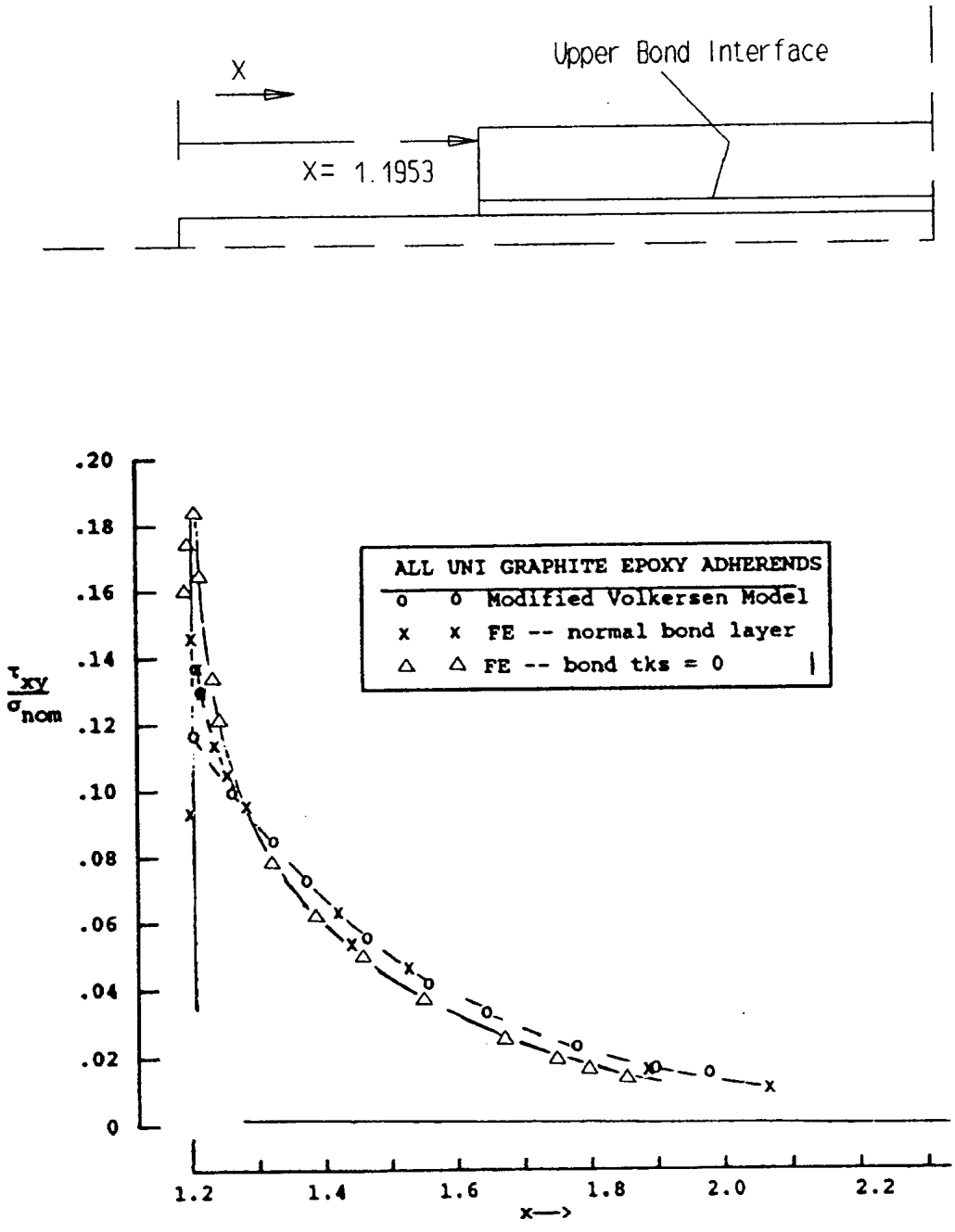

FIGURE 5.2.3.6(b) *Finite element predictions of shear stress distribution along bond-upper adherend interface, double lap joint shown in Figure 5.2.3.6(a).*

5.3 MECHANICALLY FASTENED JOINTS

5.3.1 Introduction

Mechanically-fastened joints for composite structures have been studied since the mid-1960's when high modulus, high strength composites first came into use. It was found early in this period that the behavior of composites in bolted joints differs considerably from what occurs with metals. The brittle nature of composites necessitates more detailed analysis to quantify the level of various stress peaks as stress concentrations dictate part static strength to a larger extent than in metals (no local yielding). As a result, composite joint design is more sensitive to edge distances and hole spacings than metal joint designs. Low through-the-thickness composite laminate strength has led to specialized fasteners for composites and eliminated the use of rivets. The special fasteners feature larger tail footprint areas which improve pull-through and bearing strengths. Galvanic corrosion susceptibility between carbon and aluminum has all but eliminated the use of aluminum fasteners.

Mechanically-fastened joints can be divided into two groups - single row and multi-row designs. Typical lightly loaded non-critical joints require a single row of fasteners. The root joint of a wing, or a control surface, is an example of a highly loaded joint, where all the load accumulated on the aerodynamic surface is off-loaded into another structure. The bolt pattern design, consisting of several rows, distributes the load for more efficient transfer.

There have been numerous government and privately funded programs for the purpose of developing composite mechanically-fastened joint analysis methods. A majority of these efforts has been concentrated on developing two-dimensional analyses to predict stresses and strength at a single fastener within the joint. This is because existing analysis techniques for determining multi-fastener joint load apportionment (in metals) have proven adequate. Additional analysis methods (Section 5.3.2) have been developed to address composite-related stress variations in stepped and scarf (i.e., tapered thickness) joints.

The material presented here reflects the state of the art as practiced primarily in the aircraft industry. The objective is to give the reader some insight into the key factors that control the behavior of mechanically-fastened joints in composite structures. The discussion that follows is arranged primarily to achieve that objective.

5.3.2 Structural analysis

5.3.2.1 Load sharing in a joint

Most of the mechanical joints encountered in aircraft structures have multiple fasteners. The number and type of fasteners needed to transfer the given loads are usually established by airframe designers by considerations of available space, producibility, and assembly. Although the resulting joint design is usually sufficient for finite element (FE) modeling purposes, further structural analyses are required before joint design drawings are released for fabrication. These analyses should consist of two distinct calculations: (1) computation of individual loads and orientation at each fastener with possible optimization to obtain near equal loading of each equal diameter fastener, and (2) stress analysis of load transfer for each critical fastener using fastener loads from previous analysis.

An example of a joint is shown in Figure 5.3.2.1(a). In order to obtain individual fastener loads for this or any other joint configuration (including single in-line row of fasteners), overall loading, geometry, plate stiffnesses, and individual fastener flexibilities must be known. Two structural analysis approaches have evolved in the aircraft industry. One performs the analysis in two steps, the first step being a calculation of individual bolt flexibilities followed by FE analysis with the fastener flexibilities as input. The second type includes the computation of the joint flexibility as a special FE in the overall FE analysis. An example of the latter is the SAMCJ code developed for the Air Force, Reference 5.3.2.1(a). Both approaches approximate a nonlinear joint load-displacement response, Figure 5.3.2.1(b), by a bilinear representation.

This simplification permits the overall finite element problem to be linear. Recently a closed form analytical model has been developed and programmed for the personal computer to deal with the multiple hole joint strength problem (Reference 5.3.2.1(b)).

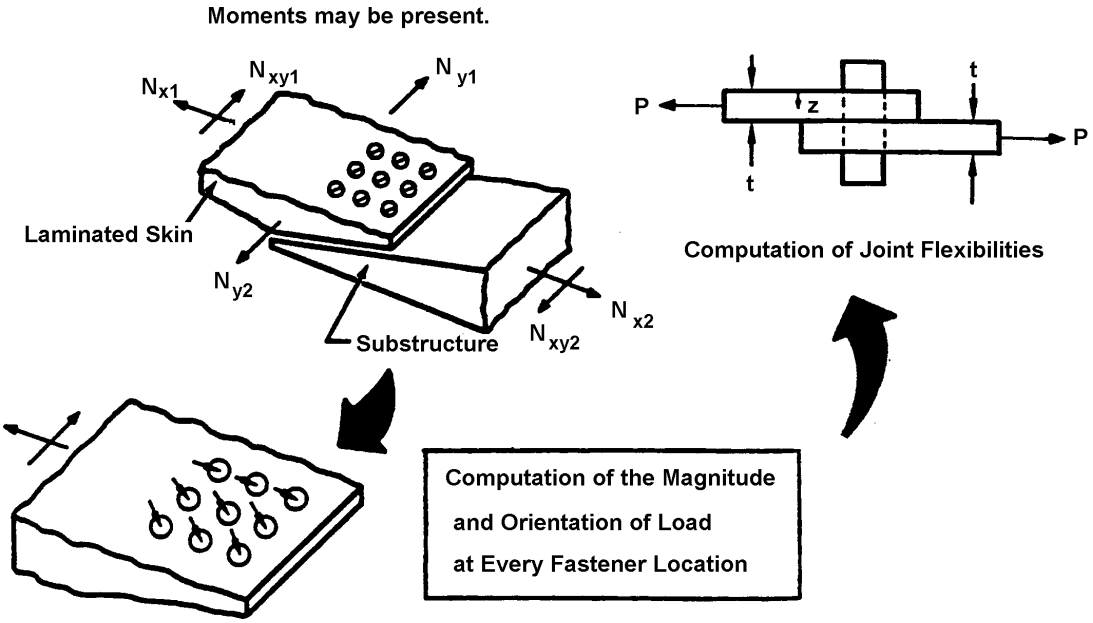

FIGURE 5.3.2.1(a) *Overview of the strength analysis of bolted structures.*

Fastener flexibility is based on joint displacement not only due to the axial extension of the joining plates but to other effects not easily modeled. These are fastener deflection in shear and bending, joint motion attributable to localized bearing distortions, and fastener rigid body rotation in single shear joints. Additionally, for composite laminates the value of joint flexibility should reflect the material orientation, ply fractions, and the stacking sequence of the laminates being joined. Other variables to be considered are the fit of the pin in the hole, presence of a free edge close to the hole, and head/tail restraint. Because of the many variables, test data for joint flexibility is the best type of input for the overall FE model of the multi-fastener joint. However, the data is not always available for all the different design situations. Hence, various modeling schemes have evolved to obtain flexibility values. Calculation of joint flexibility can be quite complex if the joint contains multiple stack-ups of plates with gaps. Analytical models to solve for the joint flexibility range from representing plates as springs to those where the fastener is idealized as a flexible beam on an elastic foundation provided by the plate or laminate.

For thick plates fasteners, flexibility may not be as important a parameter as for thin plates. Reference 5.3.2.1(c) has shown that good correlation between test and analysis for bolt load distribution using rigid inclusions to represent bolts. Reference 5.3.2.1(c) also included effects of the contact problem with and without gaps to calculate bearing stress distributions.

Load sharing in mechanically fastened joints is strongly dependent on the number and the diameter and material of the bolts, and the stiffness of joining members. For a single in-line row of bolts the first and the last bolt will be more highly loaded, if the plates are of uniform stiffness. This is illustrated in Figure 5.3.2.1(c) in which, in addition to the equal stiffness members (configuration 2), other combinations of fastener diameters/plate configurations are shown, which can alter the bolt distributions appreciably.

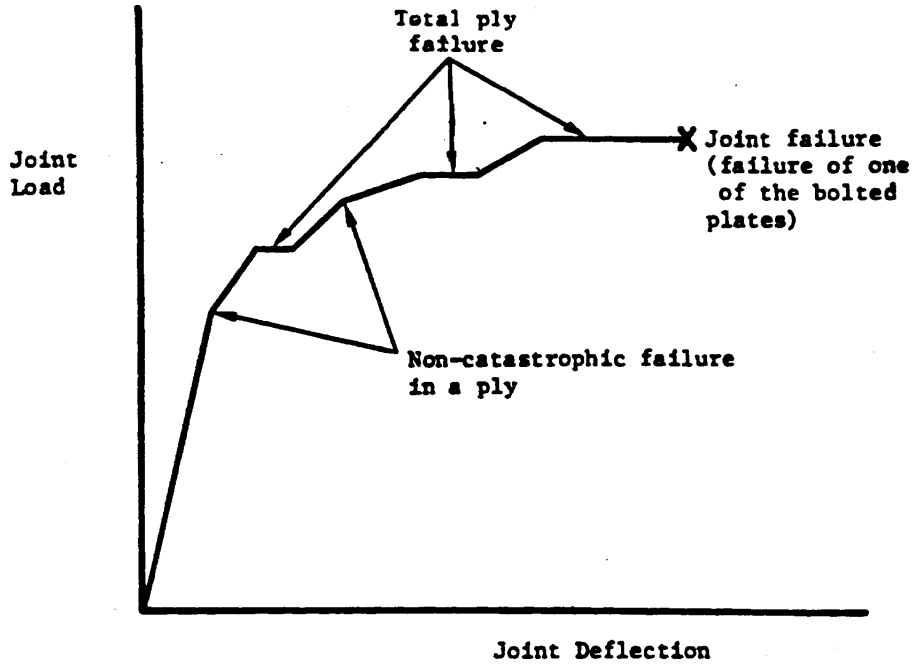

FIGURE 5.3.2.1(b) *A schematic representation of the overall load versus deflection response of the joint.*

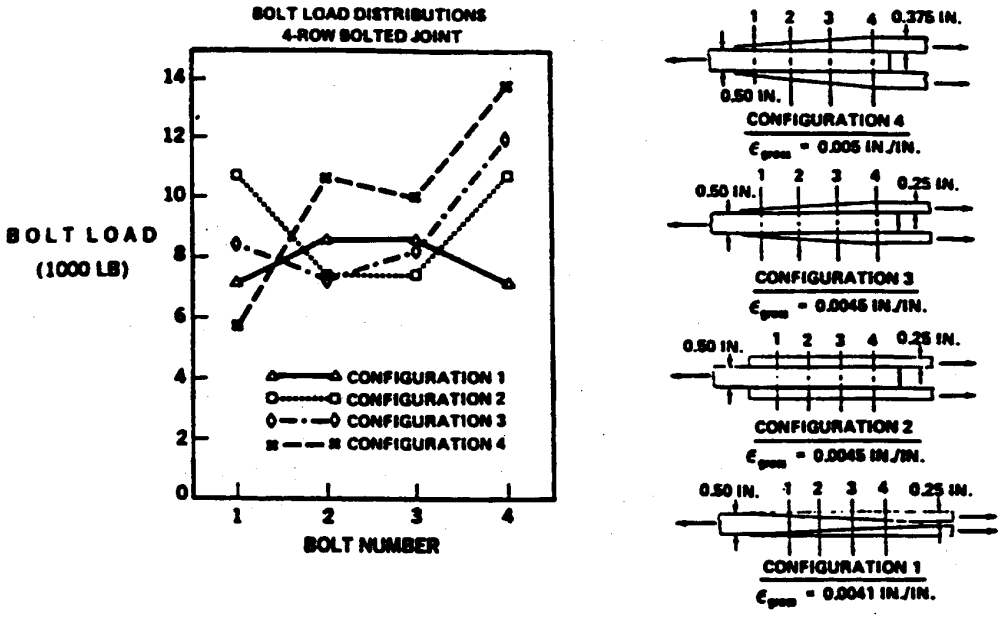

FIGURE 5.3.2.1(c) *Effect of joint configuration on fastener load distribution (Reference 5.3.2.1(d)).*

5.3.2.2 Analysis of local failure in bolted joints

Once the load sharing analysis has been performed, bolted joint analysis reduces to modeling a single bolt in a composite plate as shown in a free body diagram in Figure 5.3.2.2.(a). A number of analysis codes have been developed that perform the stress analysis and provide useful failure predictions for problem of Figure 5.3.2.2.(a). One cannot depend on analysis alone, and the design of a bolted composite joint will entail an extensive test program involving various joint configurations, laminates, and bearing/bypass ratios. However, because of the variety of laminates and load conditions present in a complex structure, testing frequently cannot cover all conditions of interest. Therefore, analytical methods are needed to extend the applicability of the test data to a wider range of cases.

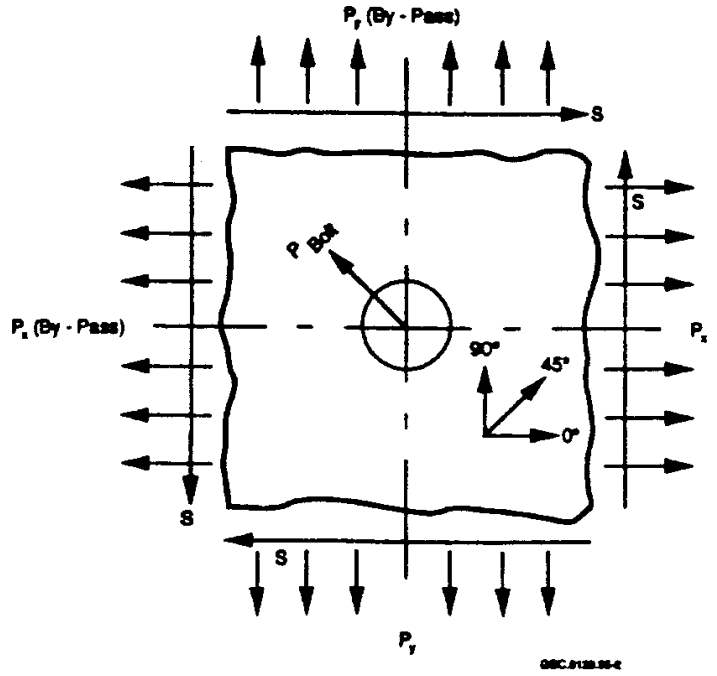

FIGURE 5.3.2.2(a) *Bolted joint under generalized loading.*

There are multiple failure modes that must be considered. The first is net section failure of the composite. Alternatively, the laminate may fail immediately ahead of the bolt due to bearing pressure or the specimen will fail by pull-through. Depending on hole spacing, edge distances, or lay-up, shear-out may occur before bearing failure is reached. Delaminations may also be present but these are not the primary cause of failure. Finally, failure of the fastener must be considered. A more comprehensive description of possible failure modes is discussed in the next section.

The analysis of fiber dominated in-plane failure modes, such as net-section failure, has typically been accomplished using variations of the approach by Whitney and Nuismer (Reference 5.3.2.2(a)), or the semi-empirical model of Hart-Smith (Reference 5.3.2.2(b)). The basis of the approach is to evaluate a ply-level failure criterion at a characteristic distance, d_0 away from the edge of the hole. The characteristic distance accounts for two experimentally observed effects. First, the strength of laminates containing a hole is greater than would be implied by dividing the unnotched strength by the theoretical stress concentration for the open hole. Second, the strength is observed to be a function of hole diameters, with strength decreasing as hole diameter increases. The use of a fixed d_0 simulates these effects, Figure 5.3.2.2(b).

The characteristic distance is treated as it was a laminate material property, and is determined by correlating the analysis to the ratio between the unnotched and open-hole strengths of laminates. More extensive correlations may reveal that d_0 is a function of the laminate ply fractions. The value of d_0 will also depend on the ply-level failure criterion used.

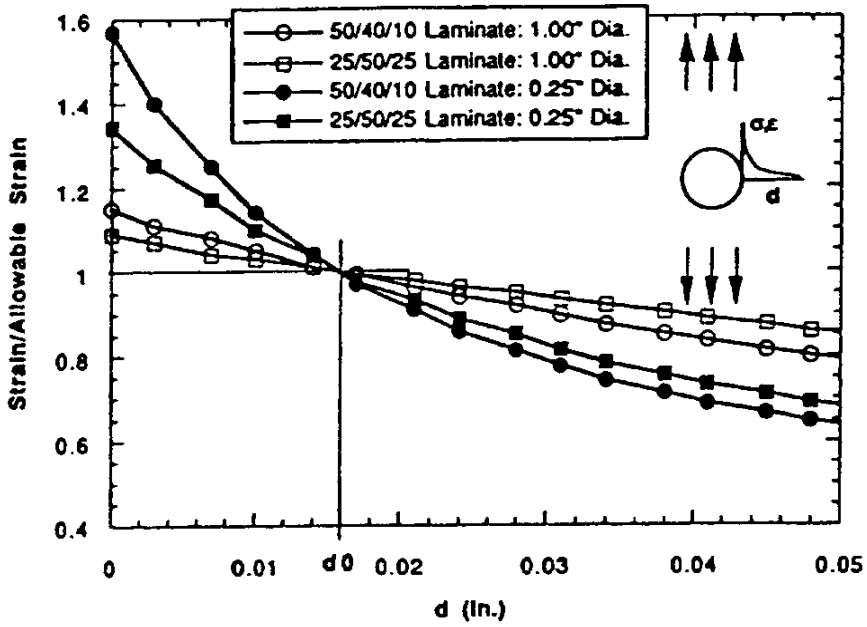

FIGURE 5.3.2.2(b) *Strain distributions near an open hole for different hole diameters and tape laminates. Applied far field load is equivalent to the expected failure load. Laminates are given as percentages of 0°/±45/90°. Crossing point of curves defines characteristic distance, d_o.*

The establishment of laminate material allowables for the failure prediction must include a consideration of the material variability, and the inherent inability of current failure theories to completely account for changes in laminate stacking sequence, joint geometry, and hole size. One approach is to establish B-basis allowables for the ply-level failure criterion based on unnotched ply data. The d_0 is then selected such that the predicted values of failure are equivalent to the B-basis value of the notched laminate tests. The B-basis d_0 can also be obtained directly from notched laminate tests if sufficient number of different laminates with various hole sizes are tested.

Although the Whitney-Nuismer method was originally conceived for failure under uniaxial tension, the method has been applied to compression, and biaxial loading. The compression d_0 will be different than the tension value and the edgewise shear d_0 different from either. Reference 5.3.2.2(c) suggests a smooth characteristic curve for connecting the tension and compression values. When biaxial loads are introduced, one must search for the most critical location around the hole. A search algorithm is needed even for the case of uniaxial loading as it can be shown that the maximum circumferential stress may not occur at a point tangential to the load direction when the percentage of ±45° plies is large, or when an off-axis laminate is considered.

Use of this failure criterion for predicting failure implies that an accurate stress solution for the vicinity of the hole is available. A solution for a hole in an infinite, anisotropic sheet was given by Lekhnitskii

(Reference 5.3.2.2(d)). This solution can be extended to the case of an assumed pressure distribution for a loaded bolt, and can be combined with boundary integral techniques to include the effects of nearby boundaries and multiple holes. General boundary element methods and finite element methods have also been applied. Care should be exercised in the use of finite-element techniques due to the high stress gradients present at the hole. The finite element model should be compared against the theoretical stress concentration at the edge of the hole to ensure sufficient mesh refinement.

The behavior of joints with bearing-loaded bolts has often been simulated by assuming a pressure distribution around the perimeter of the hole, although the actual behavior is governed by the displacement condition corresponding to the circular cross section of the bolt bearing into the surrounding plate. A typical assumption in the modeling of the joint is that the radial pressure due to the bolt follows a cosine function distribution over a 180° contact zone (Figure 5.3.2.2(c) part (A)) and zero pressure elsewhere (with zero tangential stresses around the whole circumference). In many cases this gives satisfactory results for predicting the critical stress peaks, e.g., the peak net-section stress at the 90 degree points around the fastener. Figure 5.3.2.2(c) in Reference 5.3.2.2(e) shows a comparison of the predicted stress concentration factors for an assumed "half-cosine" radial *pressure* distribution vs. the more accurate solution which assumes a radial *displacement* condition along the edge of the hole. The "K" values tabulated at the left side of the figure represent peak stresses normalized with respect to the gross stress, P/Wt (thus the subscript "G"), including the peak net section stress (K_G^{nt}) at =90°, peak bearing stress (K_G^{b}) at =0° and peak shear stress (K_G^{s}) at = 45°. These results were predicted for W/D= 2, e/W=1 and a neat fitting fastener. For these conditions, the stress concentration factors obtained from the two approaches are not substantially different, suggesting that the "half cosine" radial pressure distribution is an adequate approximation for the more accurate analysis which solves for the radial displacement distribution.

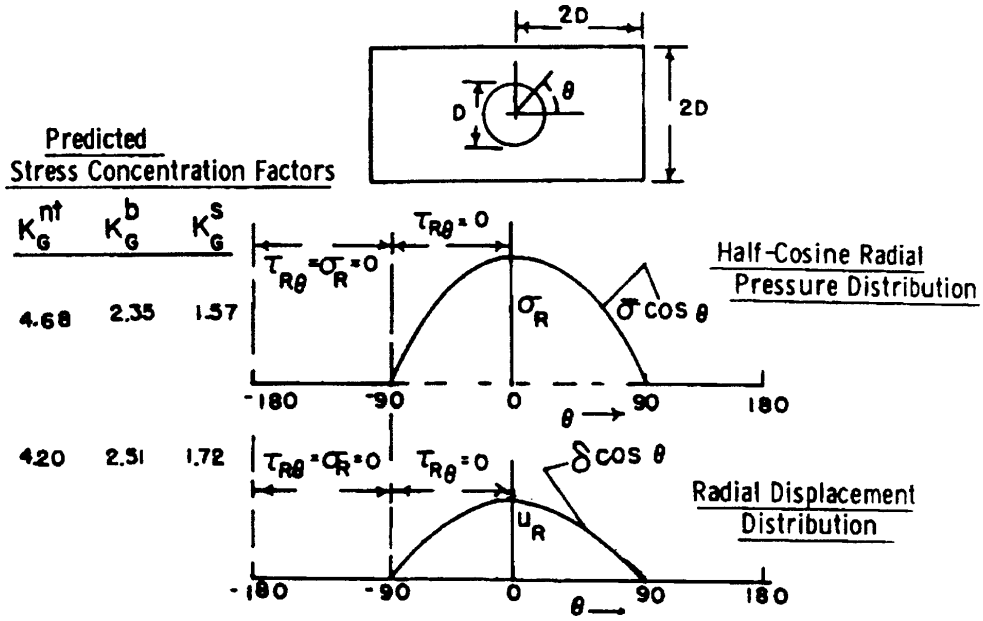

FIGURE 5.3.2.2(c) *Comparison of predicted stress concentrations for assumed radial pressure distribution vs. radial displacement distribution (Reference 5.3.2.2(e)).*

There are some important situations for which the "half cosine" pressure distribution will give poor results, however. Figure 5.3.2.2(d), which compares a variety of situations, includes one case in which the edge distance is relatively small (square symbols, e/W=0.375, W/D = 2); the radial pressure distribution is

characterized by a dip in the pressure near $\theta=0$. This corresponds to the tendency for the part of the plate in front of the fastener to deform as if in beam bending (Figure 5.3.2.2(e)) in the case of short edge distances, relieving the pressure in front of the fastener so as to account for the drop in radial pressure near $\theta=0°$ which is seen in Figure 5.3.2.2(d).

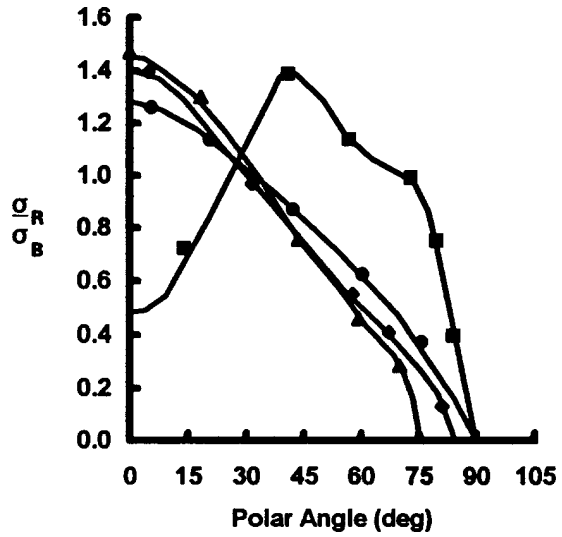

Symbol	e/W	W/D	Material
■	0.375	2	0° Glass/Epoxy
●	0.5	5	0° Glass/Epoxy
♦	Infinite Plate		0±45° Boron/Epoxy
▲	Infinite Plate		0° Glass/Epoxy (0.026% clearance)

FIGURE 5.3.2.2(d) *Radial pressure distributions for various joint configurations (Reference 5.3.2.2(e)).*

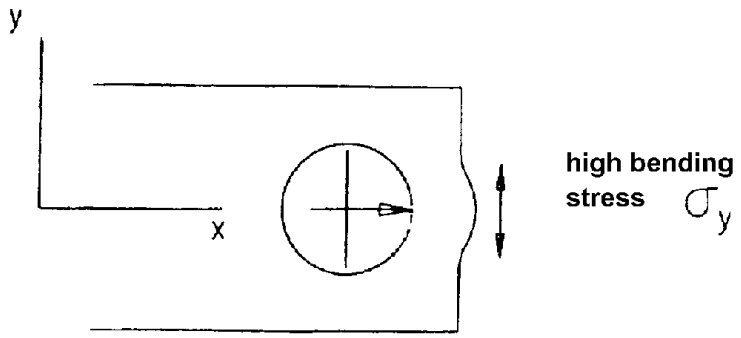

FIGURE 5.3.2.2(e) *Development of bending deflection in front of fastener for small e/D.*

In addition to the case of small edge distances, combined bearing and bypass loads can result in radial pressure distributions which deviate excessively from the "half=cosine" distribution. This can be understood in terms of the displacement behavior illustrated in Figure 5.3.2.2(f), for pure bypass loading in which there are two gaps between the plate and fastener centered about 0° and 180°, vs, the case of pure

bearing load in which a single gap located between θ=90° and 270° occurs. For low bypass loads one would, therefore, expect a single region of contact centered about θ =0°, while for large bypass loads a split contact region would be expected. In terms of the notation defined in Figure 5.3.2.2(g), this type of behavior is predicted by stress analyses which correctly model the contact situation between the fastener and plate as illustrated in Figure 5.3.2.2(h). Note in Figure 5.3.2.2(g) that P_{TOT} is the total load at the left of end of the joint, which is the sum of P_F, the fastener load, and P_{BP}, the bypass load.

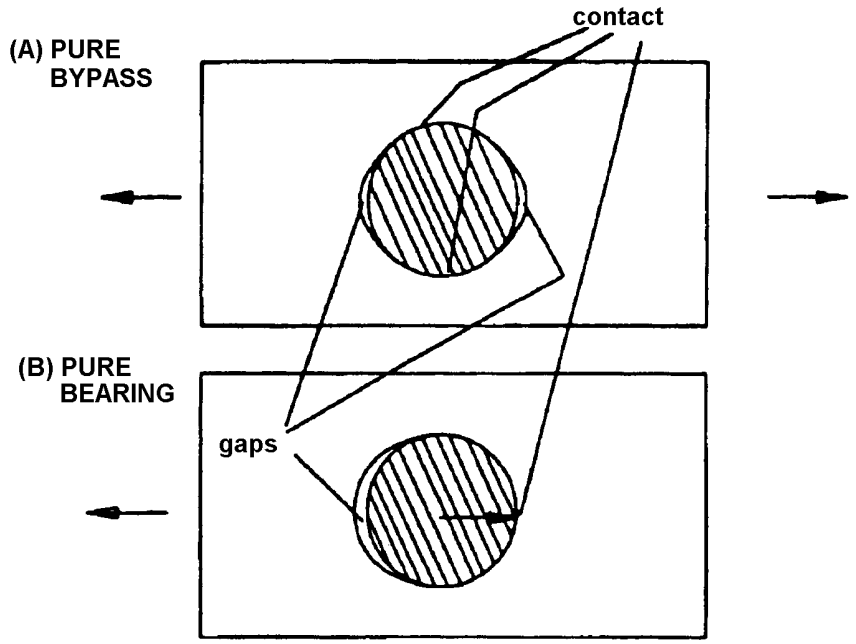

FIGURE 5.3.2.2(f) *Bolt shank/hole contact regions for pure bypass vs. pure bearing loads.*

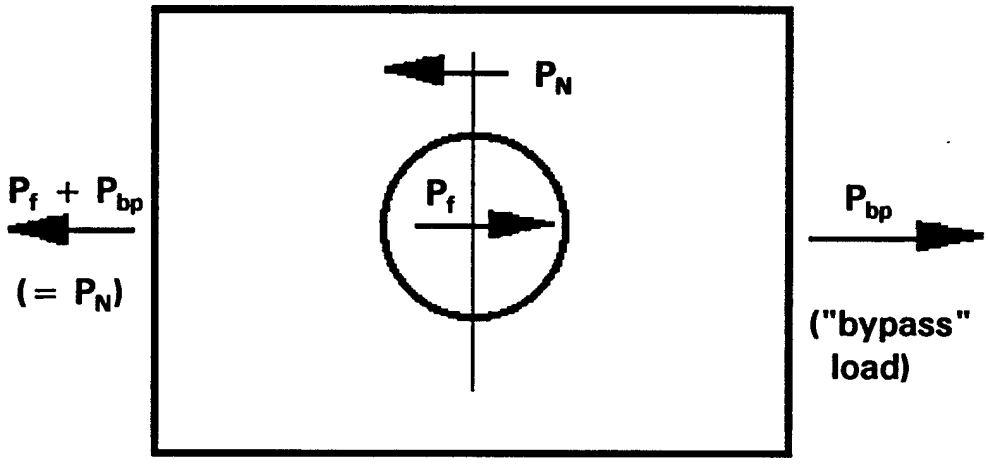

FIGURE 5.3.2.2(g) *Load definitions for combined bearing and bypass loads.*

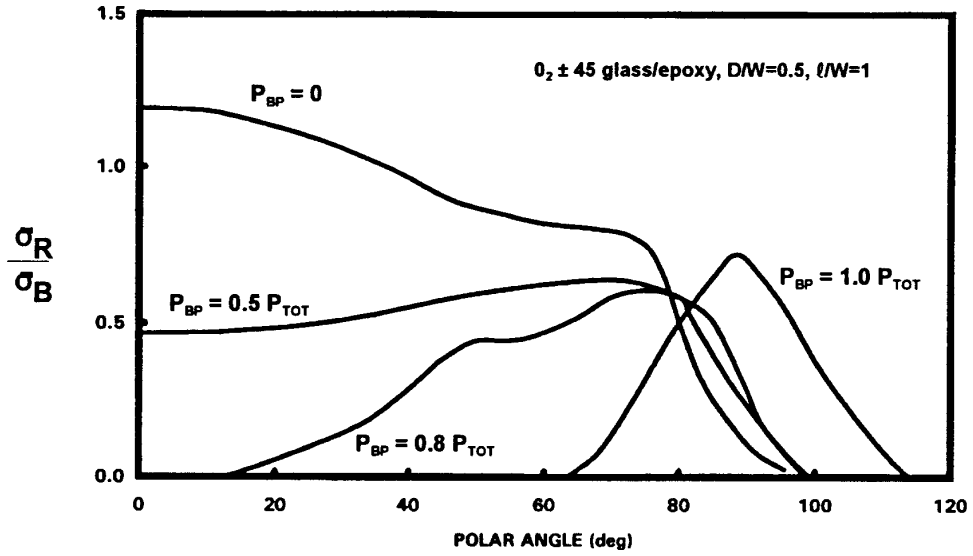

FIGURE 5.3.2.2(h) *Effect of bearing/bypass load ratio on radial pressure distribution (Reference 5.3.2.2(e)).*

Figure 5.3.2.2(i) illustrates how taking into account the effect of the radial displacements at the edge of the hole can influence predictions of the net section stress peaks. In this figure, predictions of K_G^{nt} (peak net section stress divided by gross stress) for the conventional superposition approach obtained by a linear combination of K_G^{nt} values for pure bearing load and pure bypass load (denoted "linear approximations" in Figure 5.3.2.2(i)), are compared with the corresponding results obtained when the contact problem is taken into account (open circles and squares). For the latter case, the curves are fairly flat over most of the range of load ratios, dropping rapidly near the high bypass end to a little above 3, the classical open hole value for isotropic plates having boundaries at infinity. Strength values for joints under combined bearing and bypass loading should follow similar trends with respect to the load ratio.

The above results apply to cases of exact fastener fits. Additional complications occur with clearance fits corresponding to tolerances which are representative of available machining practice. Clearance fit cases have been analyzed extensively by Crews and Naik (Reference 5.3.2.2(f)) for clearances on the order of 0.0025 in. (0.04 mm) with fastener diameters of 0.25 in. (6.3 mm), i.e., clearances about 1% of the fastener diameter[1]. Significant changes in the radial pressure distribution occur with respect to the exact fit case. The angle subtended by the contact region becomes a function of load for this case, starting at zero for incipient loads and growing to only about 60° on either side of the axial direction for typical peak loads. The reduction of the angle of contact by the effects of clearance results in significant increases in the peak bearing stress. Again, the "half-cosine" load distribution can not be used to predict this type of behavior.

Crews and Naik also addressed the applicability of the superposition method for predicting failure under combined bearing and bypass loading, on the basis of their analytical results with the Nuismer Whitney correction taken into account. They observed that the superposition approach gives adequate accuracy for predictions of the net-section tensile failures, although the predictions of radial pressure distributions are quite bad so that bearing failures cannot be treated by superposition.

[1]Note that the SI equivalent dimensions provided throughout Section 5.3 are “soft” conversions, that is SI dimensions for fastener sizes are provided but sizes are not converted to SI standard sizes.

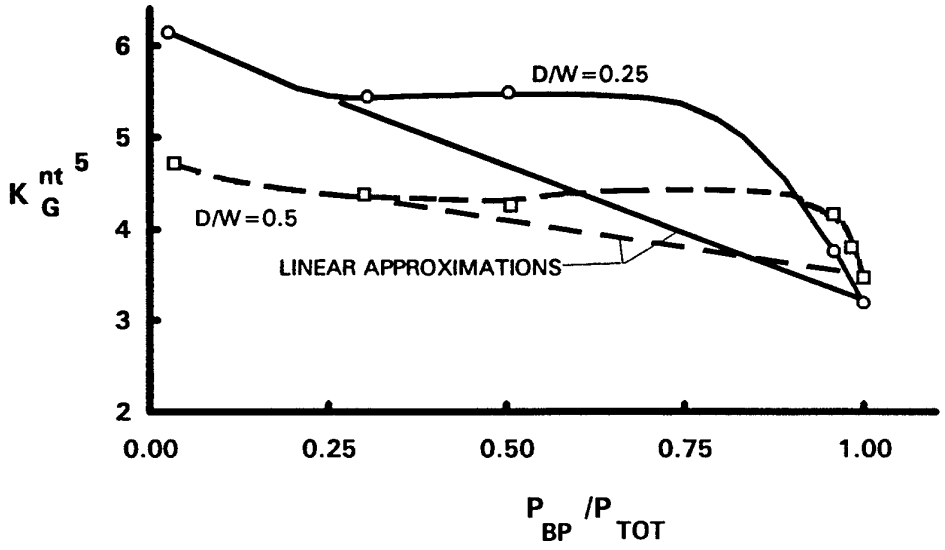

FIGURE 5.3.2.2(i) *Effect of bearing/bypass load ratio on peak net section stresses-neat fit fastener (Reference 5.3.2.2(e)).*

The basic analytical steps described above have been implemented in several computer codes. Codes developed under government sponsorship include BJSFM (Reference 5.3.2.2(g)), SAMCJ (Reference 5.3.2.2(h)), BOLT (Reference 5.3.2.2(c) and 5.3.2.2(i)), SCAN (Reference 5.3.2.2(j)), and BREPAIR (Reference 5.3.2.2(k)). BREPAIR has been specialized for the case of bolted repairs for composites, and also computes the bolt loads from the fastener and plate flexibilities.

In principle, the analysis methods described should be able to account for the shear-out failure mode if the stress analysis method used includes the effects of multiple holes and plate edges. However, because of the variety of ply-level failure criteria used, and the details of the analysis implementation, it is recommended that additional test correlation be performed before applying these methods to cases involving small edge distances, or close hole spacing.

Furthermore, current analysis methods should not be relied upon to predict matrix dominated modes such as bearing failure. Generally, the analysis codes can be used to predict net-section failures, while bearing failure is checked by direct comparison of the average bearing stress (P/dt) to test data.

The actual bearing pressure due to a bolt varies considerably through the thickness of the laminate. For this reason, the test configuration must closely match the actual joint geometry in terms of laminate thickness, gaps and shims, and configuration (double versus single shear) and type of fastener. The bearing strength will depend on factors such as the countersink depth and angle, joint rotation under load, and the type of fastener head. The though-thickness distribution of bearing stresses can be estimated by treating the bolt as a beam, and the laminate as an elastic foundation (Reference 5.3.2.2(l)). These methods are suitable for estimating the changes in the bearing stress due to changes in gap distances or laminate thickness. They may also be useful for determining the moment and shear distribution in the bolt to predict fastener failure.

Clamp-up forces have been shown to have a significant effect on laminate failure, particularly under fatigue loading. Clamp-up can suppress delamination failure modes, and changes the fastener head restraint. This effect cannot be included in the two-dimensional analysis methods described above. Before taking advantage of the beneficial effects of clamp-up, long-term relaxation of the laminate stresses

should be considered. Because of this effect, minimum clamp-up (if possible) should be used when conducting bolt bearing tests, i.e., finger tight or 10-20 in.-lb (1-2 N-m) torque up on a 1/4 in. (6.4 mm) diameter bolt. This may not be the normal torque installation of the fastener.

5.3.2.3 Failure criteria

The design of a mechanically fastened joint must assure against all possible failures of the joint. These are illustrated in Figure 5.3.2.3. Accepted design practice is to select edge distances, plate thicknesses, and fastener diameters so that of all the possible failure modes probable failures would be net section and bearing. There is no consensus whether the joint should fail in net section tension/compression or bearing. Reference 5.3.2.3(a) recommends that highly loaded structural joints be designed to fail in a bearing mode to avoid the catastrophic failures associated with net section failures. Although this is a commendable goal, particularly for single bolt joints, it is impractical in most cases as the increase in edge distances adds weight to the structure. For usual width to bolt diameter ratios of 6 both, net and bearing failures are possible, and the stress engineer is satisfied if he can show a positive margin against both failure modes. He does not try to get a higher margin for net failure than for bearing failure. Steering the joint design to have bearing failures by having large bearing allowables may result in in-service problems of bolt hole wear, fuel leakage, and fastener fatigue failures. Furthermore, net tension failure is unavoidable for multi-row joints.

In contrast to metals, load redistribution in a multi-fastened joint cannot be counted on and hence a single fastener failure in bearing constitutes failure of the joint. Failure criteria in bearing should be either bearing yield, defined either as the 0.02D or 0.04D based on actual bearing load displacement curves, Figure 7.2.2.4 of Volume 1, or B-basis ultimate load, whichever is lower. The beneficial effects of clamp-up on bearing failure has to be evaluated in light of relaxation during service.

Failure criteria for single fastener joint were discussed in Section 5.3.2.2. For complex loading or proximity to other fasteners, the failure location or mode identification may not be as shown in Figure 5.3.2.3 for unidirectional loading. For thick composites, recent work (Reference 5.3.2.3(b)) has shown that net section failures do not necessarily occur at 90° to the load direction but at some other locations around the hole.

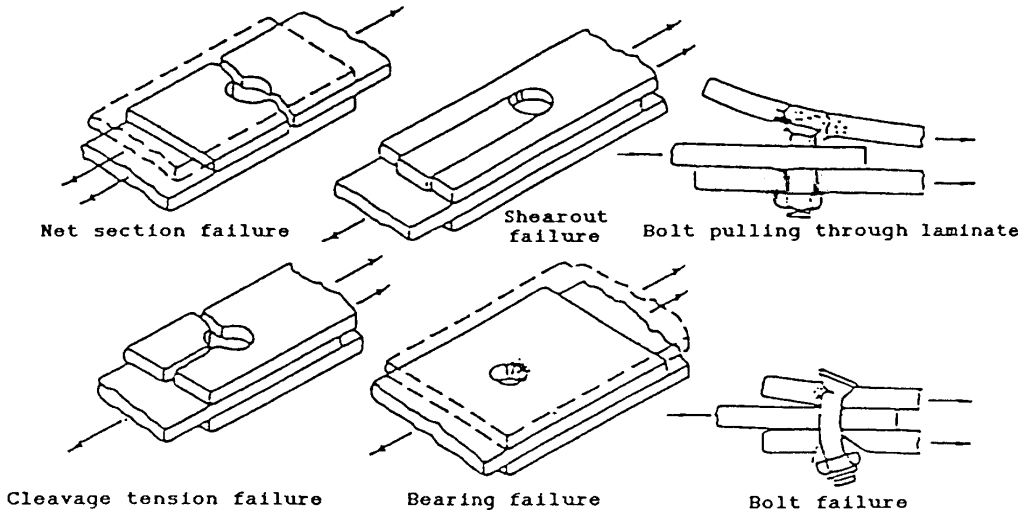

FIGURE 5.3.2.3(a) *Failure modes for mechanically fastened joints.*

5.3.3 Design considerations

5.3.3.1 Geometry

5.3.3.2 Lay-up and stacking sequence

5.3.3.3 Fastener selection

The use of mechanical fasteners to join non-metallic composite structures is bound by certain constraints which do not exist in the design of metallic joints. In other words, special care must be taken to select fasteners that are appropriate with polymer composite structures. Because of these special requirements fastener manufacturers have developed fasteners especially for use with composites. These fasteners develop the full bearing capability of the composite (which, at least for carbon/epoxy, is equal or better than aluminum) without encountering local failure modes and are not susceptible to corrosion. Therefore, these fasteners or those having such properties, should be used. Nondiscriminant use of off-the-shelf fasteners will lead to premature joint failures.

Design of mechanically fastened joints has always been guided by the principle that the material being joined should fail before the fastener, and this is the practice with composites. Although composites have high strength/stiffness to weight ratios with good fatigue resistance, it is a fact that today's composites must be treated very carefully when designing joints. The major structural limitation in this area is the insufficient through-thickness strength of the laminates. This has given rise to the term "pull-thru strength". It has become necessary to increase the bearing area of fastener heads (or tails) in order to reduce the axial stresses against the laminate when the fastener is loaded in tension.

Another area of concern is the bearing stress which a fastener applies to the edge of the hole in a composite laminate as its axis rotates due to secondary bending of the joint. This condition can impose a severe limitation on a joint with limited stiffness. Another problem is the composite's inability to support installation stresses of formed fasteners, such as solid rivets or blind fasteners with bulbed tails. In addition to surface damage, such as digging-in into composite, subsurface damage to the laminate may occur. For this reason, these fastener types are avoided in favor of two piece fasteners and blind fasteners which do not generate this type of loading during installation.

For the above reasons, tension head 100° countersunk fasteners rather than shear heads should be selected as the projected area of the tension head fastener is larger than that of a shear head fastener. The larger area improves pull-through and delamination resistance in composites, while reducing overturning forces from bolt bending. These fasteners are also recommended for double shear joints. Caution should be observed in the use of 130° countersunk head fasteners. Although this type of fastener increases the bearing area of the fastener and permits it to be used in thin laminates, pull-through strength and resistance to prying moments can be adversely affected.

The full bearing capability of composites can only be attained using fasteners with high fixity (good clamp-up). Fixity is a function of fastener stiffness, fastener fit, installation forces, torque and rotational resistance of the fastener head and collar or formed backside. However, because of relaxation with service usage, normal design/analysis practice uses data based on tests where the fasteners were installed finger tight or with light torque. As part of the allowables program, testing should also be done with fasteners installed per fastener supplier's recommended procedures.

Although close tolerance fit fasteners are desirable for use with composites, interference fit fasteners cannot be used due to potential delamination of plies at the fastener hole. There are exceptions to this rule. Some automatic high impact driving equipment which was used in production has been shown not to cause composite damage.

Presence of galvanic corrosion between metallic fasteners and non-metallic composite laminates has eliminated several commonly used alloys from consideration. Conventional plating materials are also not

being used because of compatibility problems. The choice of fastener materials for composite joints has been limited to those alloys which do not produce galvanic reactions. The materials currently used in design include unplated alloys of titanium and certain corrosion resistant stainless steels (cres) with aluminum being eliminated. The choice is obviously governed by the makeup of the composite materials being joined, weight, cost, and operational environment. Aircraft practice has been to coat fasteners with anti-corrosion agent to further alleviate galvanic corrosion.

5.3.4 Fatigue

Fatigue performance of bolted composite joints is generally very good as compared to metal joints. Under maximum cyclic load level as high as 70% of the static strength, composite bolted joints have been observed to endure extremely long fatigue life and with minimal reduction in residual strength. The predominant damage mechanism under cyclic loads is usually bearing failure in form of hole elongation with net section failure for static residual test.

Even though the general trends of fatigue behavior of bolted composites has been well established, the influence of individual parameters on the fatigue performance needs to be investigated. For bolted composite joints, the parameters include material system, geometry, attachment details, loading mode and environment. Several government funded programs have been conducted to evaluate the influence of specific design on composite bolted joints. Typical examples are given in References 5.3.4(a) - 5.3.4(e). However, the large number of design variables makes it very difficult to develop an overall understanding of the specific influence of each of the primary design parameters. Based on the results of References 5.3.4(a) - 5.3.4(e), the following paragraphs summarize the significant effects of key design parameters on the fatigue performance of bolted composite joints. Because the parameters used in each reference are significantly different, direct comparison of the results is difficult. Only the trends of the data, based on coupon tests, are discussed.

5.3.4.1 Influence of loading mode

Under a constant amplitude fatigue situation, the most severe loading condition is fully reversed loading ($R = -1$). The results in Reference 5.3.4(a) indicate that fatigue failures will occur within 10^6 cycles if the maximum cyclic bearing stress is above 35% of the static bearing strength. However, the results of Reference 5.3.4(d) show that a 10^6 cycles fatigue threshold exceeds 67% of the static strength. Failure observed in the specimens exposed to fully reversed fatigue loads were induced by local bearing and excessive hole elongation. The hole elongation increases slowly for the major portion of the specimen's fatigue life, but increases rapidly near the end of the fatigue life. That is, once the bearing mode of failure is precipitated, hole elongation increases from a low value (1 to 2% of the original hole diameter) to a prohibitive value (>10%) within a few cycles. The fatigue threshold increases with decreasing R-ratio for tension-compression loading, and tension-tension loading is the least severe constant amplitude fatigue load.

Typical aircraft spectra loading were used in References 5.3.4(a), 5.3.4(c) and 5.3.4(d) to investigate the effects of variable amplitude cyclic loading on the fatigue performance of composite bolted joints. The results in Reference 5.3.4(a) show that the specimens survived two lifetimes of a typical vertical stabilizer spectrum loading without fatigue failure. The maximum spectrum load used in these tests ranges from 0.66 to 1.25 times of the static strength. Four loading spectra were tested in Reference 5.3.4(d) to investigate the influence of spectrum profile and load truncation levels. The results of these tests showed no fatigue failure and no distinguishable difference in the fatigue life for the spectrum loading investigated. The maximum spectrum stress was 78% of the static strength and the minimum stress at -49% of the static strength.

An extensive spectrum sensitivity database for bolted composite joints was generated in Reference 5.3.4(c). In this reference, the spectrum parameters investigated included load frequency, spectrum truncation, stress level, extended life, temperature and moisture, and specimen size. With approximately 600 specimens tested in the reference, there were no fatigue failures observed within the composite portion of

the bolted joint specimens. This absence of composite fatigue failures confirmed that composite bolted joints are fairly insensitive to fatigue in tension loading at normal operating loads. Theses results also showed that composite bolted joints are insensitive to fatigue even in severe environments, such as real flight time loads and temperature, and 15 lifetimes of accelerated fatigue at 70% of the static strength in a 250°F (120°C) hot-wet condition. This does not mean that fastener failures have not occurred, sometimes precipitated by composite stiffness or fitup.

5.3.4.2 Influence of joint geometry

The influence of fastener diameter and fastener spacing on the fatigue performance of bolted composite joints is investigated in Reference 5.3.4(d). Three fastener diameters (0.25, 0.375 and 0.5 in. (6.4, 9.5, and 13 mm)) and three fastener spacing-to-diameter ratios (3.0, 4.0 and 6.0) are considered in the investigation. The results indicate that larger spacing to diameter ratio specimens have lower fatigue performance than specimens with lower ratios. The limited amount of data in the reference is not sufficient to draw a general conclusion. However, the results in Reference 5.3.4(d) are presented in terms of gross area stress, the lower fatigue performance of the wider specimens may be caused by the higher loads in the fastener and result in fastener or joint failure.

The fatigue performances of single lap joint and double lap joint are compared in Reference 5.3.4(a). Test results in the reference indicate that the threshold bearing stress value is relatively unaffected by the differences in the two joint configurations.

The effects of bolt bearing/by-pass stress interaction on the fatigue performance is also investigated in Reference 5.3.4(a). Joints with bolt-to-total load ratios of 0.0, 0.2, 0.33 and 1.0 are considered in the reference. The results of these tests show change in failure mode with bolt bearing/by-pass stress ratio. Net section failures were observed for specimens tested with a bolt bearing/by-pass ratio of 0.0 (or open hole). When 20% of the total load was introduced directly as a bearing load, half the specimens suffered a net section failure, and the other half suffered local bearing failures. For the test case where 33% of the total load was presented as the fastener bearing load, the observed failures were local bearing induced excessive hole elongation, similar to the results of full-bearing.

5.3.4.3 Influence of attachment details

The effects of attachment details on the fatigue performance of bolted composite joints are investigated in References 5.3.4(a) and 5.3.4(d). The influence of fastener fit is studied in Reference 5.3.4(d) by considering four levels of hole diameter for controlled over and under size, including slight interference. At applied cyclic load levels greater than 50% of static strength, no significant difference in fatigue performance for the different fastener fits was observed. The specimens were tested at a stress ratio of R=-1.0.

The effects of fastener torque on fatigue performance is studied in Reference 5.3.4(a). The results of these tests showed that there was no change in the failure mode and the fatigue performance improved with increased torque. The results also indicated that at low torque levels, hole elongation increased gradually with fatigue cycling and at high torque levels, the cyclic hole elongation rate was very abrupt.

The effect of countersink on joint performance was investigated in Reference 5.3.4(a). When countersunk (100° tension head) steel fasteners were used, approximately half of the tests resulted in fastener failure. The fasteners failed in a tensile mode near the head/shank boundary. Comparing these results with those with protruding head steel fasteners, the effect of the countersink is seen to be earlier elongation at a constant cyclic bearing stress amplitude. It is also seen that the fatigue threshold is lower when countersunk fasteners are used. When countersunk titanium fasteners were used instead of the steel fasteners, fastener failures occurred in every specimen.

5.3.4.4 Influence of laminate lay-up

The effect of laminate lay-up on the joint performance was investigated in Reference 5.3.4(a) by considering three laminate lay-ups--(50/40/10), (70/20/10) and (30/60/10). The results of this investigation indicated that despite the difference in static bearing strength of these laminates, the 10**6 cycle fatigue threshold is approximately equal.

5.3.4.5 Influence of environment

The effects of temperature and moisture are experimentally evaluated in References 5.3.4(a) and 5.3.4(c). The results of these studies indicate that the fatigue threshold may be lower under the hot/wet (218°F/wet (103°C/wet)) condition.

5.3.4.6 Influence of specimen thickness

The effect of laminate thickness on fatigue performance is examined in Reference 5.3.4(d) and the effect of specimen size is evaluated in Reference 5.3.4(c). The results of Reference 4 show that within the thickness of 0.25 to 0.50 inch (6.4 to 13 mm) the fatigue threshold is not significantly affected. In comparing the fatigue performance of small and large scale joints, Reference 5.3.4(c) showed that there is no significant scale up effect.

5.3.4.7 Residual strength

The extensive amount of residual strength data generated in Reference 5.3.4(c) suggested that bolted composite joints have an excellent capability of retaining static strength. This trend is also supported by the results of other investigations. The largest percentage of fatigue strength reduction observed in Reference 5.3.4(c), when compared with static strength, was 8%. There were no real time or environmental effects on residual strength reduction that were greater than this. Therefore, a design static tension strength reduction factor is appropriate to account for tension fatigue effects on bolted composite joints under practical service environments.

5.3.5 Test verification

In addition to joint coupon testing which is performed to obtain baseline data, element testing should be performed to verify joint analysis, failure mode, and location. This is particularly important for primary connections and where the load transfer is complex. The purpose of testing is to obtain assurance that the joint behaves in the predicted manner or where analysis is inadequate.

The structural joints to be tested are usually identified early in the design process and are part of the certification process, if the building block approach is used, see Section 2.1.1, Volume 1. The test specimens are classified by levels of complexity as elements, subcomponents, or components. Some examples of types of joints that are tested are shown for a fighter wing structure in Figures 5.3.5(a) and 5.3.5(b).

The bolted joint element or subcomponent tests are usually performed at ambient conditions with sufficient instrumentation to fully characterize load transfer details: direction and amplitude of bolt and by-pass loads. Tests at other than ambient conditions are necessary in cases when the low or elevated temperatures with associated moisture contents substantially change the load distributions.

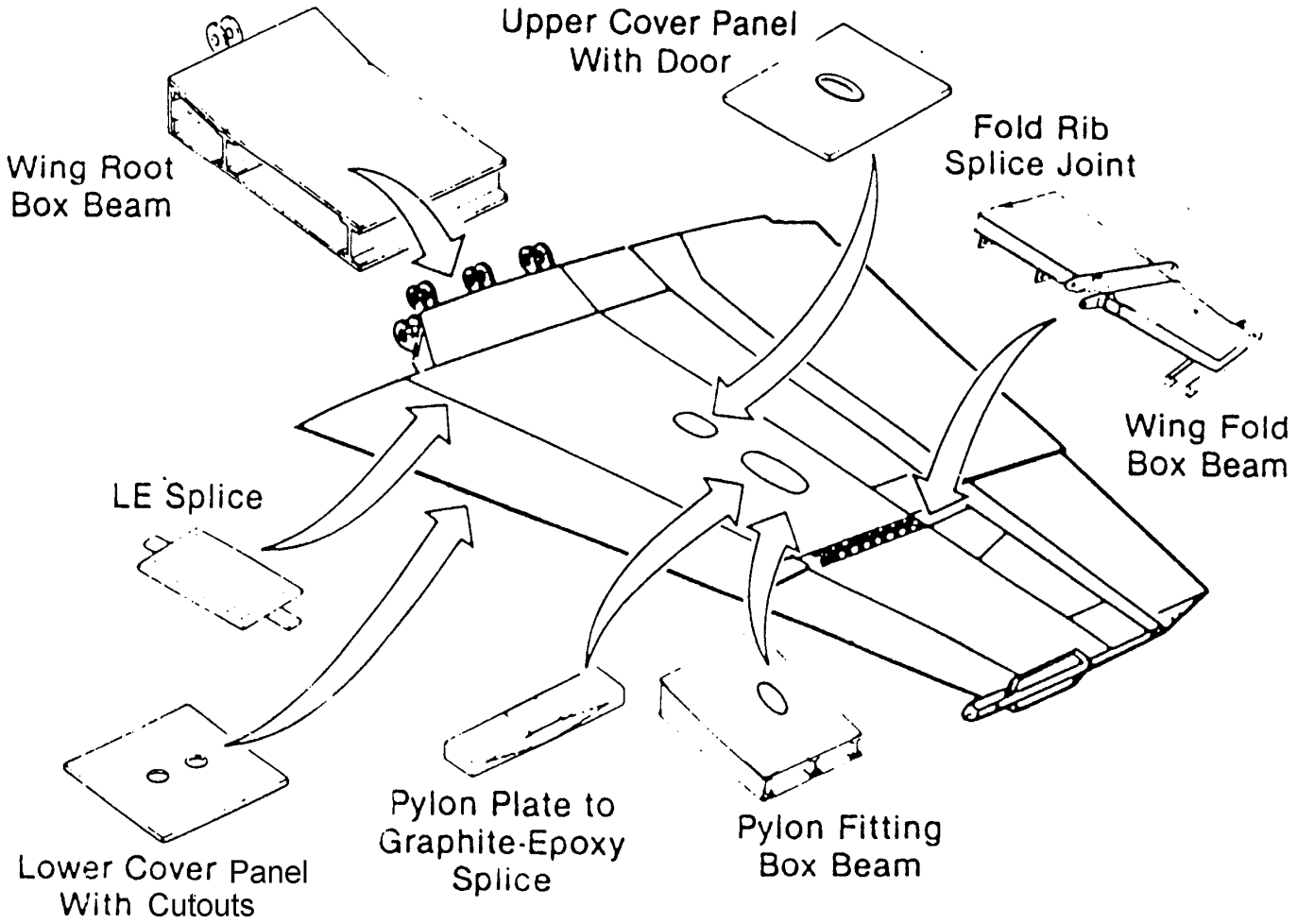

FIGURE 5.3.5(a) *Wing subcomponent tests.*

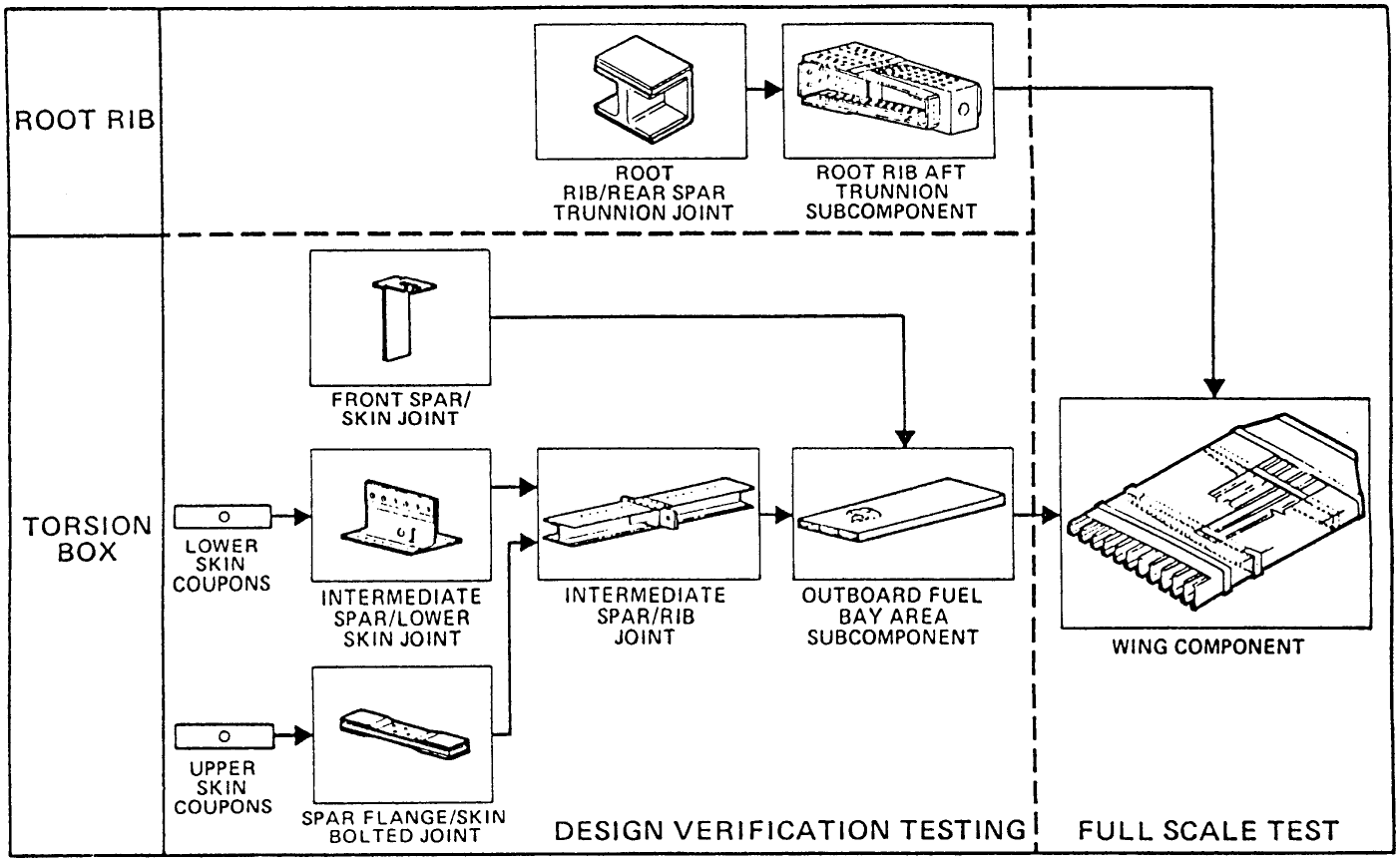

FIGURE 5.3.5(b) *Building block approach for the wing structure in the composite wing/fuselage program (Reference 5.3.5).*

REFERENCES

5.2.1(a) Volkersen, O., "Die Nietkraftverteilung in Zugbeanspruchten Nietverbindungen mit Konstanten Laschenquerschnitten," *Luftfahrtforschung*, Vol 15, 1938, pp. 4-47.

5.2.1(b) Goland, M. and Reissner, E., "Stresses In Cemented Joints," *Journal of Applied Mechanics*, Vol 11, 1944, pp. A17-A27.

5.2.1(c) Kutscha, D. and Hofer, K., "Feasibility of Joining Advanced Composite Flight Vehicle Structures," Air Force Materials Laboratory Report AFML-TR-68-391, 1968.

5.2.1(d) Dickson, J.N., Hsu, T.N., and McSkinney, J.N., "Development of an Understanding of the Fatigue Phenomena of Bonded and Bolted Joints In Advanced Filamentary Composite Materials, Volume I, Analysis Methods," Lockheed Georgia Aircraft Company, USAF Contract Report AFFDL-TR 72-64, Volume I, June 1972.

5.2.1(e) Grimes, G.C., Wah, T., et al, "The Development of Non-Linear Analysis Methods for Bonded Joints in Advanced Filamentary Composite Structures," Southwest Research Institute, USAF Contract Report AFML-TR-72-97, September 1972.

5.2.1(f) Renton, W.J., "The Analysis and Design of Composite Materials Bonded Joints Under Static and Fatigue Loadings," PhD Thesis, University of Delaware, 1973.

5.2.1(g) Renton, W.J. and Vinson, J.R., "The Analysis and Design of Composite Materials Bonded Joints under Static and Fatigue Loadings," Air Force Office of Scientific Research Report TR-73-1627, 1973

5.2.1(h) Oplinger, D.W., "Stress Analysis of Composite Joints," *Proceedings of 4th Army Materials Technology Conference*, Brook Hill Publishing Co., Newton MA, 1975, pp 405-51.

5.2.1(i) Hart-Smith, L.J., AFFDL-TR-72-130, pp 813-856.

5.2.1(j) Hart-Smith, L.J., "Adhesive Bonded Double Lap Joints," NASA Langley Contractor Report NASA CR-112235 1973.

5.2.1(k) Hart-Smith, L.J., "Adhesive Bonded Single Lap Joints," NASA Langley Contractor Report NASA CR-112236, 1973.

5.2.1(l) Hart-Smith, L.J., "Adhesive Bonded Scarf and Stepped-Lap Joints," NASA Langley Contractor Report NASA CR-112237, 1973.

5.2.1(m) Hart-Smith, L.J., "Analysis and Design of Advanced Composite Bonded Joints," NASA Langley Contractor Report NASA CR-2218, 1973.

5.2.1(n) Hart-Smith, L.J., "Advances in the Analysis and Design of Adhesive-Bonded Joints in Composite Aerospace Structures," *SAMPE Process Engineering Series*, Vol 19, SAMPE, Azusa, 1974, pp 722-737.

5.2.1(o) *Primary Adhesively Bonded Structure (PABST) Technology*, Air Force Contract F33615-75-C-3016, 1975.

5.2.1(p) Thrall, E.W., "Primary Adhesively Bonded Structure Technology (PABST) Phase 1b: Preliminary Design," Air Force Flight Dynamics Laboratory Report AFFDL-TR-76-141, 1976.

5.2.1(q) Shannon, R.W., et al, "Primary Adhesively Bonded Structure Technology (PABST) General Material Property Data," Air Force Flight Dynamics Laboratory Report AFFDL-TR-77-101 1977.

5.2.1(r) Land, K.L., Lennert, F.B., et al, "Primary Adhesively Bonded Structure Technology (PABST): Tooling, Fabrication and Quality Assurance Report," USAF Technical Report AFFDL-TR-79-3154, October 1979.

5.2.1(s) Hart-Smith, L.J., "Adhesive Bond Stresses and Strains at discontinuities and Cracks in Bonded Structures," *Transactions of the ASME, Journal of Engineering Materials and Technology*, Vol 100, January 1978, pp. 15-24.

5.2.1(t) Hart-Smith, L.J., "Differences Between Adhesive Behavior in Test coupons and Structural Joints," Douglas Aircraft Company paper 7066, Presented to ASTM Adhesives Committee D-14 Meeting, Phoenix, Arizona, 1981.

5.2.1(u) Hart-Smith, L.J., "Design Methodology for Bonded-Bolted Composite Joints," Douglas Aircraft Company, USAF Contract Report AFWAL-TR-81-3154, Vol I and II, February 1982.

5.2.1(v) Thrall, E.W., Jr., "Failures in Adhesively Bonded Structures," AGARD-NATO Lecture Series No. 102, "Bonded Joints and Preparation for Bonding," Oslo, Norway, and The Hague, Netherlands, April 1979 and Dayton, Ohio, October 1979.

5.2.1(w) Hart-Smith, L.J., "Further Developments in the Design and Analysis of Adhesive-Bonded Structural Joints," Douglas Aircraft Co. Paper No. 6922, presented at the ASTM Symposium on Joining of Composite Materials, Minneapolis MN April 1980

5.2.1(x) Hart-Smith, L.J., "Adhesive Bonding of Aircraft Primary Structures," Douglas Aircraft Company Paper 6979, Presented to SAE Aerospace Congress and Exposition, Los Angeles, California, October 1980.

5.2.1(y) Hart-Smith, L.J., "Stress Analysis: A Continuum Analysis Approach" in *Developments in Adhesives - 2*, ed. A. J. Kinloch, Applied Science Publishers, England, 1981, pp. 1-44.

5.2.1(z) Hart-Smith, L.J., "Effects of Adhesive Layer Edge Thickness on Strength of Adhesive-Bonded Joints" Quarterly Progress Report No. 3, Air Force Contract F33615-80-C-5092, 1981.

5.2.1(aa) Hart-Smith, L.J., "Effects of Flaws and Porosity on Strength of Adhesive-Bonded Joints" Quarterly Progress Report No. 5, Air Force Contract F33615-80-C-5092, 1981.

5.2.1(ab) Hart-Smith, L.J. and Bunin, B.L., "Selection of Taper Angles for Doublers, Splices and Thickness Transition in Fibrous Composite Structures," *Proceedings of 6th Conference On Fibrous Composites in Structural Design*, Army Materials and Mechanics Research Center Manuscript Report AMMRC MS 83-8, 1983.

5.2.1(ac) Nelson, W.D., Bunin, B.L., and Hart-Smith, L.J., "Critical Joints in Large Composite Aircraft Structure," *Proceedings of 6th Conference On Fibrous Composites in Structural Design*, Army Materials and Mechanics Research Center Manuscript Report AMMRC MS 83-8, 1983.

5.2.1(ad) Oplinger, D.W., "A Layered Beam Theory for Single Lap Joints," U.S. Army Materials Technology Laboratory Report MTL TR 91-23, 1991.

5.2.1(ae) Oplinger, D.W., "Effects of Adherend Deflections on Single Lap Joints," *Int. J. Solids Structures*, Vol 31, No. 18, 1994, pp. 2565-2587.

5.2.2.1(a) Hart-Smith, L.J., "Adhesively Bonded Joints in Fibrous Composite Structures," Douglas Aircraft Paper 7740; presented to the International Symposium on Joining and Repair of Fibre-Reinforced Plastics, Imperial College, London, 1986.

5.2.2.1(b) Hart-Smith, L.J., "Induced Peel Stresses in Adhesive-Bonded Joints," Douglas Aircraft Company, Technical Report MDC-J9422A, August 1982.

5.2.2.6(a) Hart-Smith, L.J., Brown, D. and Wong, S., "Surface Preparations for Ensuring that the Glue will Stick in Bonded Composite Structures," *10th DoD/NASA/FAA Conference on Fibrous Composites in Structural Design*, Hilton Head Is, SC, 1993.

5.2.2.6(b) Hart-Smith, L.J., Ochsner, W., and Radecky, R.L., "Surface Preparation of Fibrous Composites for Adhesive Bonding or Painting," *Douglas Service Magazine*, First quarter 1984, pp 12-22.

5.2.2.6(c) Hart-Smith, L.J., Ochsner, W., and Radecky, R.L., "Surface Preparation of Fibrous Composites for Adhesive Bonding or Painting," *Canadair Service News*, Summer 1985, 1985, pp. 2-8.

5.2.2.7(a) Frazier, T.B. and Lajoie, A.D., "Durability of Adhesive Joints," Air Force Materials Laboratory Report AFML TR-74-26, Bell Helicopter Company, 1974.

5.2.2.7(b) Becker, E.B., et al, "Viscoelastic Stress Analysis Including Moisture Diffusion for Adhesively Bonded Joints," Air Force Materials Laboratory Report AFWAL-TR-84-4057, 1984.

5.2.2.7(c) Jurf, R. and Vinson, J., "Effects of Moisture on the Static and Viscoelastic Shear Properties of Adhesive Joints," Dept. of Mechanical and Aerospace Engineering Report MAE TR 257, University of Delaware, 1984.

5.2.2.7(d) Mostovoy, S., Ripling, E.J., and Bersch, C.F., "Fracture Toughness of Adhesive Joints," *J. Adhesion*, Vol 3, 1971, pp. 125-44.

5.2.2.7(e) DeVries, K.L., Williams, M.L., and Chang, M.D., "Adhesive Fracture of a Lap Shear Joint," *Experimental Mechanics*, Vol 14, 1966, pp 89-97.

5.2.2.7(f) Trantina, G.G. "Fracture Mechanics Approach to Adhesive Joints," University of Illinois Dept. of Theoretical and Applied Mechanics Report T&AM 350, Contract N00019-71-0323, 1971.

5.2.2.7(g) Trantina, G.G., "Combined Mode Crack Extension in Adhesive Joints," University of Illinois Dept. of Theoretical and Applied Mechanics Report T&AM 350, Contract N00019-71-C-0323, 1971.

5.2.2.7(h) Keer, L.M., "Stress Analysis of Bond Layers," *Trans. ASME J. Appl. Mech.*, Vol 41, 1974, pp 679-83.

5.2.2.7(i) Knauss, J.F., "Fatigue Life Prediction of Bonded Primary Joints," NASA Contractor Report NASA-CR-159049, 1979.

5.2.2.7(j) Wang, S.S. and Yau, J.F., "Analysis of Interface Cracks in Adhesively Bonded Lap Shear Joints," NASA Contractor Report NASA-CR-165438, 1981.

5.2.2.7(k) Johnson, W.S. and Mall, S., "A Fracture Mechanics Approach for Designing Adhesively Bonded Joints".

5.2.3.6 Oplinger, D.W. "Effects of Mesh Refinement on Finite Element Analysis of Bonded Joints," U.S. Army Research Laboratory Study (Unpublished), 1983.

5.3.1 Whitman, B., Shyprykevich, P., and Whiteside, J.B., "Design of the B-1 Composite Horizontal Stabilizer Root Joint," *Third NASA/USAF Conference on Fibrous Composites in Flight Vehicles Design*, Williamsburg, VA, November 4-6, 1976.

5.3.2.1(a) Ramkumar, R.L., Saether, E.S., Appa, K., "Strength Analysis of Laminated and Metallic Plates Bolted Together by Many Fasteners," AFWAL-TR-86-3034, July, 1986.

5.3.2.1(b) Xiong, Y. and Poon, C., "A Design Model for Composite Joints with Multiple Fasteners," National Research Council, Canada, IAR-AN-80, August 1994.

5.3.2.1(c) Griffin, O.H., et. al., "Analysis of Multifastener Composite Joints," *Journal of Spacecraft and Rockets*, Vol 31, No. 2, March-April 1994.

5.3.2.1(d) ACEE Composite Structures Technology, *Papers by Douglas Aircraft Company*, ed. M. Klotzsche, NASA-CR-172359, August 1984.

5.3.2.2(a) Whitney, J.M. and Nuismer, R.J., "Stress Fracture Criteria for Laminated Composites Containing Stress Concentrations," *J. Composite Materials*, Vol 8, July, 1974, pp. 235-265.

5.3.2.2(b) Hart-Smith, J., "Mechanically-Fastened Joints for Advanced Composites Phenomenological Considerations and Simple Analysis," *Fibrous Composites in Structural Design,* ed. Edward M. Lenoe, Donald W. Oplinger, John J. Burke, Plenum Press, 1980.

5.3.2.2(c) Chang, F., Scott, R.A., Springer, G.S., "Strength of Mechanically Fastened Composite Joints," Air Force Wright Aeronautical Laboratories Technical Report AFWAL-TR-82-4095.

5.3.2.2(d) Lekhnitskii, S.G., *Anisotropic Plates*, Gordon and Breach Science Publishers, New York, 1968.

5.3.2.2(e) Oplinger, D.W., "On the Structural Behavior of Mechanically Fastened Joints" in *Fibrous Composites in Structural Design,* ed. Edward M. Lenoe, Donald W. Oplinger, John J. Burke, Plenum Press, 1980.

5.3.2.2(f) Crews, J.H., and Naik, R.A., "Combined Bearing and Bypass Loading on a Graphite/Epoxy Laminate," *Composite Structures,* Vol 6, 1968, pp. 21-40.

5.3.2.2(g) Garbo, S.P. and Ogonowski, J.M., "Effect of Variances and Manufacturing Tolerances on the Design Strength and Life of Mechanically Fastened Composite Joints, Volume 3 - Bolted Joint Stress Field Model (BJSFM) Computer Program User's Manual," Air Force Wright Aeronautical Laboratories Technical Report AFWAL-TR-81-3041, April 1981.

5.3.2.2(h) Ramkumar, R.L., Saether, E.S., and Appa, K., "Strength Analysis of Laminated and Metallic Plates Bolted Together by Many Fasteners," Air Force Wright Aeronautical Laboratories Technical Report AFWAL-TR-86-3034, July 1986.

5.3.2.2(i) Chang, F., Scott, R.A., and Springer, G.S., "Strength of Bolted Joints in Laminated Composites," Air Force Wright Aeronautical Laboratories Technical Report AFWAL-TR-84-4029.

5.3.2.2(j) Hoehn, G., "Enhanced Analysis/Design Methodology Development for High Load Joints and Attachments for Composite Structures," Naval Air Development Center Technical Report.

5.3.2.2(k) Bohlmann, R.E., Renieri, G.D., Horton, D.K., "Bolted Repair Analysis Methodology," Naval Air Development Center Technical Report NADC-81063-60, Dec. 1982.

5.3.2.2(l) Harris, H.G., Ojalvo, I. U., and Hooson, R.E., "Stress and Deflection Analysis of Mechanically Fastened Joints," Air Force Flight Dynamics Laboratory Technical Report AFFDL-TR-70-49, May 1970.

5.3.2.3(a) Ramkumar, R.L., Saether, E.S., Cheng, D., "Design Guide for Bolted Joints in Composite Structures," Air Force Wright Aeronautical Report AFWAL-TR-86-3035, March 1986.

5.3.2.3(b) Cohen, D., Hyer, M. W., Shuart, M. J., Griffin, O. H., Prasad, C., Yalamanchili, S. R., "Failure Criterion for Thick Multifastener Graphite-Epoxy Composite Joints," *Journal of Composites Technology & Research*, JCTRER, Vol . 17, No. 3, July 1995, pp. 237-248.

5.3.4(a) Ramkumar, R.L., and Tossavainen, E.W., "Bolted Joints in Composite Structures: Design, Analysis and Verification, Task I Test Results--Single Fastener Joints," AFWAL-TR-84-3047, August 1984.

5.3.4(b) Garbo, S.P., and Ogonowski, J.M., "Effects of Variances and Manufacturing Tolerances on the Design Strength and Life of Mechanically Fastened Composite Joints," Vol 1, 2 and 3, AFWAL-TR-81-3041, April 1981.

5.3.4(c) Jeans, L.L., Grimes, G.C., and Kan, H.P., "Fatigue Spectrum Sensitivity Study for Advanced Composite Materials, Volume I - Technical Summary," AFWAL-TR-80-3130, Vol I, December 1980.

5.3.4(d) Walter, R.W., and Tuttle, M.M., "Investigation of Static and Cyclic Failure Mechanisms for GR/EP Laminates," *Proceedings of the Ninth DoD/NASA/FAA Conference on Fibrous Composites in Structural Design*, DOT/FAA/CT-92-25, September 1992, p. I-167.

5.3.4(e) Walter, R.W., and Porter, T.R., "Impact of Design Parameters on Static, Fatigue and Residual Strength of GR/EP Bolted Joints," *Proceedings of the Tenth DoD/NASA/FAA Conference on Fibrous Composites in Structural Design*, NAWCADWAR-94096-60, p. III-75, April 1994.

5.3.5 Whitehead, R.S., et al., "Composite Wing/Fuselage Program," AFWAL-TR-883098, Vol 1-4., February, 1989.

This page intentionally left blank

Index Worksheet